NASA CR-134671

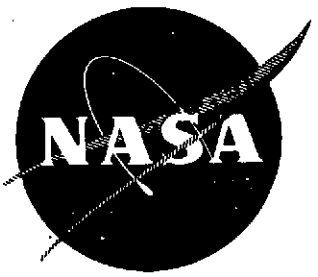

STUDY TO DEFINE BEHAVIOR OF LIQUID LUBRICANTS IN AN ELASTOHYDRODYNAMIC CONTACT

by

James L. Lauer

SUN OIL COMPANY

prepared for

NATIONAL AERONAUTICS AND SPACE ADMINISTRATION

NASA Lewis Research Center

NAS3-17593

1. Report No.	2. Government Accession No.	3. Recipient's Catalog No.
NASA CR-134671		

4. Title and Subtitle	5. Report Date
STUDY TO DEFINE BEHAVIOR OF LIQUID LUBRICANTS IN AN ELASTOHYDRODYNAMIC CONTACT	October 17, 1974
	6. Performing Organization Code
7. Author(s)	8. Performing Organization Report No.
James L. Lauer	
9. Performing Organization Name and Address	10. Work Unit No.
Sun Oil Company P. O. Box 1135 Marcus Hook, PA 19061	11. Contract or Grant No.
	NAS 3-17593
12. Sponsoring Agency Name and Address	13. Type of Report and Period Covered
National Aeronautics and Space Administration Washington, D. C. 20546	Contractor Report
	14. Sponsoring Agency Code

15. Supplementary Notes

Project Manager, W. R. Jones, Jr. Lubrication Branch
NASA Lewis Research Center
Cleveland, Ohio

16. Abstract

As an initial step in a program designed to determine state and composition of fluids in EHD contacts by infrared spectroscopy, the spectra of an ester and a saturated hydrocarbon polymer were obtained at pressures ranging from ambient to 2 GN/m^2 (20 kilobar) and at temperatures between ambient and 180°C in absorption and between 150°C and 210°C in emission. To simulate contact conditions the fluids were contained in the tiny sample volume of a diamond cell, i.e., the hole in a metal spacer separating two diamonds pressed against each other in a nut cracker-like arrangement. Pressures could be deduced from bandshifts and states of aggregation from bandwidths in the fluorescence spectrum of a ruby crystal immersed in the fluids. An infrared Fourier transform spectrometer was used with attachments specially designed to analyze the radiation passed through the sample and both diamonds (absorption technique) or the radiation emanating from the heated sample and passing through only one diamond (emission technique). The latter technique is applicable to operating EHD contacts. Spectral changes pointing to possible glass transitions and composition changes were observed. Emission and absorption spectra were generally equivalent. Some emission bandshapes appear to be temperature sensitive enough to be useful as internal temperature probes.

17. Key Words (Suggested by Author(s))	18. Distribution Statement
Elastohydrodynamic lubrication; infrared absorption spectroscopy; infrared emission spectroscopy; phase changes; traction; diamond anvil cell; ruby fluorescence; high pressures; glass transitions	Unclassified - Unlimited

19. Security Classif. (of this report)	20. Security Classif. (of this page)	21. No. of Pages	22. Price*
Unclassified	Unclassified	95	$3.00

* For sale by the National Technical Information Service, Springfield, Virginia 22151

FOREWORD

This research was conducted under NASA Contract NAS 3-17593 by the Applied Research Division of the Sun Oil Company of Pennsylvania in their laboratory at Marcus Hook, PA. The work was done by Dr. James L. Lauer, Principal Investigator, and by Mr. Melvin E. Peterkin, Research Chemist. The project was managed by the NASA Project Manager, Mr. William R. Jones, Jr., Lubrication Branch, NASA-Lewis Research Center, Cleveland, Ohio 44135.

Because of a failure of our apparatus, the timely execution of the program was made possible only by a generous loan of vital electronic equipment by the Food and Drug Administration, U. S. Department of Health, Education, and Welfare, for which Dr. George W. Yang, its normal user, Mr. David B. Moody, Administrative Officer, and Mr. Carl E. Feight, Chief Associate Commissioner for Administration, deserve special credit. The method used to determine pressure in the diamond cell was adapted from work by Drs. G. J. Piermarini, S. Block, and J. D. Barnett at the National Bureau of Standards. Drs. Piermarini and Block also gave us their personal assistance when needed and supplied us with detailed information of their cell design. Their help is gratefully acknowledged.

Thanks are also due to Dr. Walter P. Siegmund of the American Optical Company, Fiber Optics Division, Southbridge, Massachusetts, for supplying us with a specially constructed fiber optics bundle for use in pressure determinations by the N.B.S. method.

TABLE OF CONTENTS

TABLE OF CONTENTS (continued)

SUMMARY

A program has been initiated to probe the state and composition of fluids in EHD contacts by infrared Fourier transform spectroscopy. This technique is orders of magnitude more sensitive than dispersive infrared absorption spectroscopy and is applicable to the analysis of emissions and reflections. As a first step, absorption and emission spectra have been obtained over the 600-1000 cm^{-1} region for two model fluids contained in a diamond anvil high pressure cell, which simulated an EHD contact in many respects except for shearing motion. The fluids were (a) an ester, pentaerythritol tetraheptanoate, having good lubricating characteristics, and (b) a hydrocarbon polymer fluid having good traction characteristics. Pressures varied from ambient to 2 GN/m^2 (20 kilobars) and temperatures were between 25° and 210°C. These conditions are reasonable to expect in true contacts.

The objective of finding spectral changes with temperature and pressure, attributable to phase and compositional changes, was clearly realized for the hydrocarbon polymer fluid and less so for the ester fluid. Furthermore these changes depended on rates of pressurization and temperature history, factors likely to be of major importance in operating contacts. The principal change is from a liquid to a glass under high pressure. The work has also been successful in demonstrating the applicability of infrared emission spectroscopy to EHD contacts since emission spectra could be obtained from the small fluid volumes contained in a diamond cell and these spectra were found to be equivalent to absorption spectra. Emission spectroscopy is obviously more practical in bearing situations, since only one window and no external source is required. The temperature dependence of certain bands in these emission spectra is also useful (after calibration) as an internal temperature gauge of a fluid -- a highly desirable bonus. However, the study also pointed out limitations of the infrared emission techniques: The fluid temperatures must be well above ambient, but not too high or most characteristic bands become submerged in a blackbody background. For this reason, film thickness and infrared band intensities must be appropriately matched. The spectral region chosen proved to be a good compromise, and its principal features, the CH_2-rocking/twisting mode of hydrocarbon chains and its harmonics, very sensitive to aggregational state and molecular weight. Often spectral features are attributable to steric configurations of molecules, and they can also change with pressure.

The deductions on state could be confirmed by our application of a new procedure developed at the National Bureau of Standards primarily for use as a pressure gauge for fluids in the diamond cell. This technique is based on the pressure sensitivity of the peak frequency of the strongest fluorescence band of ruby at 6942 °A. A small crystal is immersed in the test fluid contained in the diamond cell and its fluorescence spectrum is recorded. As long as the crystal is in a strictly hydrostatic environment, its fluorescence bands are sharp, but when the surrounding fluid becomes glassy, the pressure distribution over the crystal surface causes them to spread out. By recording both peak position and band width, both pressure and state can be obtained.

An EHD test rig to be used in the next phase of this work was designed, which incorporates many of the results of this study, and primarily the method chosen for observing infrared emission spectra with our Fourier interferometer.

1. INTRODUCTION

Infrared spectroscopy is still the most generally used technique to obtain structural information on chemical compounds. The vibrational spectrum of a material is strongly dependent on its molecular structure and phase. Hence the application of infrared spectroscopy to EHD contacts is likely to enhance our knowledge about the state of the fluid there very considerably. However, most work in the past concerned absorption spectra at ambient temperature, since they are relatively easy to obtain and to interpret. As soon as the sample temperature is different from that of the detector, emission of radiation must be considered. With few exceptions, infrared emission has been considered a nuisance to be corrected for, since very few infrared spectrometers can differentiate between absorption and emission and regard emission as a perturbation of the absorption spectrum. To do that, an instrument is required which has the chopper (producing the usual modulated signal) between the source and the sample rather than -- as is usual -- between the sample and the detector. Since EHD contacts are at elevated temperatures, emission or absorption spectra must be separately gathered. Furthermore, it is necessary to obtain spectra of high resolution from very small sample volumes. Here an interferometer is invaluable because its sensitivity is much greater than that of a standard grating spectrometer. In addition, computerized data processing is needed to get spectra sensitive enough to detect the small changes caused by the EHD environment and to permit their interpretation to some degree of confidence.

2. EXPERIMENTAL

2.1 FLUIDS STUDIED

The two fluids used were selected for us by NASA. One of them is a so-called traction fluid manufactured by Sun Oil Company, which will be called the "Sun Fluid" below, and the other is a pure chemical compound, pentaerythritol tetraheptanoate, which will be referred to as the "Ester Fluid". These materials are obviously quite different in their properties, which are shown -- to the extent we determined them here for identification purposes -- in Table I. The pour point of the ester fluid should be noted. Its hysteresis is characteristic of fatty materials undergoing a variety of phase transformations. Standard identification infrared absorption spectra were also run (Figs. 1 and 2). These infrared spectra were, of course, obtained under ambient conditions and in a large absorption cell. They can be compared with those we obtained interferometrically (vide infra) in the high pressure cell over a limited spectral region (Figs. 14 and 23). The tremendous power (much greater detail under very adverse conditions) of the interferometric procedure is immediately apparent.

2.2 HIGH PRESSURE DIAMOND ANVIL CELLS

The high pressure cell with which all the work described in this report was carried out was purchased from High Pressure Diamond Optics. It is a standard cell described in the literature.[1] The high pressure region is contained between two parallel and opposing diamond faces which are forced against each other in a nutcracker-type of arrangement by a spring which, in turn, is compressed by a screw. Solids can be compressed directly between the diamond faces, but liquids must be contained in a hole of a metal gasket sandwiched between the diamonds. For absorption measurements the diamond cell is mounted in a Perkin-Elmer 4X beam condenser placed in the sample compartment of the Fourier interferometer. Resistance wires surrounding the diamonds allow their heating up to 200°C, the temperatures being measured by a thermocouple.

It should be noted that only type II diamonds are sufficiently transparent in the far infrared to permit spectral analysis. These diamonds are also very rugged and the very best heat conductors in existence, their thermal conductivity exceeding that of silver by more than 100%.

TABLE I

Physical and Chemical Properties Determined for Identification

	Ester Fluid	Sun Fluid
Molecular Weight by Vapor Phase Osmometry	585	300
Saponification Number (mg KOH/g)	387.5; 391.8	---
d_4^{20}	0.9816	0.8809
n_C^{20}	1.4530	1.4811
Viscosity (KV)		
100°F	24.77	40.9
210°F	4.49	4.97
Pour	freezes at -30° and will not pour until +30°	
Traction*	0.013	0.053
Percent Aromatics	not detected	~ 3%
Decomposition Temp.** (°C) (isoteniscope)	314	291 (traction component) 266 (VI component)

*By the method of Reference 16

**Stability tests by W. R. Jones, Jr., at NASA

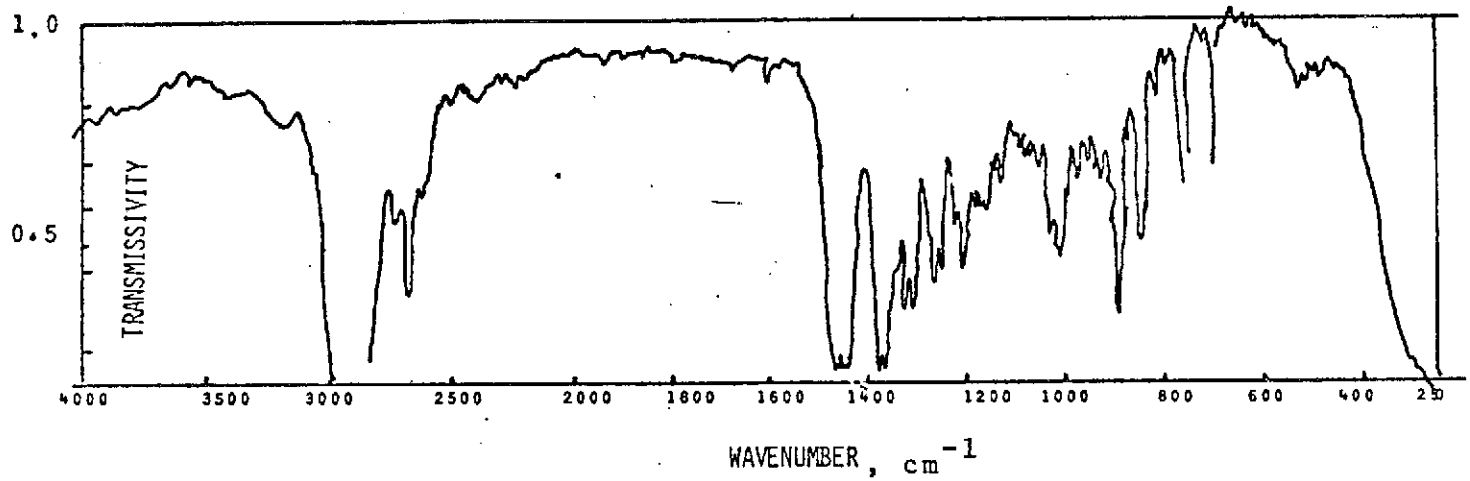

Fig. 1 - Standard Infrared Spectrum of Sun Fluid

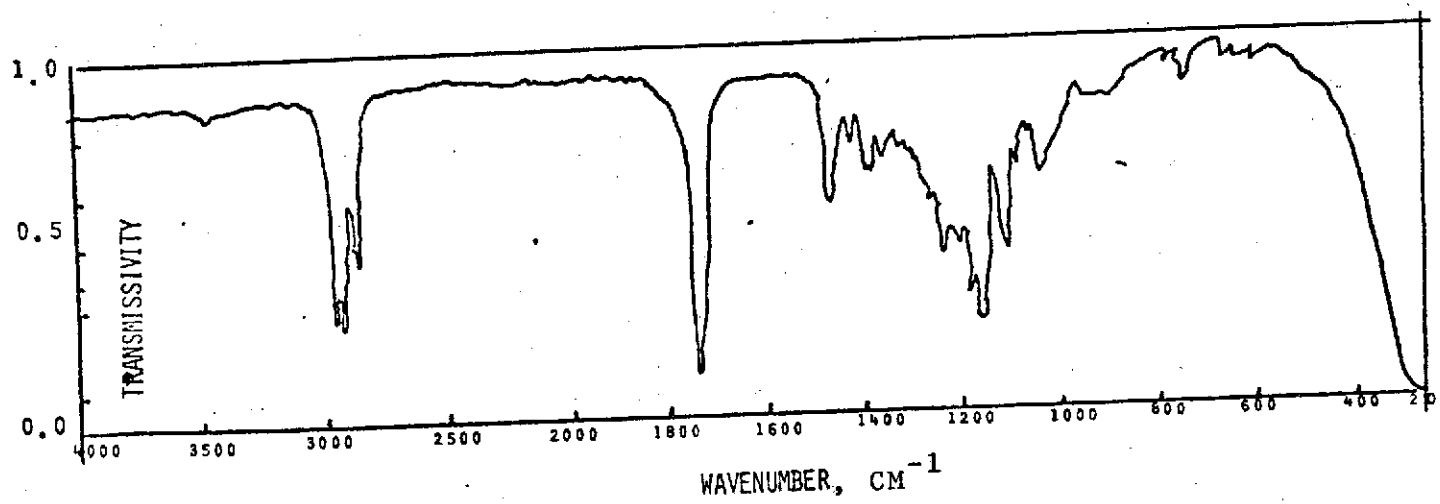

Fig. 2 - Standard Infrared Spectrum of Ester Fluid

The attainable pressures vary with the nature and thickness of the gasket as well as with the common area of the opposing diamond faces. Since the thickness determines the optical path through the sample which should be optimized for a given spectral region as much as possible, the pressure variation is often limited (the gasket must flow to allow the liquid to be compressed). Our diamond faces are about one millimeter in diameter, but the largest gasket hole useable without leakage turned out to be only half that size.

The alignment of the diamond faces in this cell presented some difficulties. The diamonds are set in plaster which needed frequent renewal because the fluids studied leaked into it. Then the faces might not be parallel on remounting. The main virtue of the new cells which were recently constructed for us in our machine-shop are ball-and-socket diamond holders which are automatically centered and easy to align. These cells will make future work much faster for us and allow us to go to much higher pressures. They follow in detail the most recent design of Dr. Piermarini[2] at the National Bureau of Standards.

Inconel gaskets were used throughout, varying in thickness from 125 to 360 micrometers originally (under pressure the thickness may decrease to half these values). They provided optimum optical pathlengths for the 630-930 cm^{-1} wavenumber region on which we concentrated our attention. The thicknesses of the fluid films in an EHD contact region are typically one percent of these values. Spectra from such thin layers will require the usual scale expansions and reductions of noise by appropriate techniques, all of them requiring longer running times of the interferometer. Because of pressure for time, experiments of this nature had to be postponed for these samples. It will also be possible, of course, to select other spectral regions containing more intense infrared bands. Although Inconel gaskets do not work-harden very much, they do to some extent under pressure cycling and then give rise to different fluid pressures for the same number of turns of the screw. In the absence of a proper pressure sensor for most of this work -- a situation that has now been corrected with the construction of an N.B.S. pressure-measuring device based on changes in the ruby fluorescence spectrum (vide infra) --, a calibration of screw turns versus the known freezing pressures of standard fluids (benzene, decane, chloroform) was carried out. It gave us the relationship of 0.15 GN/m^2 (1.5 kilobar) per screw trun, which we used for the work below. New gaskets had to be used for every series of experiments.

In some instances we measured gasket thickness as a function of screw turns (pressure) with the fluids contained in the cell. The hole size was also measured with a microscope and found to be constant. The results of Table II can therefore be interpreted as volume changes of the fluids. They are consistent with Bridgman's results[3] for similar materials.

TABLE II

Gasket Thickness Changes for "Ester Fluid"

Turns of Screw		Hole Size	Gasket Thickness (in mils**)
0			10
2	(∿ 0.3 GN/m^2)	0.5 mm	8.8
8	(∿ 1.2 GN/m^2)	0.5 mm	8.5
16	(∿ 2.4 GN/m^2)	0.5 mm	7.4
leave overnight*			
16	(∿ 2.4 GN/m^2)	0.5 mm	6.9
8	(∿ 1.2 GN/m^2)	0.5 mm	7.5
2	(∿ 0.3 GN/m^2)	0.5 mm	8.0

*note hysteresis, showing the need for a standard operating routine

**1 mil = 25.4 μm

Because of experimental limitations, gasket thickness (which was measured directly with a micrometer screw across the jaws of the "nutcracker") and hole size could only be determined at ambient temperature. Since the spring compressing the jaws of the diamond cell is never heated, it is assumed to exert the same pressure on the gasket regardless of temperature, and the pressure on the fluids is also assumed to remain constant. This assumption may not be true (e.g. the gasket material may flow more readily at higher temperatures and expansion should occur) and will be checked in the near future. However, the errors made by it are considered small.

A number of experiments were carried out to obtain fluid pressures and temperatures from band broadenings and band intensities of probe materials dissolved in small concentrations. An ideal probe material consists of highly symmetric small molecules having strong absorption bands that are not overlapped by those of the fluid under investigation. In this respect chloroform turned out to be most successful, particularly its 665 cm^{-1} band. Figure 3 shows the changes brought about by one percent of chloroform in the Sun Fluid under pressure. Clearly some of the overlapping absorption bands are so severely broadened that they distort the entire spectrum, but the 665 cm^{-1} does appear to be a good indicator. This area will be explored further, especially since it may provide information on viscosity (from the bandshape) as well as on pressure and temperature. Viscosity can be inferred from the broadening of ruby fluorescence bands as illustrated in the following section.

2.3 PRESSURE AND STATE MEASUREMENTS BY THE METHOD OF THE NATIONAL BUREAU OF STANDARDS.

While it is relatively simple to obtain high pressures in condensed phases with the diamond anvil cell, it has been almost impossible to know these pressures accurately. When working with solids no gaskets are needed between diamond anvils and it is possible, for calibration, to substitute for the unknown material a crystal whose color change with pressure is known. Then, of course, the assumption must be made that spring tensions and geometry can be exactly reproduced, which is not an easy task since the pressure varies over the area shared by the two opposing diamond faces. Nevertheless reasonably good estimates of pressure have been made on the basis of various metal-organic complexes that are pressure-sensitive, some shifting visible absorption to the red, some to the blue, of which nickel dimethylglyoxime is an outstanding example. The absorption spectrum in the visible is then used as a pressure-sensitive meter. When liquids are studied under pressure, they must be contained in the hole of a gasket separating the two opposing diamond faces and it has been very difficult to align a small crystal in the liquid space with respect

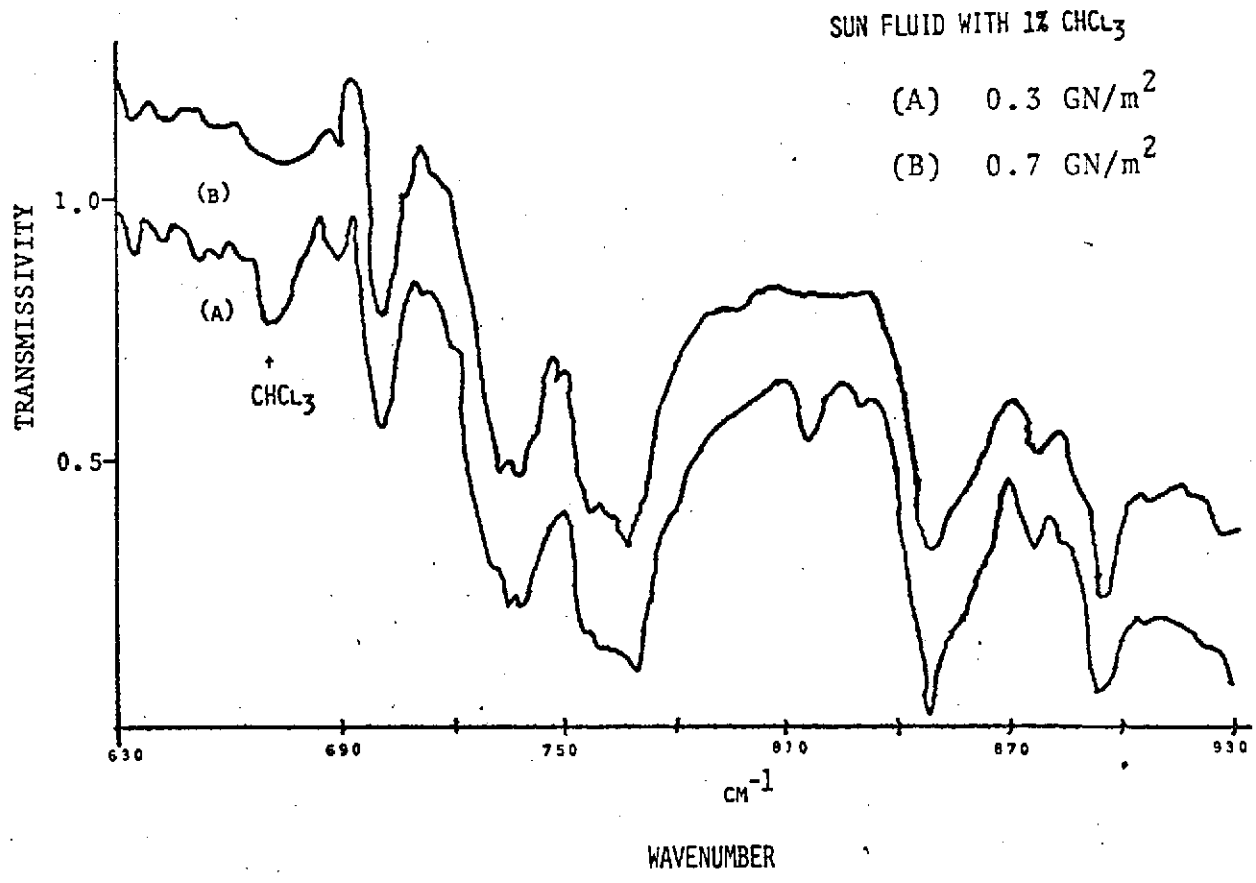

Fig. 3 - Effect of 1% Chloroform on an Infrared Absorption Spectrum at High Pressure; note that all the ordinates of curve (B) are uniformly displace upward by 0.3 units

to the optical path to obtain an absorption spectrum of the crystal. A microspectrophotometer is required, allowing simultaneous visual observation of the crystal and alignment and yet the crystal must remain small enough not to obscure an adequate radiation path through the fluid for its subsequent examination by infrared spectral analysis. Most authors, including ourselves, used some empirical measure of pressure, such as the number of turns of the screw compressing the spring acting on the anvils and then correlated the number of turns with spring tension and geometry and with known freezing pressures of standard substances. This procedure requires not only reproducibility of the spring tension and alignment of a gasket hole on the diamond faces, but of the compression of both liquid and gasket. Unfortunately most metals do work-harden, even Inconel, so that the results of this type of calibration can be in considerable error.

In a few articles that appeared recently, Piermarini[4] and his colleagues described a method ideally designed for the determination of the pressure in fluids contained in the diamond cell. A small inorganic fluorescent crystal, of which ruby (alumina containing a trace of chromium ion) is an outstanding example, is placed with the fluid into the sample space and the fluorescence emanating from it is examined. Usually the fluid does not itself fluoresce, at least not in the region where ruby does. The crystal is unreactive and insoluble in the liquid and small enough not to interfere with its observation by visual and infrared spectroscopy. Under high pressure the frequencies of the fluorescence bands of the crystal shift toward the red by small amounts (in terms of wavelength by $+0.0365A°/GN/m^2$). They also shift with temperature (by $+0.068A°/°C$) but temperature can be separately measured by a fine thermocouple attached to the gasket. To obtain the resolution required to measure pressure within ± 0.05 GN/m^2 or better, Piermarini and coworkers are using an echelle grating spectrometer. They also are using a microscope coupled to a TV-pickup, which enables them to zero in on a particular spot in the sample cavity where a ruby crystal is located. Other workers have adapted the N.B.S. system and modified it to suit their need, e.g. Drs. Ben Welber and Max Brotsky at IBM's Yorktown Heights Research Center have been using a high intensity laser source for the N.B.S. mercury arc, which has enabled them to substitute a modest grating monochromator for the N.B.S. echelle, and Dr. Holzapfel of the Max Planck Institute für Festkörperforschung in Stuttgart, Germany, has been experimenting with a Fabry-Perot interferometer.

Our own version of the National Bureau of Standards (N.B.S.) method is the most modest of all and is shown in Fig. 4. Radiation from a high intensity zirconium arc is filtered by a blue filter and condensed on the sample space of a diamond cell. The fluorescence excited in a ruby crystal in the cell is then picked up by a light fiber bundle of circular cross-section at one end and rectangular cross-section at the other, so as to transfer most of the radiation from the cell into the slit of a grating monochromator. This light fiber bundle was especially constructed for us by Dr. Siegmund of the American Optical Company's Fiber Division at

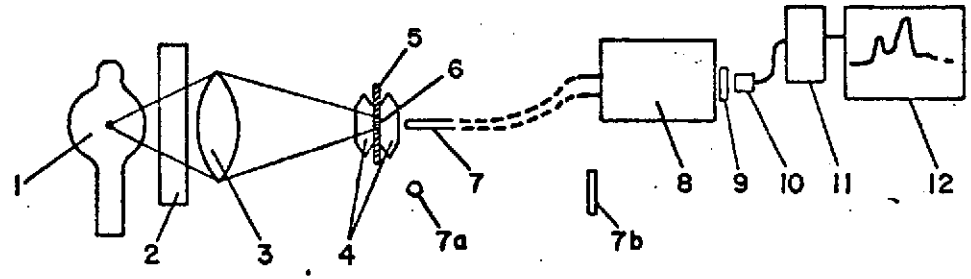

1. ZIRCONIUM ARC
2. $CuSO_4$ FILTER
3. LENS
4. DIAMOND ANVILS
5. GASKET
6. FLUID SAMPLE
7. LIGHT FIBER BAND
   - 7a. CROSS SECTION AT ANVIL
   - 7b. CROSS SECTION AT SLIT
8. GRATING MONOCHROMATOR WITH SCANNING DRIVE
9. INTERFERENCE FILTER
10. PHOTOMULTIPLIER DETECTOR
11. HIGH IMPEDANCE ELECTROMETER
12. STRIP CHART RECORDER

Fig. 4 - Apparatus to Measure Pressure in The Diamond Anvil Cell

Southbridge, Massachusetts, and it turned out to be essential to the success of our device. Because the individual optical fibers of this bundle are much thinner than those normally obtainable and arranged in perfect order, the resolution and the intensity of the fluorescence spectrum were much improved over our own previous achievements. Our grating monochromator is a Bausch and Lomb 500 mm focal length instrument, provided with a 102 mm grating containing 600 grooves per millimeter. We added a slow constant speed scanning drive and a photomultiplier detector (an RCA C31034 end-on tube). In front of the photomultiplier we placed a narrow bandwidth (100A°) filter centered about the 6942A° ruby line to eliminate all the stray light generated by the intense blue exciting radiation. The photomultiplier current is then conducted to a Keithley Model 602 High Impedance Electrometer and finally recorded on a standard strip chart recorder. In general, our currents have been of the order of 10^{-10} amperes. Two blips are introduced into the circuitry by the drive at exactly reproducible positions on the wavelength scale. They serve as markers.

An example of a pressure/fluorescence measurement is shown in Fig. 5. The displacement corresponding to a pressure change of .2 GN/m^2 is clearly noticeable.

The N.B.S. procedure may provide not only a pressure, but a measure of the state of the medium surrounding an immersed ruby crystal as well. For, as Piermarini already has pointed out, as long as the crystal finds itself in a truly hydrostatic environment, the width of a fluorescence band is at a minimum. When the viscosity of the surrounding medium is high compared to the time scale of a measurement, e.g. when the surrounding medium is glassy, the crystal is subjected to different pressure gradients in different directions and the width of a fluorescence band is naturally greater. This observation is of considerable importance in our work. Fig. 6 shows a series of such observations. When the pressure is increased from 0.1 to 0.5 GN/m^2 (1-5 kilobar) (as determined from the ruby fluorescence band positions) the bandwidth of the stronger fluorescence band (R-1) is hardly changed, indicating that the medium (here the Sun fluid at ambient temperature) was still liquid. Between 0.5 and 0.6 GN/m^2 (5-6 kilobar) of pressure a sharp change of width occurred (indicating formation of a highly viscous material and confirming a deduction from changes in the infrared absorption spectra). The next measurement at 1 GN/m^2 (10 kilobar) of pressure was made a little time after the pressure increase (about 20 minutes or so) and it is likely that the width observed was not the maximum, for after standing overnight the width had decreased to nearly the original one. We believe that the fluid here, i.e. the Sun fluid, had reached a very high viscosity at this pressure, so that it took several hours to equilibrate. This work is only at a very early stage; it will be expanded and calibrations will be carried out to enable us to measure viscosity at high pressures by the N.B.S. method.

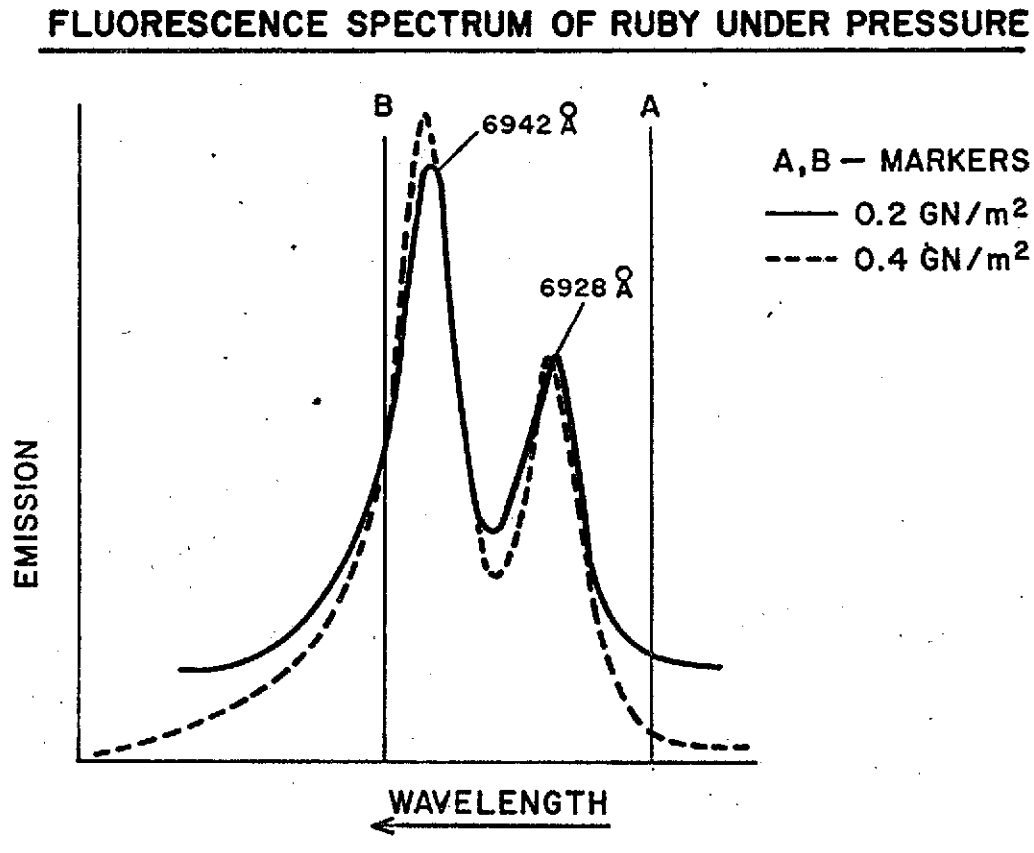

Fig. 5 - Pressure Dependence of Ruby Fluorescence

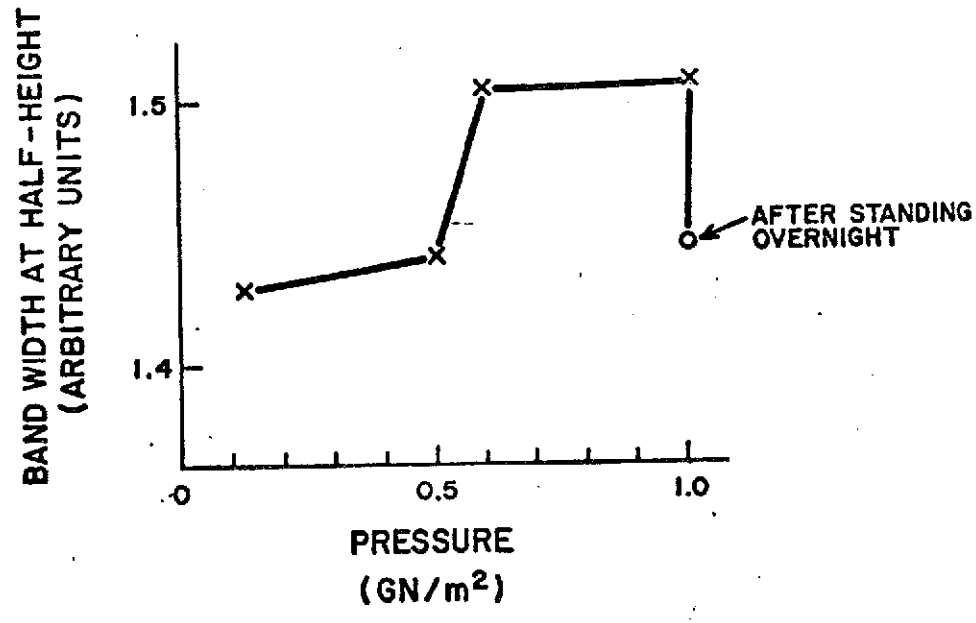

Fig. 6 - Bandwidth of Ruby R-1 Fluorescence Band as a Function of Pressure in Surrounding Sun Fluid

At this stage our main use of the N.B.S. method has been in the calibration of the diamond cell screw for pressures with different gaskets. An example is shown in Fig. 7. As the gasket compression under the force of the spring is not instantaneous, the pressure changes with time as indicated by the two different curves. As expected, these changes are less at higher pressures. The calibration curve is obviously not linear over the entire pressure range studied. Most of the work reported in this report still gives the pressure in screw turns, for our version of the N.B.S. method was not developed until rather recently. We will use it exclusively in our future program.

2.4 INFRARED ABSORPTION SPECTRA FROM THE DIAMOND CELL

Our interferometer is an RIIC Model FS-720 Far Infrared Interferometer, which we had previously modified to extend its range from the 400 cm^{-1} upper frequency limit to about 1100 cm^{-1}. Since the modification was described in some of our recent publications[5], it will not be detailed here. Indeed, for various reasons described below, the spectral region of 630 cm^{-1} to 930 cm^{-1} (occasionally to 1050 cm^{-1}) turned out to be the most useful one for this work. After some exploratory runs, it became clear that band shifts of about 1 cm^{-1} had to be clearly detectable above the noise level -- a difficult task in view of the small amount of radiant energy passed through the sample. Accordingly, a standard operating procedure was developed in which four times as many points were sampled as theoretically necessary for the spectral resolution required and the excess points were used to remove noise by mathematical filtering and smoothing procedures. Since the time required per spectrum was thereby brought to about two hours, care had to be exercised to insure constancy of temperature and other conditions over this period. The resulting spectra were calculated for separations of 0.61 cm^{-1} and were found to reproduce well within ± 1.22 cm^{-1}, as can be seen from the empty cell background spectra of Fig. 8, which were run at different temperatures. These spectra also show that there was no appreciable change of detector sensitivity as a function of cell temperature. Nevertheless, for purposes of consistency, all the fluid spectra were ratioed to the empty cell spectra at the same temperature. All fluid spectra were recorded both as plots of transmissivity versus wavenumber (ratioed plots) by an automated plotter taking data from computer files and as numerical tabulations on IBM output sheets (of course, the empty cell spectra had to be "single-beam", i.e. unratioed plots of detector signal versus wavenumber).

The optical path lengths in the diamond cell were chosen experimentally to provide good spectra over the chosen region; the ester fluid, being polar, was found to absorb more strongly than the hydrocarbon Sun fluid. Because of this variation all spectra were plotted in a "normalized form", i.e. expanded or contracted to range over the same amplitudes. We believe all spectra are there-

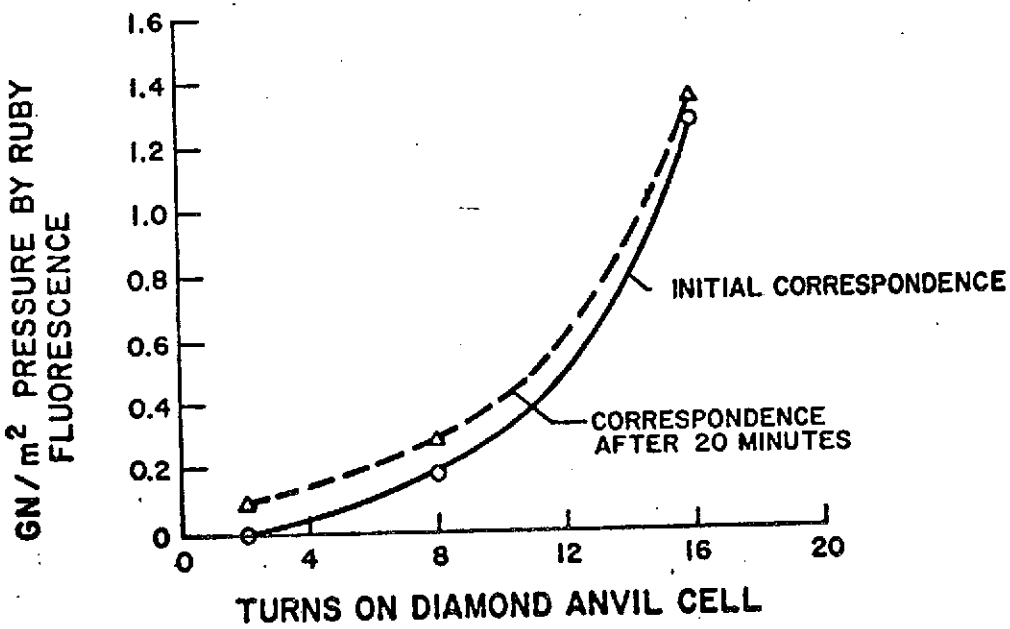

Fig. 7 - Calibration of a Diamond Cell Gasket by the National Bureau of Standards Method

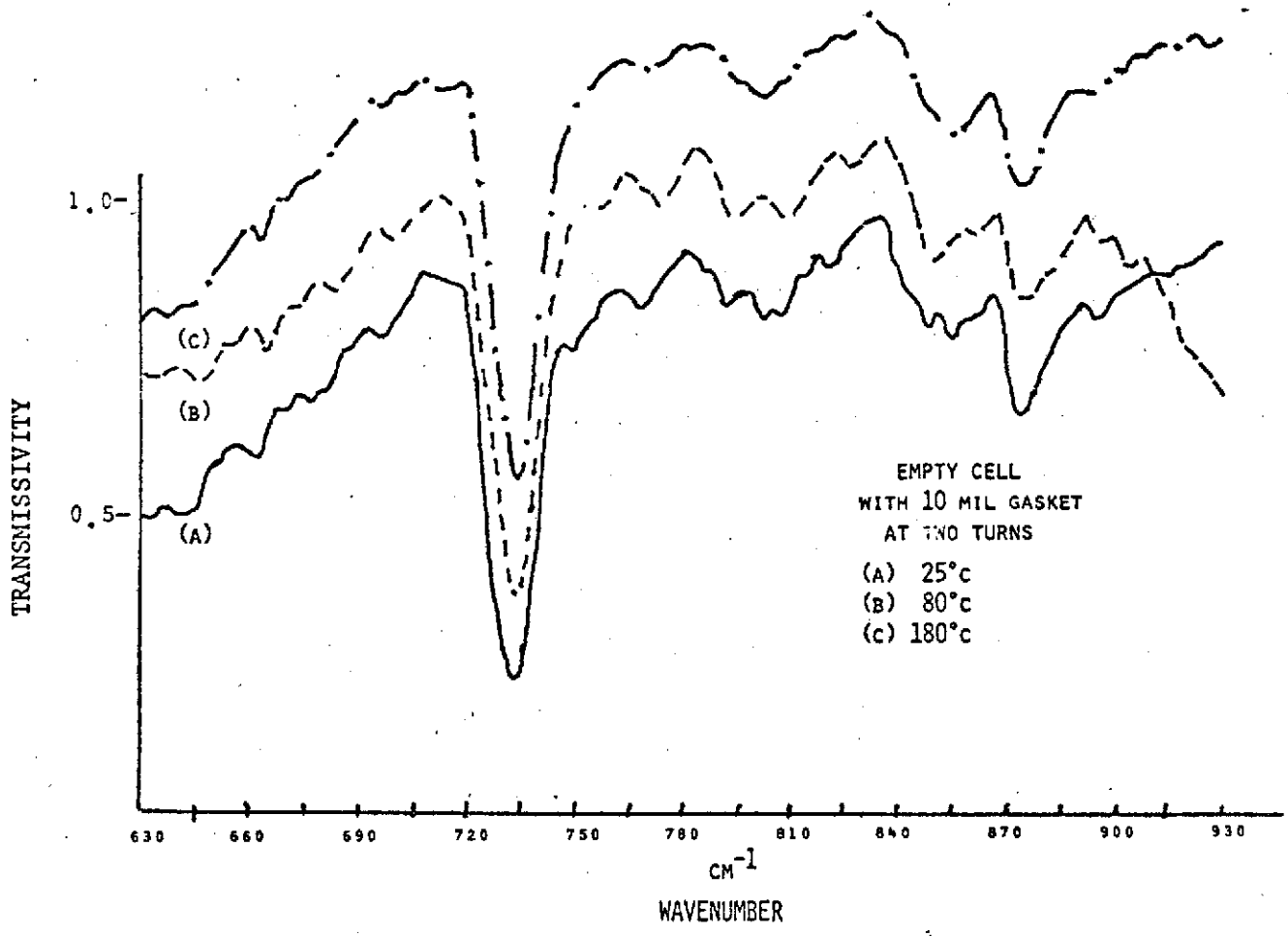

Fig. 8 - Empty Diamond Cell Spectra at Different Temperatures (Note that the ordinates of curves (B) and (C) are uniformly displaced upward by 0.2 and 0.4 units respectively)

fore comparable. It should be noted that since the spectra were drawn from computer files, it is an easy matter to change scales, or to draw several spectra exactly superimposed on the same plot.

Since degassed samples were tightly sealed into the diamond cell, oxidative degradation is excluded. Decomposition temperatures, measured by W. R. Jones, Jr. at NASA, lie considerably above all our temperatures. Since, furthermore, the spectral changes observed to occur with pressure and temperature changes were found to be reversible in every instance explored, chemical degradation over the course of an experiment (about 30 minutes at elevated temperatures) appears unlikely.

2.5 INFRARED EMISSION BANDS OF LIQUIDS

Several references exist in the literature, showing that infrared emission spectra are similar to absorption spectra and in principle, more easily obtained. The sensitivity of a Fourier spectrometer is often sufficient to measure emission from fluids in the infrared even when the temperature difference between the fluid and the reference is only 50°C, as for example Low[6] and Griffith[7] have shown. Indeed these authors obtained some very respectable spectra under such conditions. Griffith pointed out that the thickness of the fluid layer played an important role with respect to the quality of the spectra, thinner layers giving generally sharper bands. These bands appear to be located on top of generally black body type emission.

To detect infrared spectral features of fluids in simulated bearing contacts, the emission technique is obviously easier to apply than the absorption technique since only the radiation coming through one window must be analyzed. It would be rather difficult to pass radiation through the bearing surfaces and the oil, although significant reflection techniques can be visualized and reflection may be tried in our further work as a viable alternative to emission. A simple mathematical analysis of the radiation emanating from the fluid layer in a bearing through a window is evidently helpful to an understanding of the factors involved and will now be outlined.

The problem has been reduced to the simplest terms -- a more refined analysis will be undertaken later -- as illustrated in Fig. 9. We consider a homogeneously emitting fluid layer bounded by parallel walls, one being represented by a perfectly transparent window and the other by a perfectly reflecting metal. This model, analogous to McMahon's[8] for a slab of a glass, approximates the situation of a simulated EHD contact, e.g. the rotating ball sliding by a window in a stationary plate, which we will be using in future experiments.

Let $p(\omega,t)$ be the radiant power per unit volume in the wavenumber region ω to $\omega + d\omega$ at temperature t, $k(\omega,t)$ be the absorption coefficient at that wavenumber and temperature, and x the distance from the layer to the boundary. The emitted radiation from the fluid and arriving at the window/liquid boundary (and normal to it)

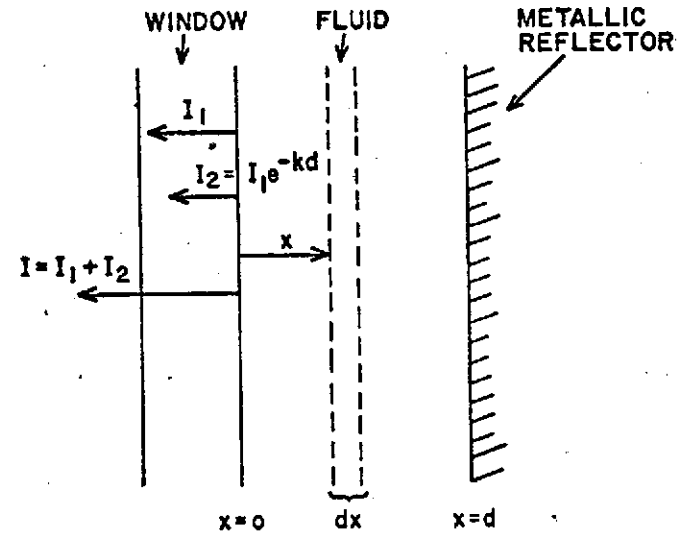

Fig. 9 - Fluid Layer Emitting Infrared Radiation

from a fluid layer dx will be proportional to

$$p(\omega,t)e^{-k(\omega,t)x} \tag{1}$$

The intensity from the entire layer arriving at that boundary without reflection will be

$$I_1 = \int_o^d pe^{-kx}\,dx = \frac{p}{k}(1-e^{-kd}) \tag{2}$$

An underlying assumption is that radiation absorbed is not reradiated. An equal flux of radiation is emitted in the opposite direction and reflected by the metal surface. The intensity of this radiation, at the fluid/window interface will be

$$I_2 = I_1 e^{-kd} = \frac{p}{k}(1-e^{-kd})e^{-kd} \tag{3}$$

Thus the total emission arriving at the fluid/window interface, all of which is assumed to be perpendicular to it, will be

$$I = I_1 + I_2 = \frac{p}{k}(1-e^{-kd})(1+e^{-kd}) = \frac{p}{k}(1-e^{-2kd}) \tag{4}$$

If kd is large, the layer becomes opaque and the intensity of its emitted radiation approaches that of a black body. Hence,

$$\frac{p}{k} = cR_b \tag{5}$$

where $R_b(\omega,t)$ is the emissive power of a black body for the same wavenumber ω and temperature t and c is a constant dependent on the apparatus. Accordingly,

$$I = cR_b\,(1-e^{-2kd}) \tag{6}$$

If we neglect reflection losses at the window, then this expression is proportional to the radiation flux that can be detected after its passage through the window. Therefore, in that case, multiple reflections are also neglected.

In terms of transmissivity

$$T = e^{-kd} \tag{7}$$

equation (6) becomes

$$I = cR_b \ (1-T^2)$$

$$(I = I(\omega,t);\ T = T(\omega,t)) \tag{8}$$

Though drastically simplified, equation (8) contains some very important results:

(a) The emission can never exceed that of a blackbody over the same frequency range and at the same temperature. Actually this result has been implied in the original assumptions.

(b) The emissivity is expressed by the factor $(1-T^2)$, which is a function of both wavenumber and temperature since the transmissivity is both temperature and wavenumber-dependent.

(c) The square of the transmissivity occurs in Eq. (8) instead of the first power, because of the reflection from the metallic surface (cf. Eq. (2) with Eq. (8)). Effectively the optical path through the absorbing layer has been doubled and Eq. (8) is basically a statement of Kirchhoff's law.

(d) Emission spectra of good quality require optical thicknesses that are half those used in absorption or, in any case, that are equivalent to those of absorption. This generalization applies, of course, only to low temperature/condensed phase spectra. When the layer thickness is excessive, the transmissivity over the region of an absorption band is very low, and the spectra are poor. In general, the transmissivity of a band peak should be 0.25 to 0.35 for good quality. Since most lubricants have absorption bands in the 10 - 15μm region (600-1000

cm^{-1}) that require optical pathlengths of about 0.015mm to meet this criterion, emission spectra under the conditions discussed would require pathlengths of about 0.008 mm or about 10 micrometers. Long electronic time constants and scale expansion have enabled the molecular spectroscopist to obtain good quality absorption spectra for optical pathlengths of 10% and even 1% of the optimum or, equivalently, for the same pathlength, to obtain such spectra at 1 - 10% dilution in a transparent solvent. Thus the achievement of good emission spectra from layers only $\sim$ 1.0 micrometers thick -- as reported by Griffith -- is not surprising. The thickness of fluid film layers in EHD contacts has been estimated at 0.1 - 1.0 micrometers under severe loads. Accordingly the emission technique is applicable to the obtaining of infrared spectra in EHD contacts, using present technology, but it will require very careful experimentation.

(e) The black-body emissive power, R_b, varies with temperature according to Planck's law. Near ambient temperature ($\sim$ 300°K), R_b has its maximum near 1000 cm^{-1}. The emission spectrum near that wavenumber will be most intense.

Of course, experimentally a temperature difference between sample and reference is required, so that samples at ambient temperature require cooled references.

From equation (8) and suitable calibration data to evaluate the constants, a transmissivity and an absorption coefficient can be derived as a function of wavenumber. At reasonably low temperatures, such as those expected to prevail in EHD contacts, an emission spectrum can supply the same information as an absorption spectrum for the assumptions specified.

The assumptions made in the foregoing derivation are, as pointed out, very drastic. The diamond window used in this work is certainly not non-reflecting and the metal surface not perfectly reflecting. From separate determinations of reflectivity as a function of wavenumber spectra of better quality could be obtained by computation. Indeed Aronson[9] has shown that the reflectivity changes over an absorption band can be very significant. Our present work does not take reflectivity changes into account, but work is planned for the future, which will enable us to do so.

2.6 DETERMINATION OF INFRARED EMISSIONS

2.6.1 Emissions from Fluids in a Standard Cell at Ambient Pressure

For this work a heated cell of large sample area was used, such as the Beckman-RIIC No. FH-01. Since the amount of infrared energy radiated by the sample was therefore relatively large, our Perkin-

Elmer Model 221 grating spectrophotometer was adequate for this work and it was unnecessary to use the more sensitive -- and more cumbersome -- interferometer.* The sample was sandwiched between sodium chloride plates and the surrounding housing was water-cooled so as not to affect the spectrometer slits in front of which the cell was attached. The cell was placed in the reference beam of the spectrometer and the attenuated radiation from a Nernst glower operated at the lowest possible temperature constituted the sample beam. Known attenuation was achieved by calibrated screens. In this way emission bands looked like absorption bands under usual operating procedures and one adjustment kept the entire spectrum on the scale of the recorder. In addition to the sample runs, identical runs were made with the empty cell and with the cell containing a "black (or gray) body" (oxidized copper) at the same temperature. As shown below, these extra runs made it possible to remove extraneous contributions from the apparent emission spectra of the sample fluid itself.

It should be noted that one very important reason for the much greater difficulty in obtaining emission spectra from fluids as compared with absorption spectra is the contribution of extraneous radiation. When an absorption spectrum is run, only the sample and windows are transparent enough to pass radiation so that the spectrometer record represents the spectrum of the sample (absorption by the windows is generally negligible). However, when an infrared emission spectrum is run on a liquid sample -- which must necessarily be contained in a sample cell - the heated cell body, the spacer or gasket keeping the fluid sandwiched between the window plates and even dust on the windows, particulate matter in the fluid, and the cell body itself will also radiate and dilute the primary spectrum. Discrimination between the sample spectrum and the background spectrum is vital. When the sample is spread over a relatively large area, i.e., an area greater than that accepted by the spectrometer (as was the case here), the background contributions are small and it was possible to reduce them sufficiently by the following computational procedure:

Suppose spectrometer readings on the "Percent Transmission" scale are respectively R_S, R_C, and R_B, for the cell containing the fluid sample, air (empty cell), and gray body, under otherwise identical conditions of temperature, location, Nernst glower reference, etc. The corresponding attenuation factors of the screens used in the sample path for the Nernst glower are F_S, F_C, and F_B.

---

*The procedure used is analogous to that of Fabbri and Baraldi[10]

The three runs give these data:

$$R_S = E_N F_S / (E_C + E_S) \tag{1}$$

$$R_C = E_N F_C / E_C \tag{2}$$

$$R_B = E_N F_B / (E_B + E_C) \tag{3}$$

where E_N, E_S, E_C, and E_B are respectively the emissions from the Nernst glower, the fluid sample, the empty cell, and the gray or black body, as seen by the spectrometer detector. E_B was assumed known from Planck's equation except for a constant factor independent of wavenumber (gray body). No corrections for reflectivities were made at this stage of the work; they will be the subject of later refinement. Algebraic manipulations of these equations lead to

$$E_S = E_B \cdot \frac{R_S F_C R_B - F_S R_C R_B}{R_S F_C R_B - R_. R_C F_B} \tag{4}$$

In practice R_C turned out to be very small compared to the other readings over the spectral region of interest. In that case (from Equation (1) and (3))

$$E_S = E_B \cdot \frac{F_B R_S}{F_S R_B} \tag{5}$$

The emissivity is given by

$$\varepsilon(\omega,t) = E_S/E_B \cdot \text{constant} \tag{6}$$

and it is the significant spectral parameter. By Kirchhoff's law, ε relates to the absorption coefficient $k = k(\omega)$. Computer programs were developed to plot spectra according to equations (4), (5), and

(6). E_B, the blackbody emission, or a quantity proportional to it, is known from Planck's equation as

$$E_B = \frac{2C_1}{\lambda^5} \cdot \frac{1}{(e^{\frac{C_2}{\lambda T}} - 1)} \qquad (7)$$

Here $C_1 = C_o^2 h = 5.953 \times 10^{-17}$ Wm^2, is the first radiation constant, and $C_2 = C_o h/k = 0.01438$ m°K, is the second radiation constant (C_o is the velocity of light in vacuo, h is Planck's constant, k is Boltzmann's, and λ is the wavelength).

2.6.2 Emissions from Fluids in the Diamond Cell at Elevated Pressures

The small window area of the diamond cell, which is an unavoidable consequence of the high pressures achievable, makes infrared emission spectroscopy orders of magnitude more difficult than in the case just discussed. Here, of course, the more sensitive interferometer (our RIIC FS-720) is the instrument to use. But it had never been used in this manner before. We anticipated difficulties and we knew that we were entering a terra incognita in almost every respect, but it turned out to be much harder than expected.

While the instrumental modifications and the construction of auxiliary apparatus were undertaken as part of our basic research contract with the Air Force Office of Scientific Research, a description of them will be given here, since they had to precede the gathering of spectral information and represent necessary background. Fig. 10 illustrates the adapter built for emission measurements with the diamond anvil cell. Since this cell simulates an EHD contact in many ways (except for movement, of course), the volume of fluid emitting radiation is a fraction of that contained in the eye of a small needle and our task can be appreciated in terms of trying to accomplish a spectral analysis of the radiation from this volume, barely more than 100°C above the temperature of the detector, and effectively six feet away from it! Furthermore the sample volume is surrounded by much larger metal gasket, which is itself radiating over the same spectral region. Because these aspects were foreseen, the adapter was designed with a number of alignment capabilities. Vital to them is the use of visual light. As shown in Fig. 10, a projection lamp can be mounted above the diamond cell to illuminate the fluid volume and since both the auxiliary optics and the interferometer optics are entirely reflecting, the locations of visual images are also the locations of the infrared images formed by the infrared radiation of the fluid volume. (When the "real" EHD contact will be studied in the next phase of our program, the convenience of straight-through illumination of the

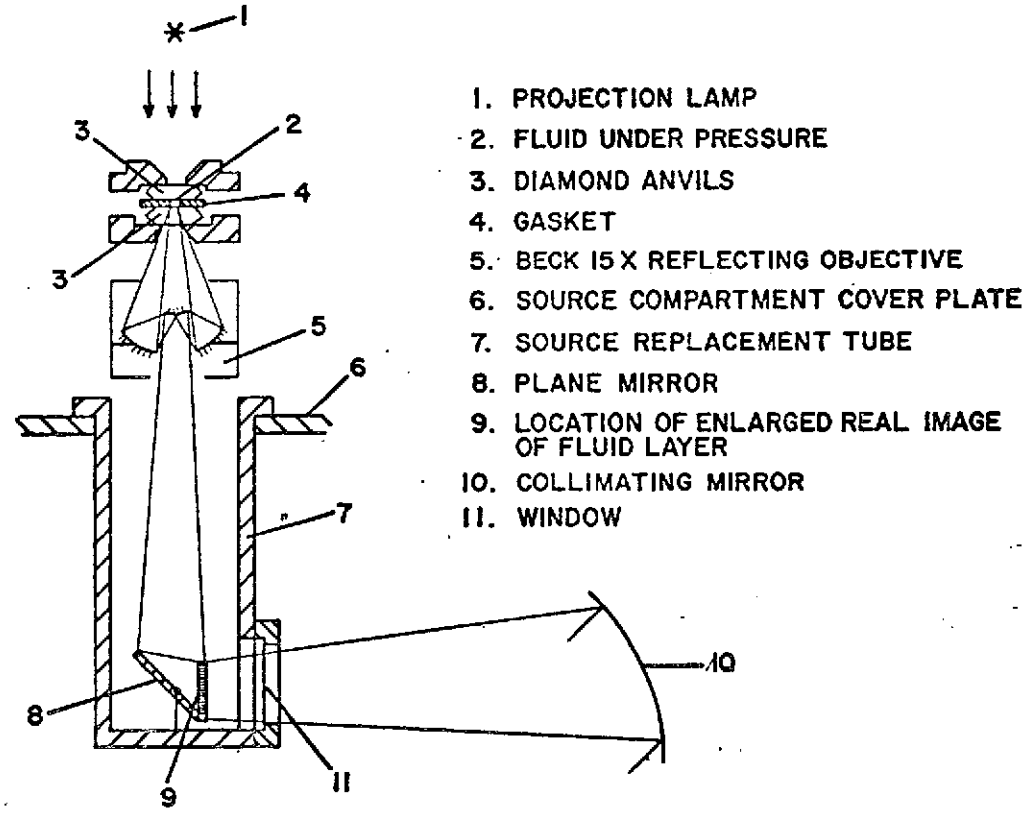

Fig. 10 - Adapter for Obtaining Infrared Emission Spectra from a Diamond Anvil Cell, Using an RIIC FS-720 Far Infrared Interferometer.

sample volume by visible light will be absent and reflected light will have to be employed.) Below the diamond cell a Beck 15X reflecting objective "lens" is placed, whose function is to form an enlarged real image of the sample at the exact location at which the mercury source lamp of the interferometer is normally placed for infrared absorption work. The plane mirror 8 at 45° angle with the vertical causes the image to be formed in a vertical plane. From there on the interferometer optics function in the normal way as shown in Fig. 11. The new source, i.e., the image of the heated fluid contained in the diamond cell, is collimated by the off-axis paraboloidal mirror 3, passed through the interferometer section 4, 5, 6 and is reconstituted in the form of the real image 12 in the so-called sample compartment (here a sample is placed for absorption measurements). After that the radiation is trapped by the cone condenser 10 and brought onto the Golay detector 11.

The availability of real images in locations 1 and 9 (Fig. 11), which can be seen makes the critical alignment possible. Image 1 must have the proper phase relationship with respect to the chopper 2, since the Golay detector and amplifier measure effectively the difference in temperature between the source and the chopper blade at ambient temperature. Both image 1, but especially image 2 must be masked to prevent most of the radiation from the gasket surrounding the sample from impinging onto the detector. Furthermore, when the visual image of the hole in the gasket between the diamonds is sharp at location 9, the interferometer section is properly aligned. Last but not least, the enlarged visual image of the sample volume makes it possible to recognize contamination in the fluid, a leaky gasket (gas bubbles), and other untoward circumstances that could cause spurious results, if allowed to go on unnoticed.

An important feature of the design of the adapter for emission measurements with the interferometer is its ready exchange for the conventional arc source. All the new accessories are mounted on a new cover plate of the source compartment; to return to the arc source this plate is removed with all its parts in one operation and the arc and the old cover plate are fastened -- no new alignment is needed and the whole operation can be accomplished in less than half an hour. The cylinder 7 (Fig. 10) dipping into the source compartment and holding mirror 8 is provided with window 11, so that a vacuum can be maintained in the rest of the instrument. It is often necessary to run the instrument under vacuum to avoid contamination of spectra by water vapor.

In contrast to the grating spectrometer used to obtain emission spectra from heated fluids at ambient pressure, the interferometer that had to be used with the diamond cell, is single-beam, i.e., not ratio-recording. As mentioned before, the detector signals are proportional to the difference between the radiation emitted by the sample and that emitted by the chopper blade, which was kept at ambient temperature. Furthermore it was inconvenient to place a black body (or even a gray body) into the diamond cell in a

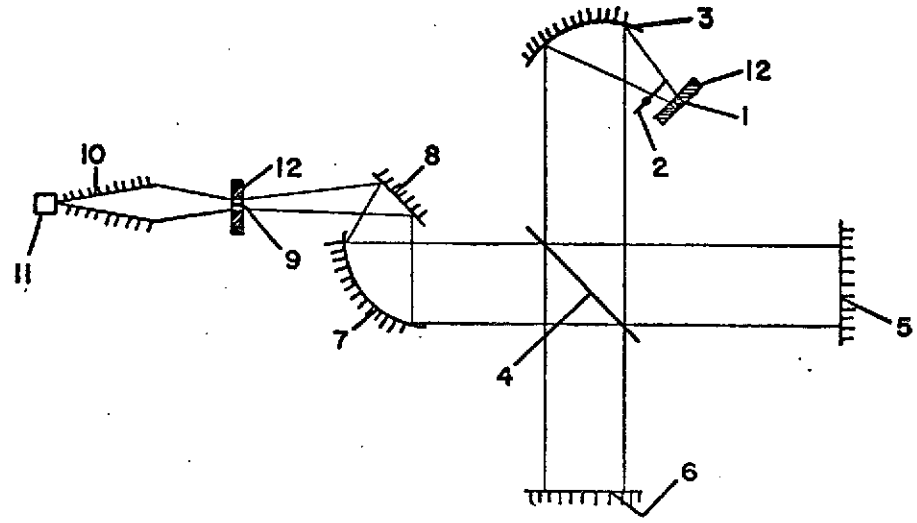

1. SOURCE OR IMAGE OF FLUID LAYER EMITTING RADIATION
2. CHOPPER
3. COLLIMATING MIRROR
4. BEAM SPLITTER
5. SCANNING MIRROR
6. STATIONARY MIRROR
7. CONDENSING MIRROR
8. FLAT MIRROR
9. REAL IMAGE OF SOURCE OR ENLARGED OF FLUID LAYER EMITTING RADIATION
10. RADIATION CONDENSING CONE
11. GOLAY DETECTOR
12. MASK

Fig. 11 - Interferometer Schematics

reproducible position and a separate black body (approximated by a cartridge heater in a blackened housing) had to be run. (A standard black body, in the form of a calibrated hollow cylinder, will be substituted for this makeshift at a later time.) These factors and the appreciable contribution of gray radiators from the cell itself made it necessary to apply a procedure for the reduction of the data from the diamond cell, which was quite different from that described earlier for the standard cell.

The detector signal at a given wavelength λ, when the cell is in place and containing fluid at temperature T_S is given by

$$S_S = K\epsilon_\lambda \, [E(T_S) - E(T_C)] \tag{1}$$

where K is the responsivity of the detector, ϵ_λ the spectral emissivity of the fluid sample, and $E(T_S)$ and $E(T_C)$ are respectively the blackbody radiations (or gray body radiations proportional to them) at the sample and chopper temperatures. When the sample cell is replaced by our black body reference (now the cartridge heater), the signal is

$$S_B = K[E(T_B) - E(T_C)] \tag{2}$$

Combining equations (1) and (2) gives for the spectral emissivity

$$\epsilon_\lambda = \frac{S_S(E(T_B) - E(T_C))}{S_B(E(T_S) - E(T_C))} \tag{3}$$

To facilitate the analysis the black body runs were made at the same temperatures as the sample runs. Under these conditions

$$\epsilon_\lambda = \frac{S_S}{S_B} \tag{4}$$

The factor marring this apparent simplicity is the very appreciable contribution of background radiation from other parts of the cell. Accordingly the detector signal S_S is not just due to the fluid itself, but both to the fluid and the background coming from the gas-

ket and other parts of the cell. Denoting this background (another gray body) by S_G, equations (3) and (4) must be modified by the substitution

$$S_S = S_F + S_G \tag{5}$$

giving

$$\varepsilon_\lambda = \frac{(S_S - S_G)G_B(E(T_B) - E(T_C))}{S_B G_S (E(T_S) - E(T_C))} \tag{6}$$

(S_F is the signal caused by the emission of the fluid alone), or for blackbody runs at the same temperatures as the sample runs

$$\varepsilon_\lambda = \frac{(S_S - S_G)G_B}{S_B G_S} \tag{7}$$

where the gains, G_S and G_B for sample and blackbody runs respectively, have been introduced.

Since the emissivity of a transparent sample is a function of the thickness, one might do better by calculating the absorption coefficient which is an intrinsic property of the material. This can be done with the help of McMahon's relation[8]

$$\varepsilon = \frac{(1-R)\ (1-T)}{1-RT} \tag{9}$$

where

$$T = e^{-kt} \text{ or } e^{-2kt} \tag{10}$$

depending on whether one measures the thickness of the fluid layer,

t, or the optical path, 2t, when reflection from the metal surface in back of the fluid layer plays a role. If the reflectivity, R, is neglected,

$$\epsilon = 1-T = 1-e^{-2kt}$$

$$\text{or} \quad 2kt = -\ln (1-\epsilon) \tag{11}$$

from which k can be computed. However, neglect of R is not properly justified and it is preferable to obtain refractive index data or reflection data separately. For normal incidence reflectivity and refractive index are related by the Fresnel equation

$$R = \frac{(n-1)^2}{(n+1)^2} \tag{12}$$

3. RESULTS

3.1 HIGH PRESSURE ABSORPTION SPECTRA OF THE "ESTER" (PENTAERYTHRITOL TETRAHEPTANOATE, abbreviated as PETH)

3.1.1 Early Experiments

The Contract called for spectra at three temperatures for each of three pressures. Very early in our work the need for standardization of the sequence grew very important, especially with the ester fluid, but with the Sun fluid as well. For example, Fig. 12 shows single beam (not ratioed) absorption spectra of the ester at a pressure of about 2 GN/m^2 (14 turns). As the temperature was increased from 25 to 80°C, the position of the main bands near 725 cm^{-1} and 765 cm^{-1} remained about the same. When the 80°C run was repeated, the band peaks had shifted toward higher frequencies and they remained so even at 180°C. Then, however, the band intensities had greatly weakened, indicating that the material was probably liquid. The second 80°C sample could have been partly liquid or another solid modification (the first two runs were very likely solid or glassy, judging from the sharp band structures and the band intensities). It should be noted that the sample was brought to the high pressure rather quickly. When the temperature cycle was reversed, i.e. the fluid was still brought to pressure rather quickly, the spectra of Fig. 13 were obtained. Here the temperature could only be dropped to 35° in one day (35°C was believed not to be significantly different here from 25°C), but a repeat run at 25°C was carried out the next day. Now a frequency shift toward lower frequencies occurred between 35 and 25°C, on standing.

Our present interpretation of this data is that the material at first was a solid or glass (polarization characteristic of crystalline material was never noted in any of the experiments reported here). Heating it to an intermediate temperature and allowing it to stand would change it into another solid modification (peaks at higher wavenumbers). Further temperature increase would cause liquefaction. The reverse heating cycle may produce the solid forms at different temperatures, because of different cooling rates, for example. We therefore, standardized on running the highest temperature first whenever possible at every pressure, and allowing the sample to cool slowly, hopefully so to reach equilibrium at every stage. Pressurizing slowly might have been preferable, but would have consumed an inordinate amount of time (a turn per hour, say).

3.1.2 Series of Runs, Standard Spectra

Spectra were obtained at three pressures (2, 8, and 16 turns, or about .3, 1.2 and 2.4 GN/m^2) and at three temperatures for each pressure (usually 180°, 80°, and 25°C). The order of temperatures

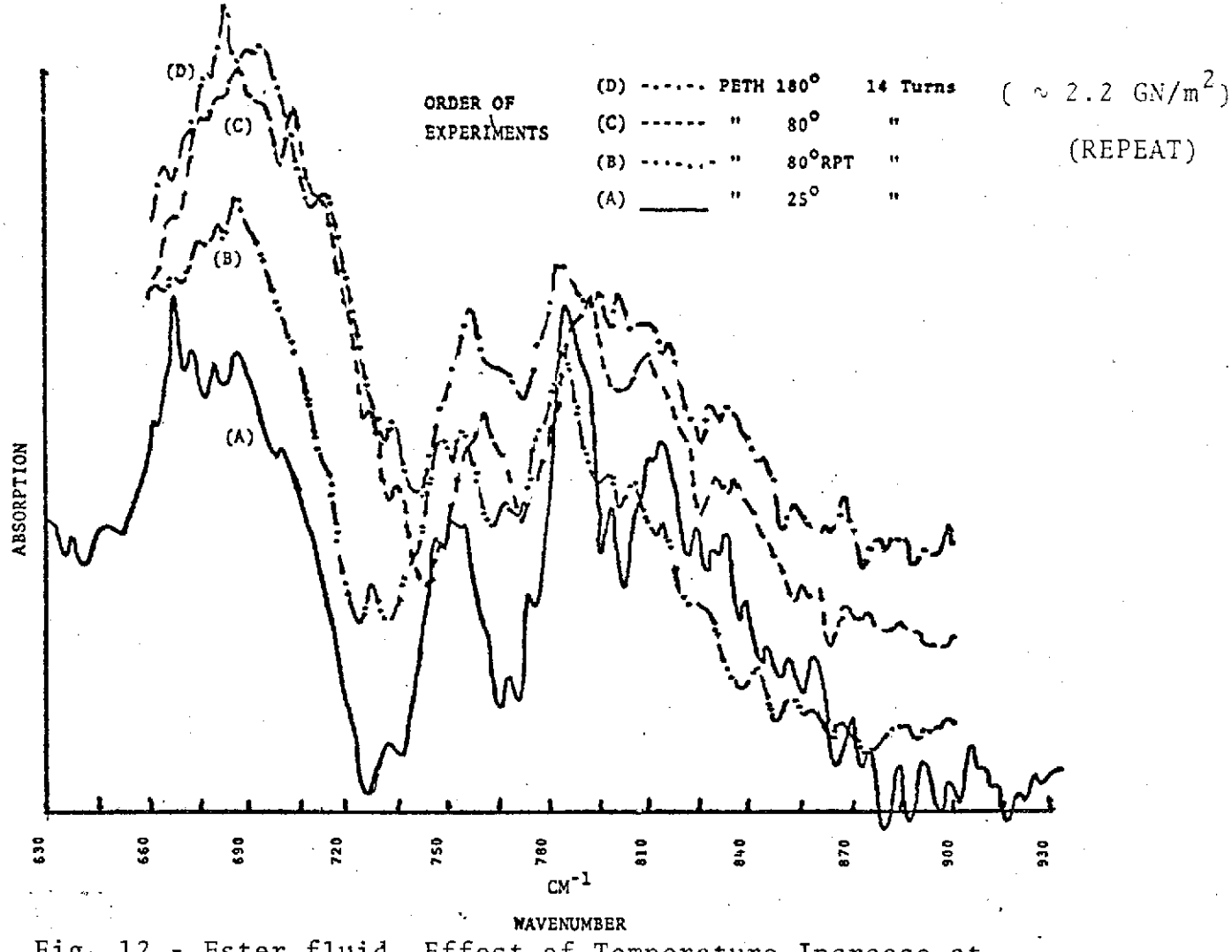

Fig. 12 - Ester fluid, Effect of Temperature Increase at Constant Elevated Pressure. (Note that the ordinates of curves (B), (C), and (D) are uniformly displaced upward).

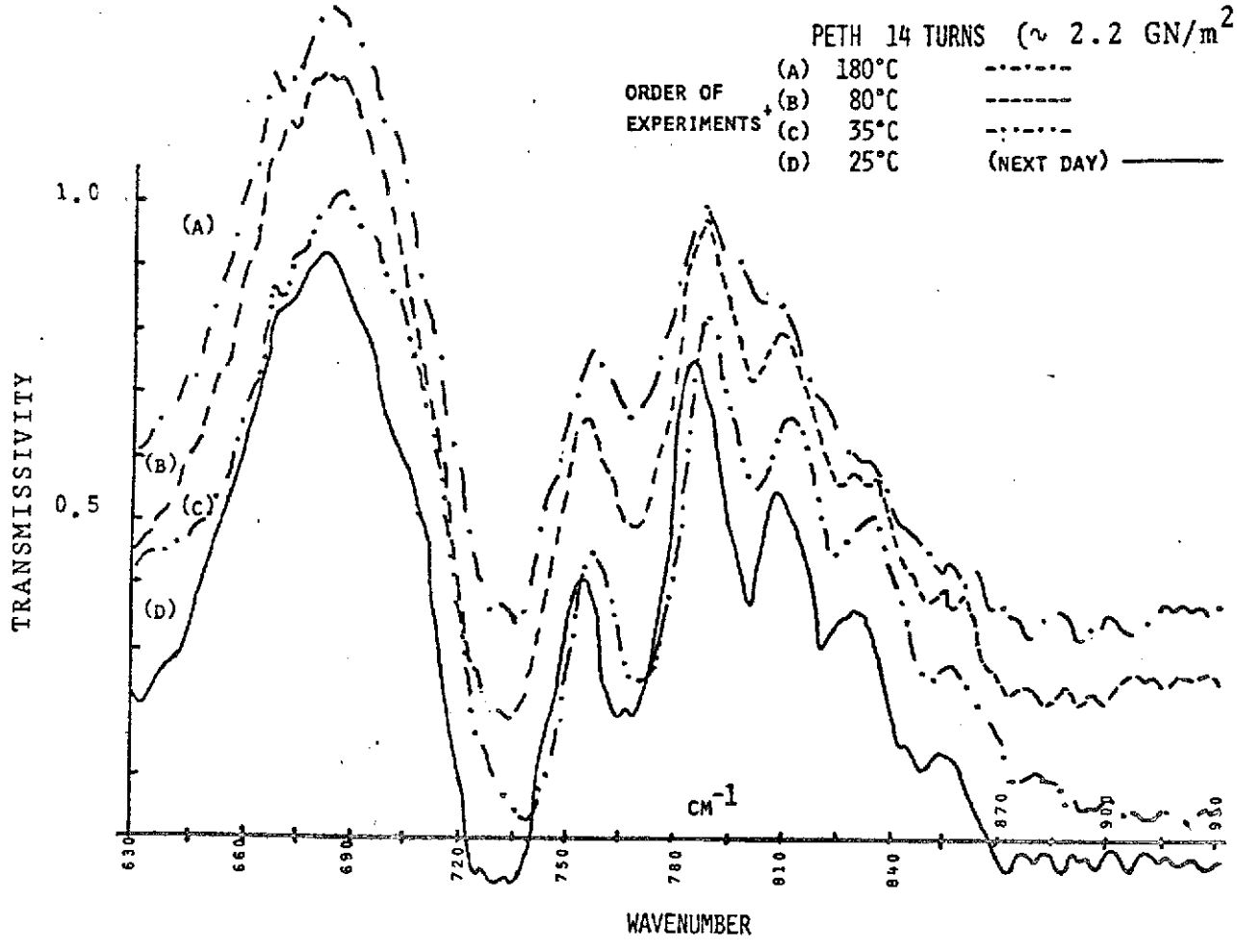

Fig. 13 - Ester fluid, Effect of Temperature Decrease at Constant Elevated Pressure. (Note that the ordinates of curves (C), (B), and (A) are uniformly displaced upward)

was usually the highest first, intermediate next, and lowest last. All the spectra were individually normalized as stated before, but for convenience of comparison three spectra were plotted per figure, every spectrum displaced from the next by a constant arbitrary amount. Hence, Fig. 14, 15 and 16 give three temperatures for every pressure and Figs. 17, 18 and 19 three pressures for every temperature. To summarize the changes of band intensities, Figs. 20 and 21 were plotted, the former showing the effect of temperature at a given pressure, the latter the effect of pressure at a given temperature. These summaries show that all but the 735 cm^{-1} band intensities decrease with temperature at any given pressure, though at various rates, but that the 735 cm^{-1} band intensity drops strongly as the pressure is increased from 8 to 16 turns, whereas the intensities of other bands may increase with increasing pressure. It should, of course, be noted that band frequency shifts are not taken into account in the summary figures.

3.1.3 Interpretation

Most of the spectral region examined contains absorption bands ascribable to the CH_2 rocking/twisting mode. The band at about 725 cm^{-1} is the fundamental and then there are overtones and band splittings caused by interactions in the solid phase. Indeed, their frequencies in the lowest melting solid phase can be used to identify the chain length of the acid part of an ester and bands split into doublets indicate two chains interacting in a unit cell (symmetric and antisymmetric rocking). For example, a band at 796 cm^{-1} (798 cm^{-1} in our spectra) is characteristic of a C_7 - triglyceride and presumably also of a C_7 - pentaerythritol. By analogy with the triglycerides, specifically trienantoin, glycerol triheptanoate, we would expect the pentaerythritol esters to exhibit more than one solid phase. These are commonly referred to -- in the order of ascending melting point -- as α, β, and β'-phases, the latter being stable over a narrow region only and having lower symmetry (hence much more structure in their absorption spectra). An indication of β-phases appears to be in Figs. 12 and 13, where much more structure (Section 1 above) was apparent. Also, the length of heating or cooling turned out to be important and this is a characteristic of β-phase formation. This aspect (rate of pressuring, rate of heating and cooling) ought to be studied in more detail. The analogy with the well-studied trienantoin spectra (at low temperatures, not at high pressures) should be further explored.

Another point is important: In many triglycerides, such as tristearin[12], a transition sequence solid I→liquid I→solid II→liquid II can occur. The structure of the semiliquid interphase between two solid phases has been described in terms of a liquid crystalline interphase. In view of our findings of rate-dependent spectra, this aspect should be explored for such esters (triglycerides and pentaerythritols) under different pressures and temperatures.

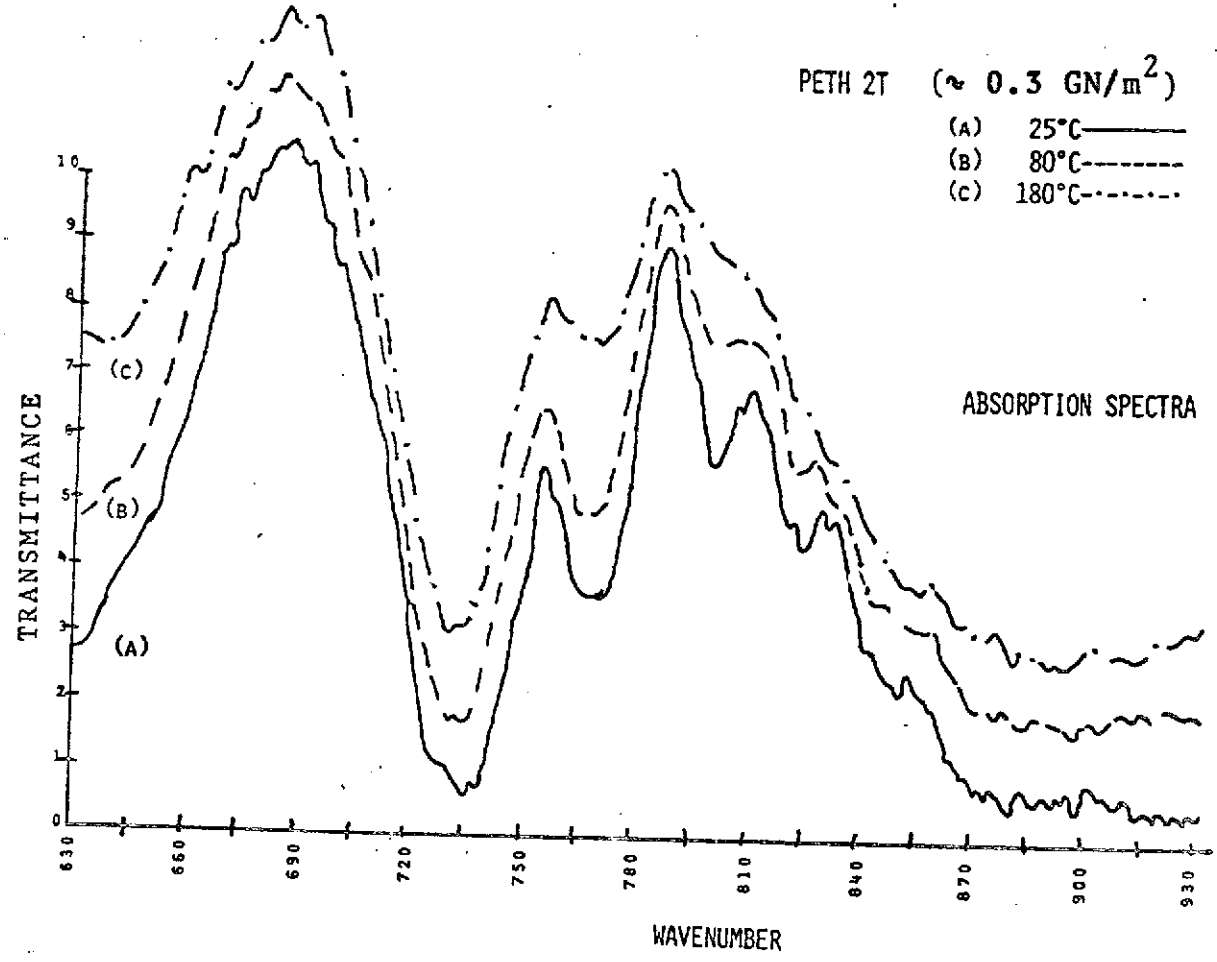

Fig. 14 - Ester fluid, Absorption Spectra at a Pressure of 2 Turns (≈ 0.3 GN/m^2), and at 25°, 80°, and 180°C (Note that the ordinates of curves B and C are uniformly displaced upward)

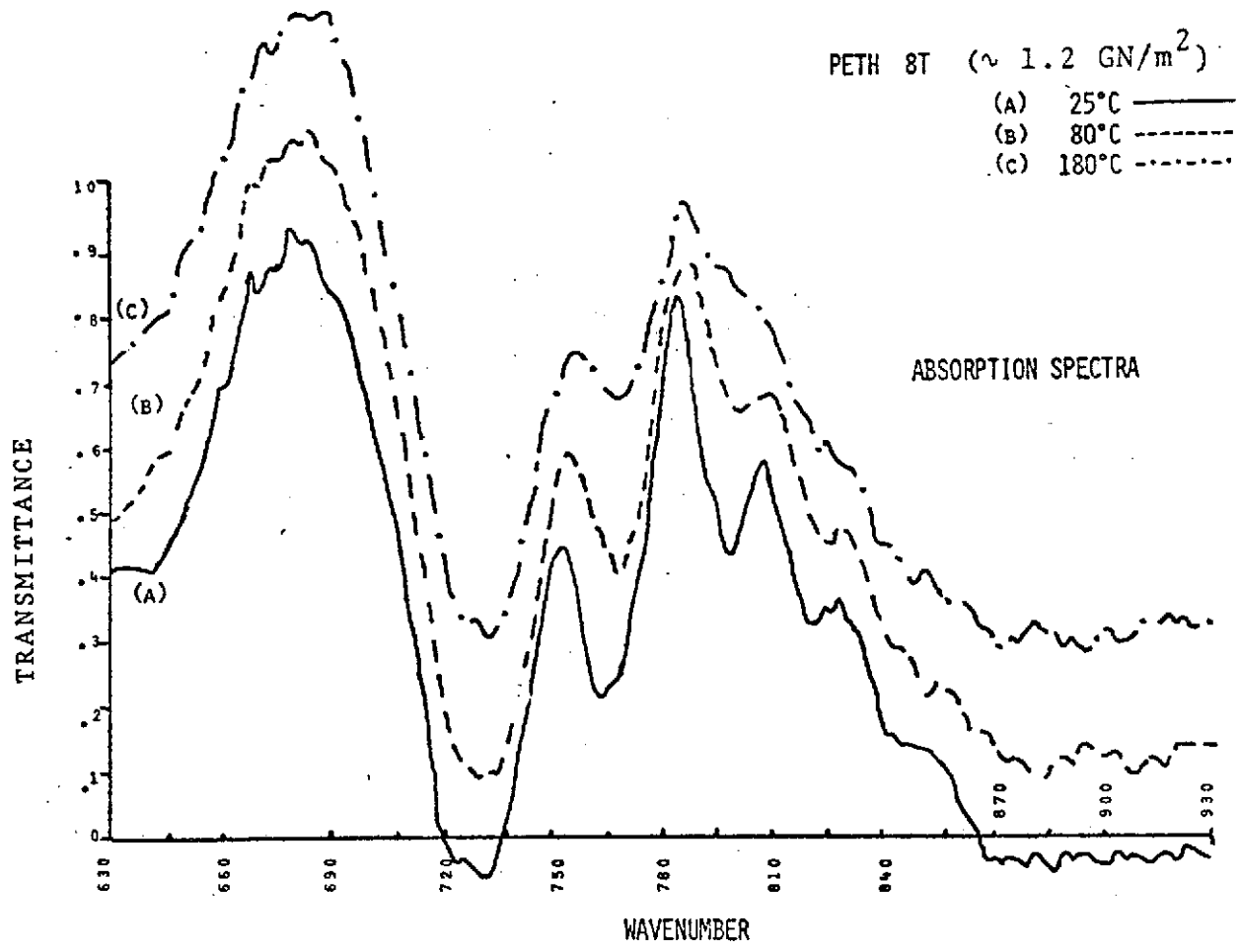

Fig. 15 - Ester fluid, Absorption Spectra at a pressure of 8 Turns (∿ 1.2 GN/m^2), and at 25°, 80°, and 180°C (Note that the ordinates of curves (C), (B), and (A) are uniformly displaced upward)

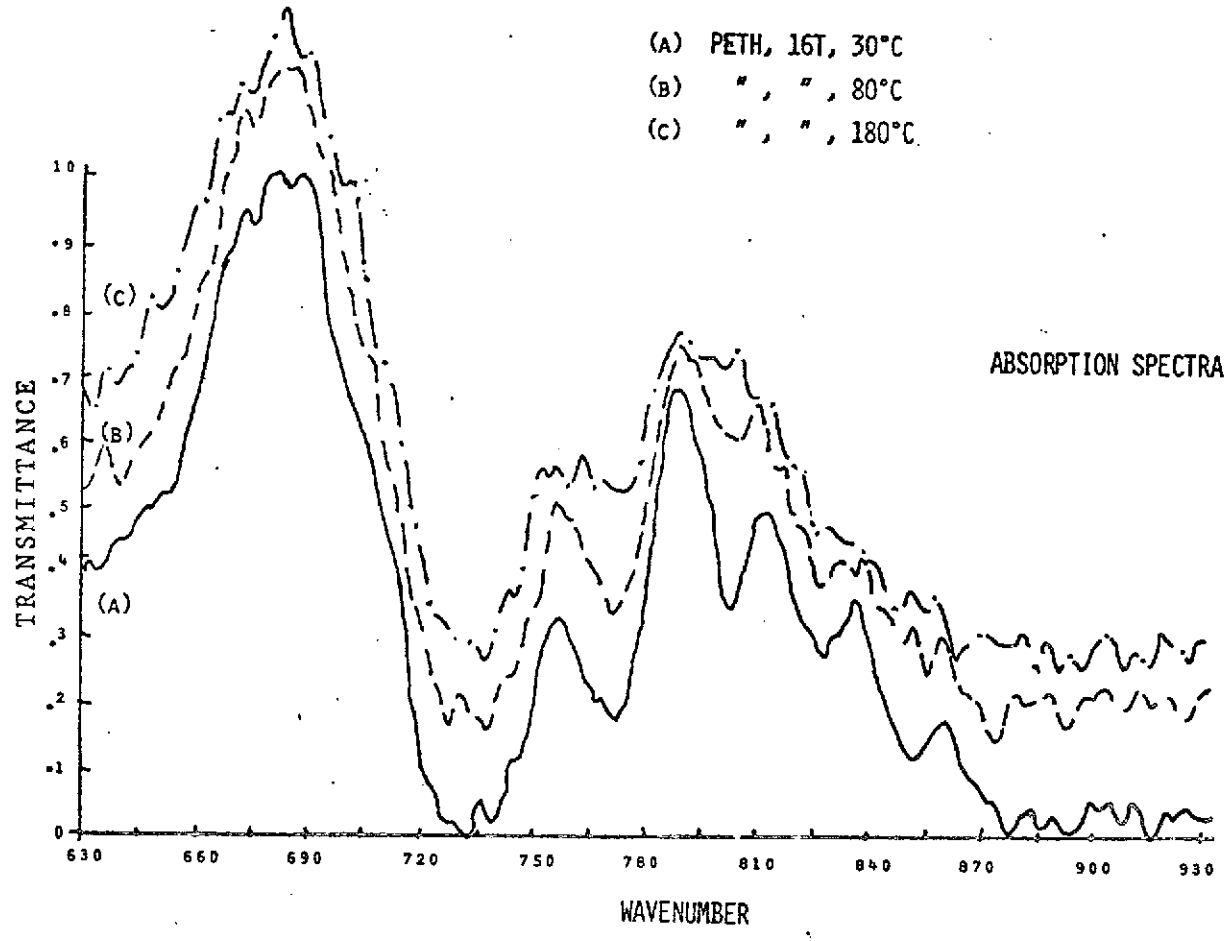

Fig. 16 - Ester Fluid, absorption spectra at a pressure of 16 Turns (~ 2.4 GN/m^2), and at 25°, 80°, and 180°C. (Note that the ordinates of curves (C), (B), and (A) are uniformly displaced upward)

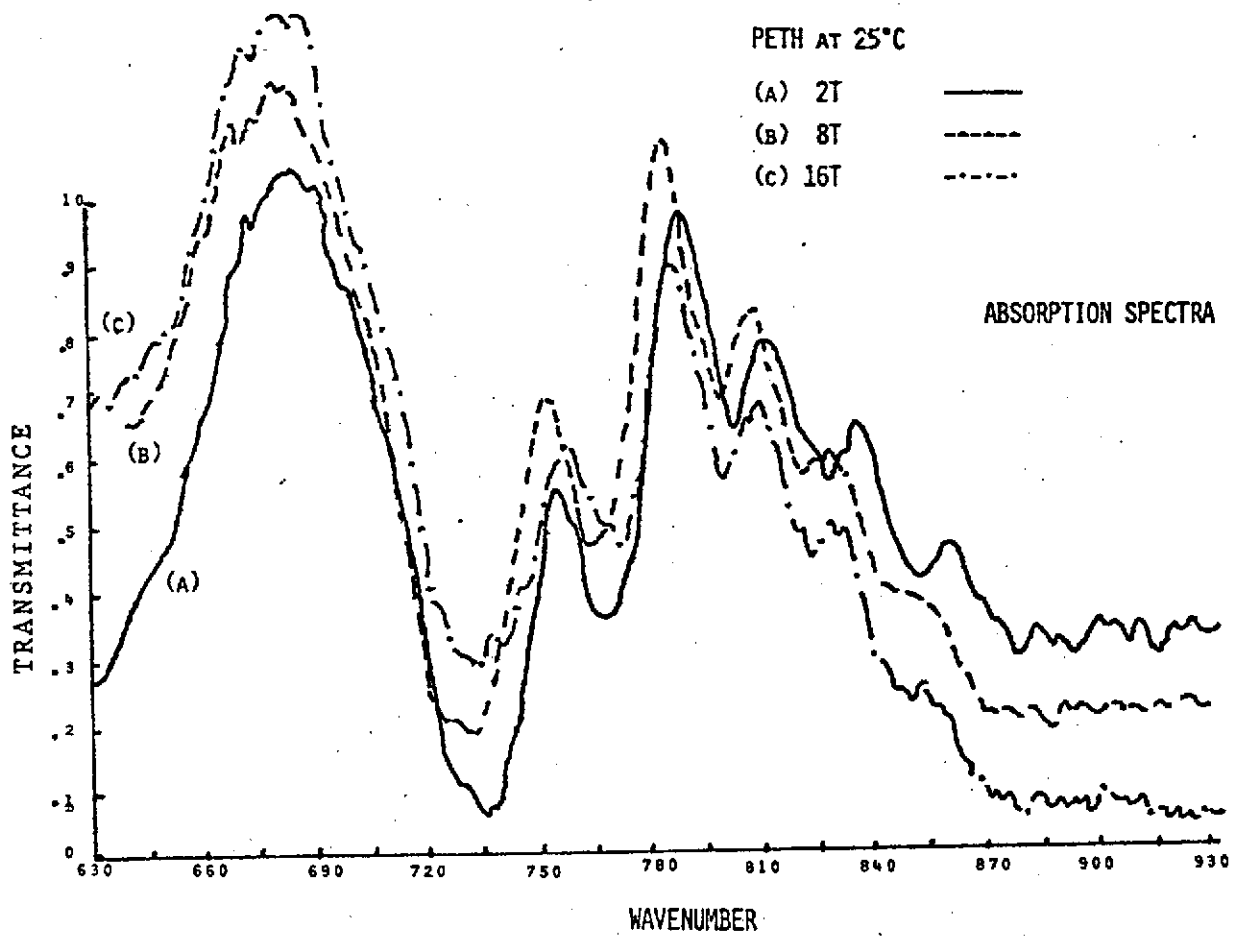

Fig. 17 - Ester fluid, Absorption Spectra at 25°C, and at Pressures of 2, 8, and 16 turns (∿ 0.3, 1.2, and 2.4 GN/m^2) [Note that the ordinates of curves (C), (B), and (A) are uniformly displaced upward]

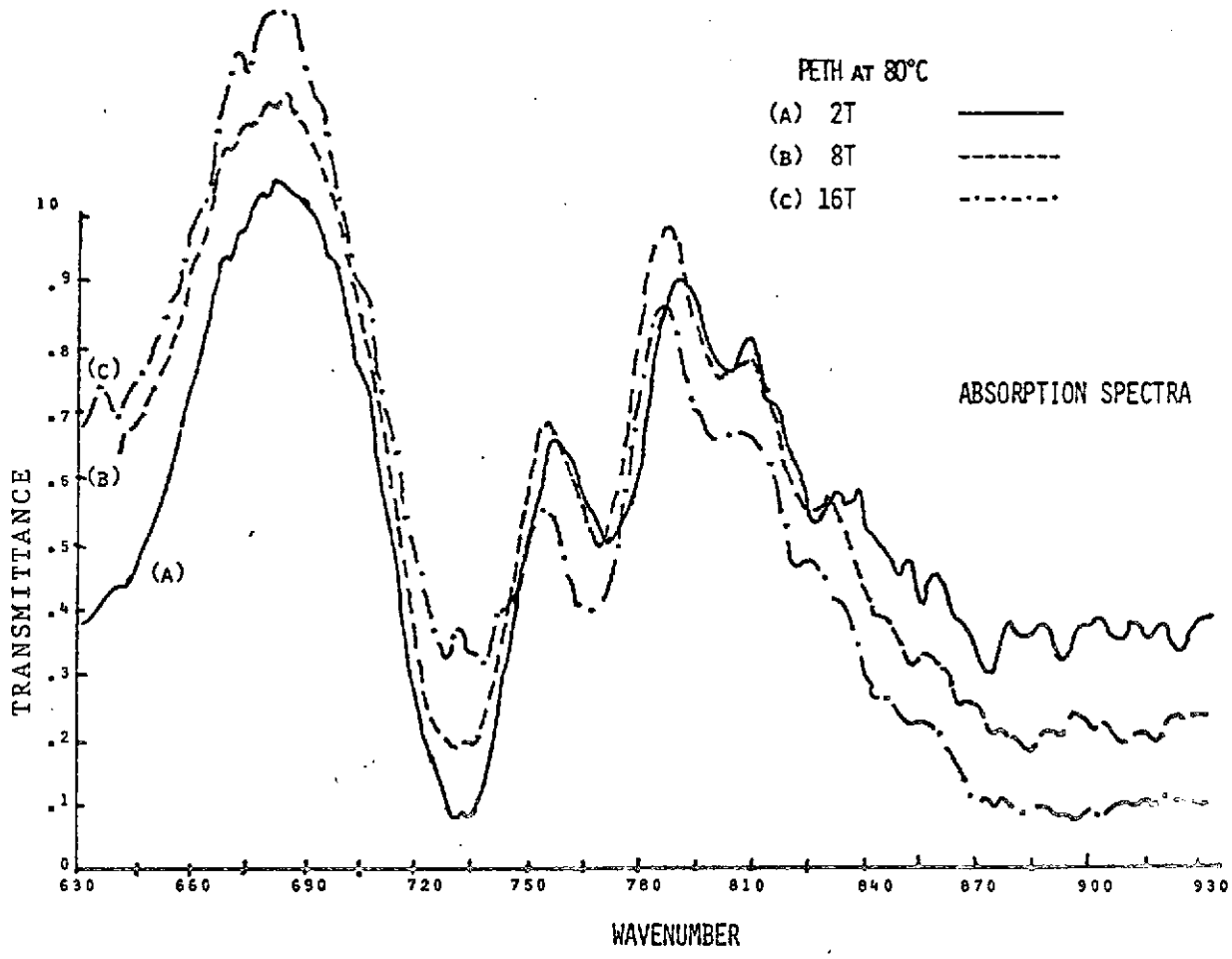

Fig. 18 - Ester Fluid, Absorption Spectra at 80°C, and at Pressures of 2, 8, and 16 turns (≈ 0.3, 1.2, and 2.4 GN/m^2) [Note that the ordinates of curves (C), (B), and (A) are uniformly displaced upward]

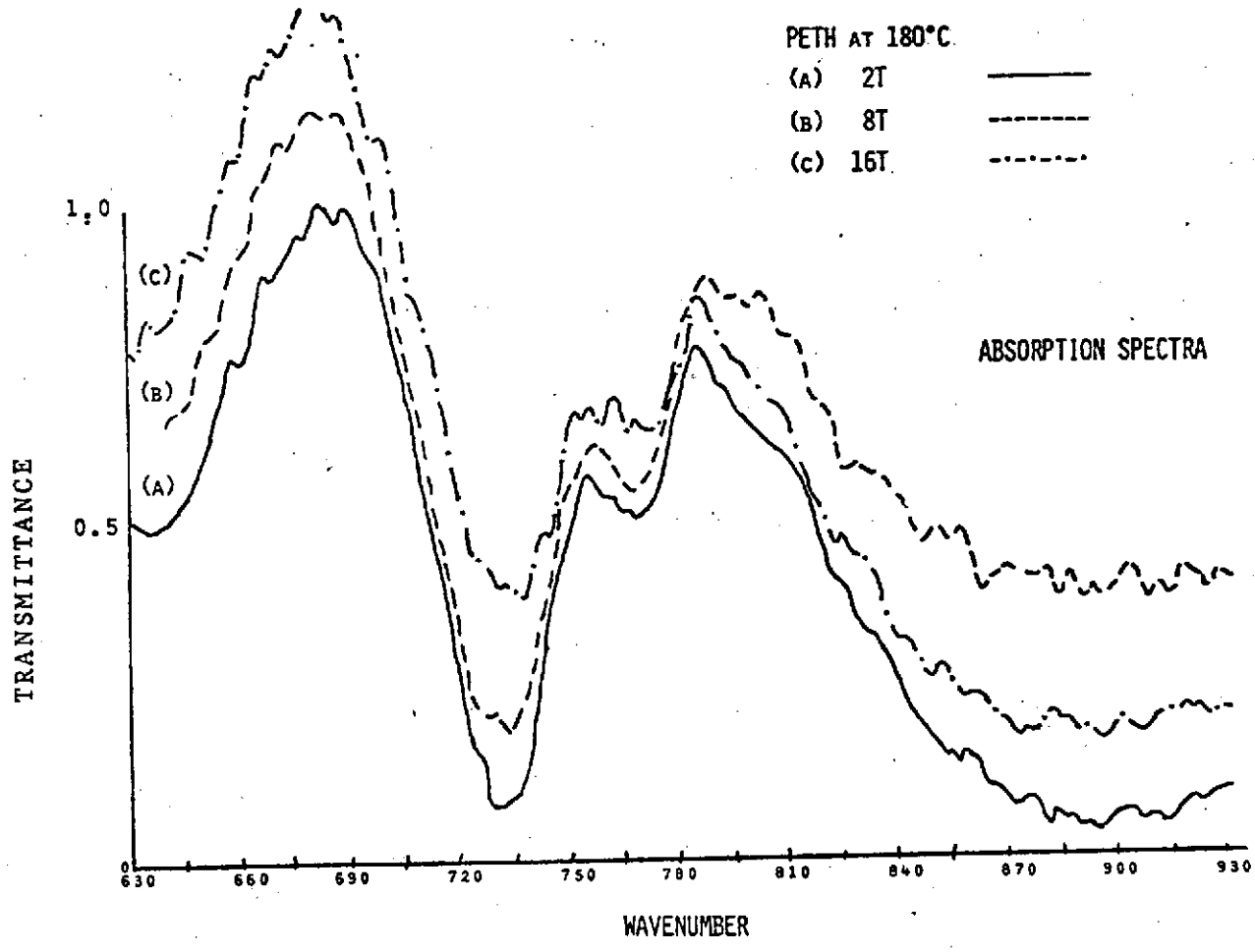

Fig. 19 - Ester Fluid, Absorption Spectra at 180°C, and at Pressures of 2, 8, and 16 turns (~ 0.3, 1.2, and 2.4 GN/m^2) [Note that the ordinates of curves (C), (B), and (A) are uniformly displaced upward]

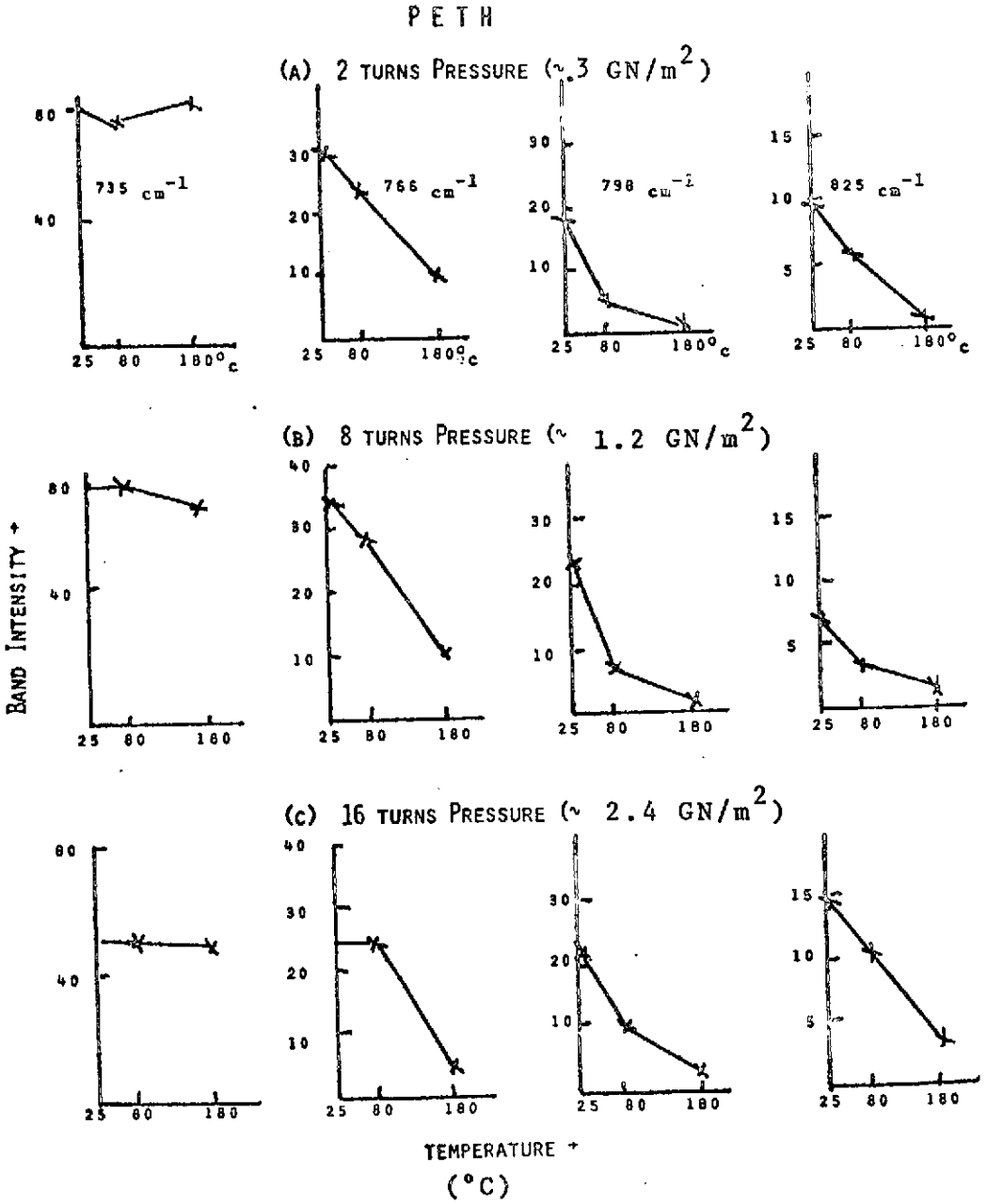

Fig. 20 - Ester Fluid, Changes of Infrared Absorption Band Intensities With Temperature at Three Pressures

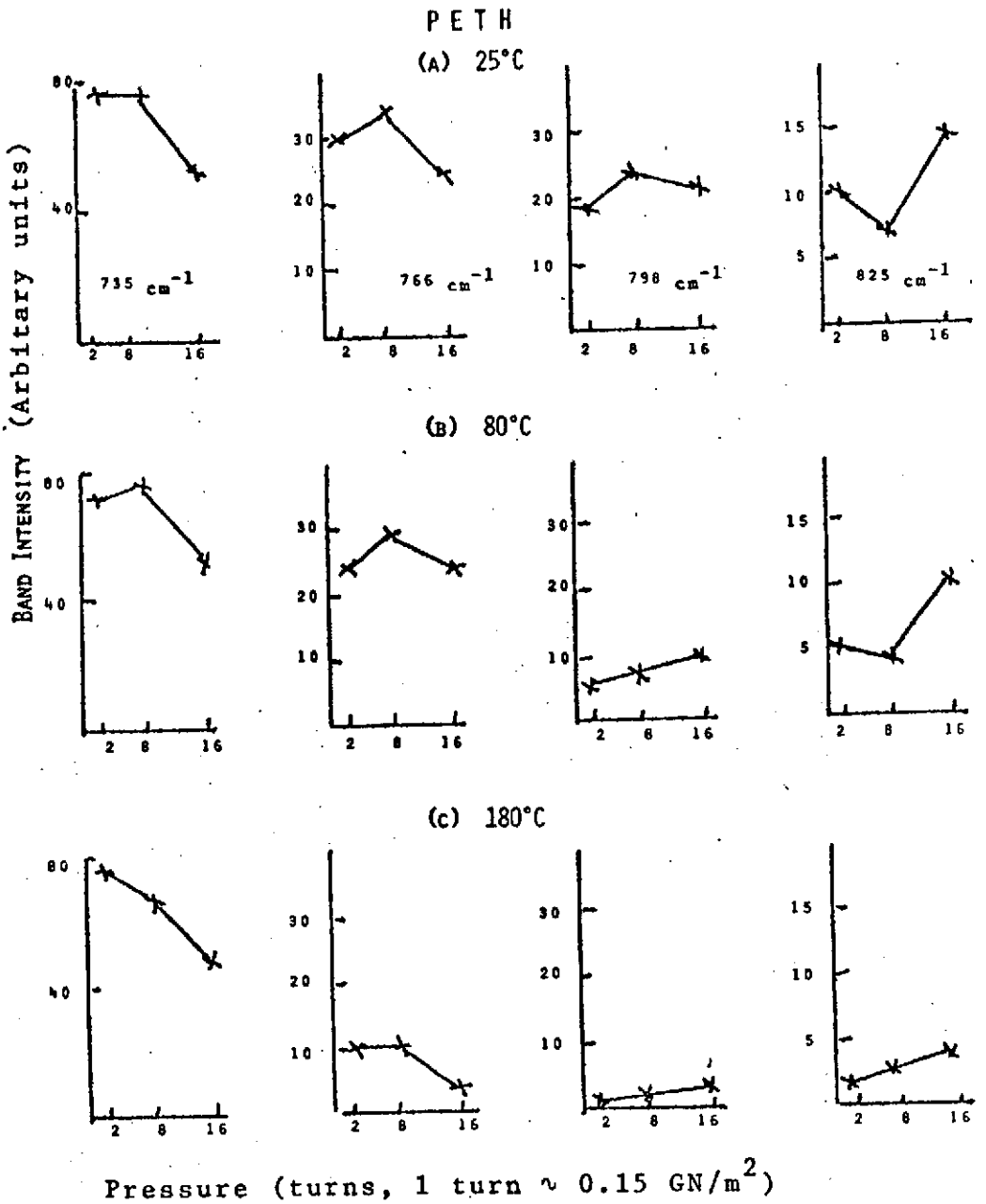

Fig. 21 - Ester Fluid, Changes of Infrared Absorption Band Intensities with Pressure at Three Temperatures

In summary then, our findings so far are indicative of the formation of some solid or glassy phases under certain pressures and temperatures. These phases may not have been observed under truly equilibrium conditions. For this reason, it has yet not been possible even to bracket the ranges of phase transition temperatures and pressures. As will now be shown, solid/liquid transitions could be shown much more clearly in the case of the Sun fluid.

3.2 HIGH PRESSURE ABSORPTION SPECTRA OF THE "SUN FLUID"

3.2.1 Early Experiments

An early series of spectra is shown in Fig. 22. Here the pressure was increased rapidly from 0 to 2, 8, and 14 turns respectively, all at constant ambient temperature. The changes are indicative of a liquid to glass, or viscous liquid (sharper and stronger bands), to solid transition (simpler and less intense structure). Because it occurred to us that rapid compression (over a few minutes) might freeze in certain phases and configurations, we decided to adopt the same routine here as in the case of the other fluid, viz. bring the fluid up to a given pressure level, increase the temperature to the maximum desired, run that spectrum, and then run other spectra at successively lower temperatures. In this way the fluid would have had the best chance to equilibrate.

3.2.2 Series of Runs, Standard Spectra

All the spectra were obtained in the way just indicated. However, they were plotted in two ways: (a) different temperatures at a given pressure, as they were run, and (b) different pressures at a given temperature (Figs. 23 to 25 and Figs. 26 to 28). These spectra are exceedingly clear and reproducible and somewhat better than those of the ester fluid, because of the generally lower infrared absorption of this material. Let us look at the latter series of plots. There are some outstanding differences produced by pressure changes at various temperatures. Take, for example, the band near 738 cm^{-1} at 25°C. This band is usually considered the solid (crystalline) part of the twin 728/738 cm^{-1}, which is the fundamental CH_2-rocking/twisting vibration in a chain of CH_2 groups (we already referred to this band in our discussion of the ester fluid). Indeed, the 738 cm^{-1} band (its precise frequency position varies slightly with different materials) has been used as a measure of crystallinity in polyethylene polymers. Now there is hardly an indication of it in the 2 turns spectrum (0.3 GN/m^2) at 25°C (see Fig. 26), but it is strongly present at the higher pressures. Simultaneous with the appearance of the 738 cm^{-1} band is the disappearance of its "liquid state twin" at

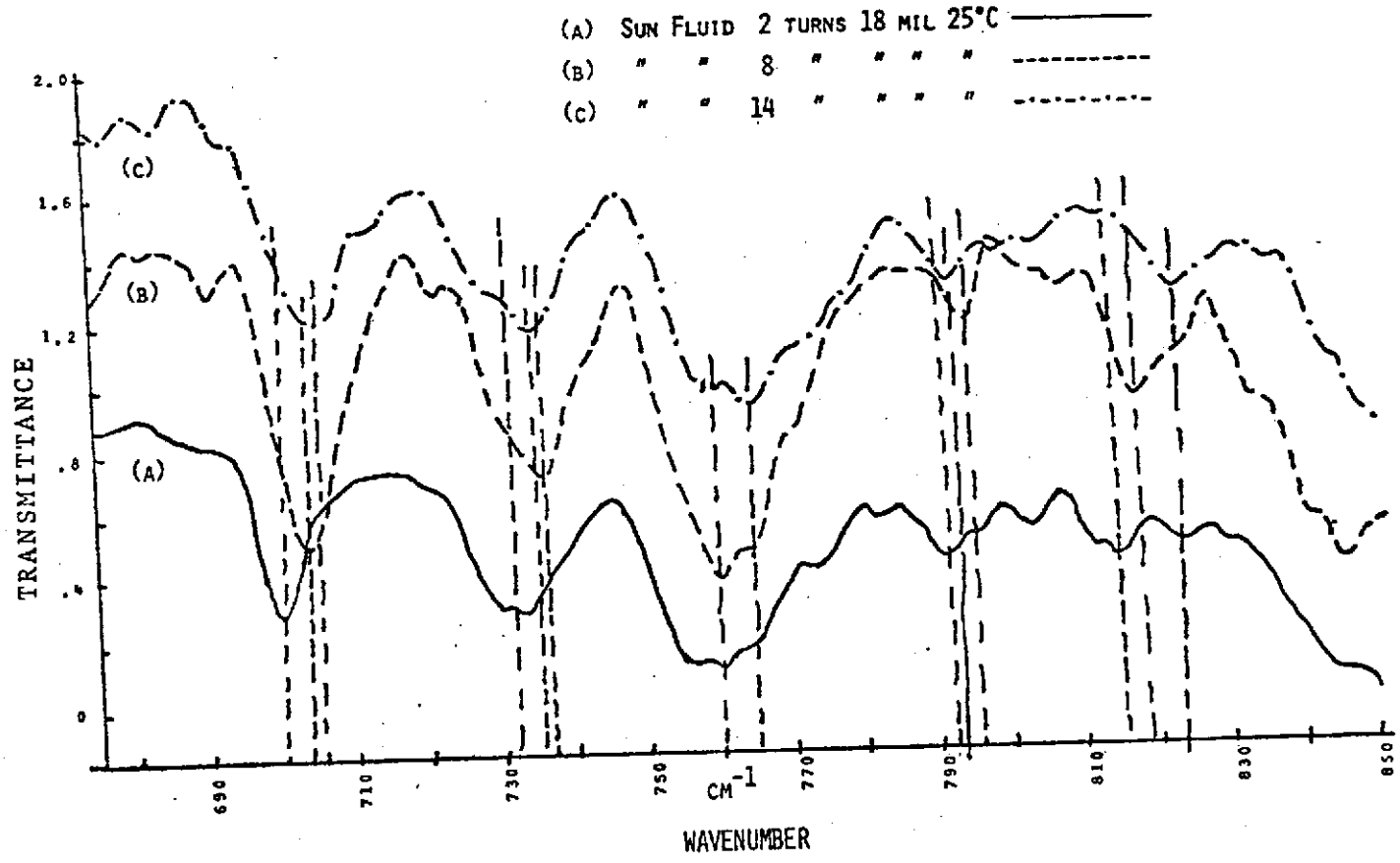

Fig. 22 - Sun Fluid, Effect on Absorption Spectra of Rapid Pressure Increase at Ambient Temperature (Note that the ordinates of curves (C), (B), and (A) are uniformly displaced upward)

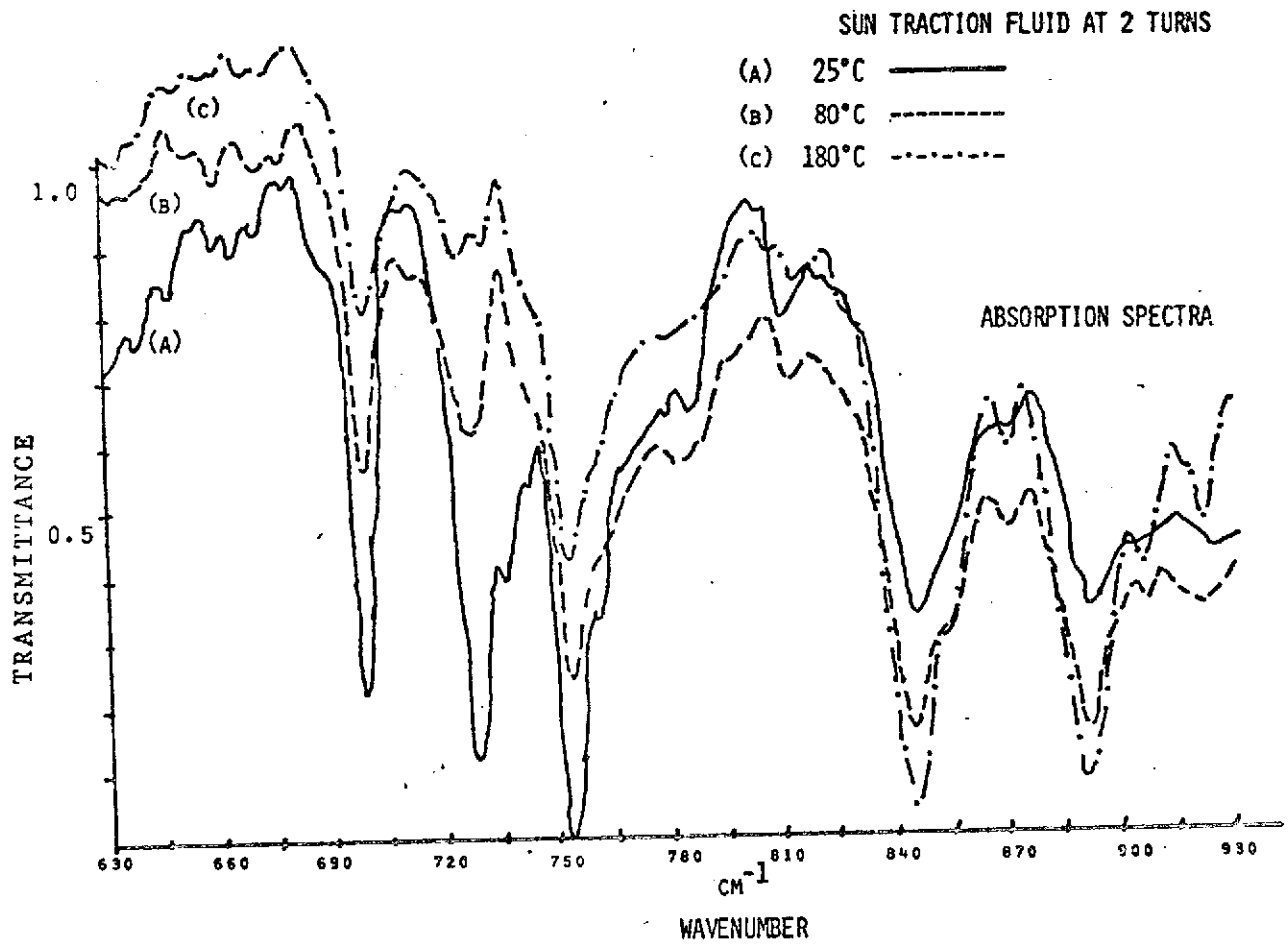

Fig. 23 - Sun Fluid, Absorption Spectra at 2 turns ($\sim$ 0.3 GN/m^2) Pressure, and at 25°, 80°, and 180°C (Note that the ordinates of curves (C), (B), and (A) are uniformly displaced upward)

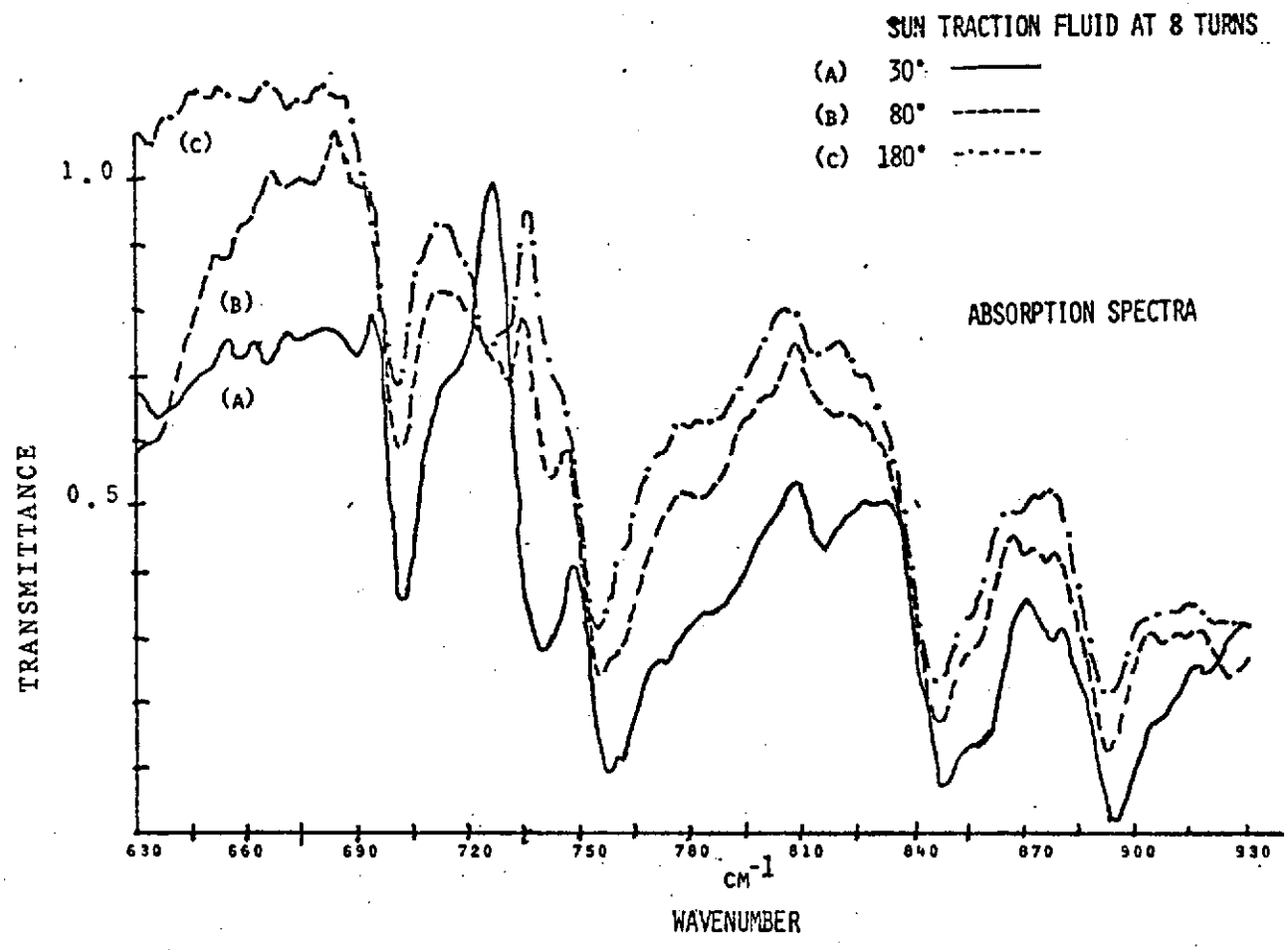

Fig. 24 - Sun Fluid, Absorption Spectra at 8 Turns (~ 1.2 GN/m^2) Pressure, and at 30°, 80°, and 180°C (Note that the ordinates of curves (C), (B), and (A) are uniformly displaced upward)

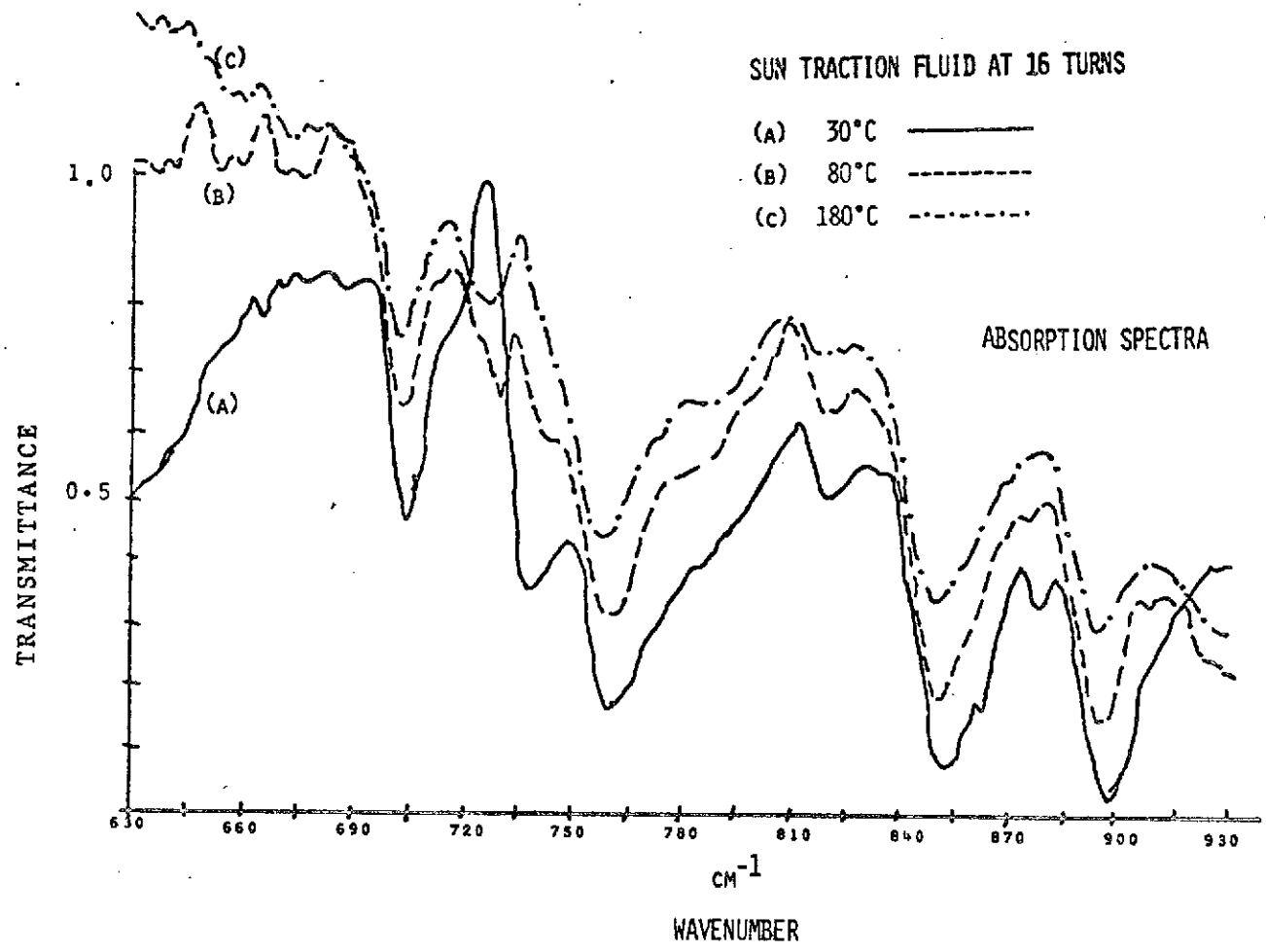

Fig. 25 - Sun Fluid, Absorption Spectra at 16 Turns ($\sim$ 2.4 GN/m^2) Pressure, and at 30°, 80°, and 180°C (Note that the ordinates of curves (C), (B), and (A) are uniformly displaced upward)

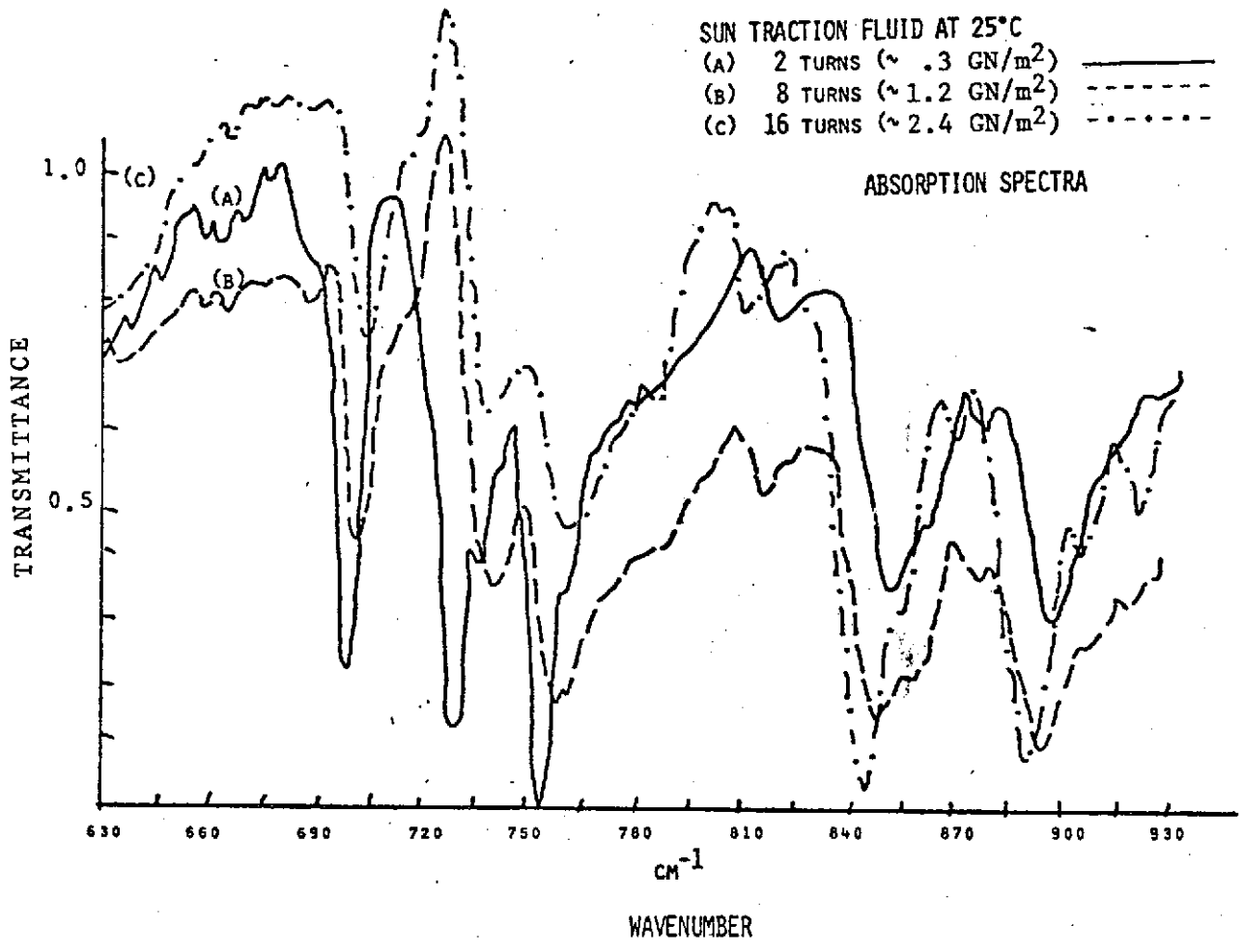

Fig. 26 - Sun Fluid, Absorption Spectra at 25°C and at Pressures of 2, 8, and 16 Turns (~ 0.3, 1.2, and 2.4 GN/m^2) (Note That the ordinates of curves (C), (B), and (A) are uniformly displaced upward)

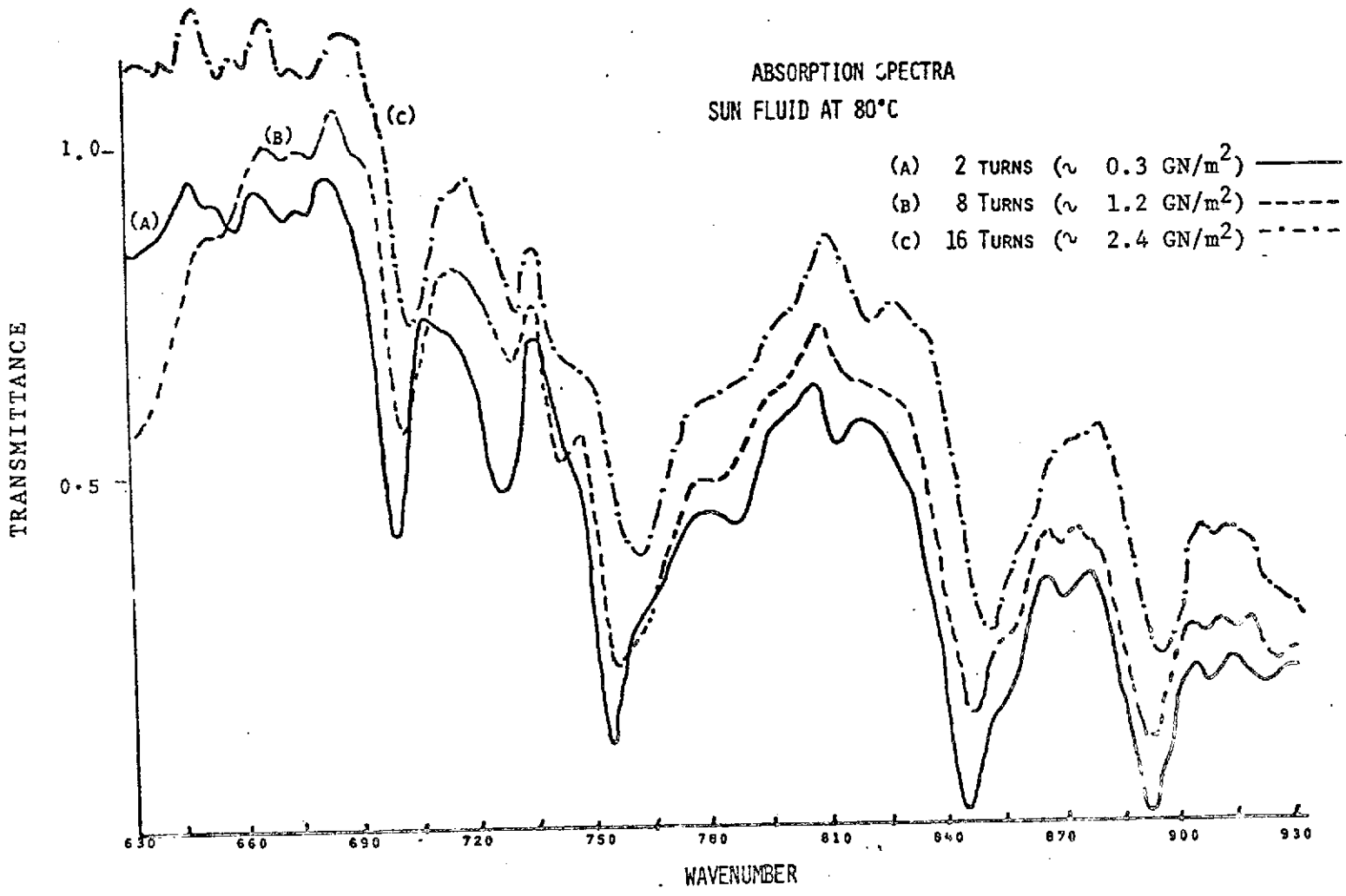

Fig. 27 - Sun Fluid, Absorption Spectra at 80°C and at Pressures of 2, 8, and 16 Turns (∿ 0.3, 1.2, and 2.4 GN/m^2) [Note that the ordinates of curves (C), (B), and (A) are uniformly displaced upward]

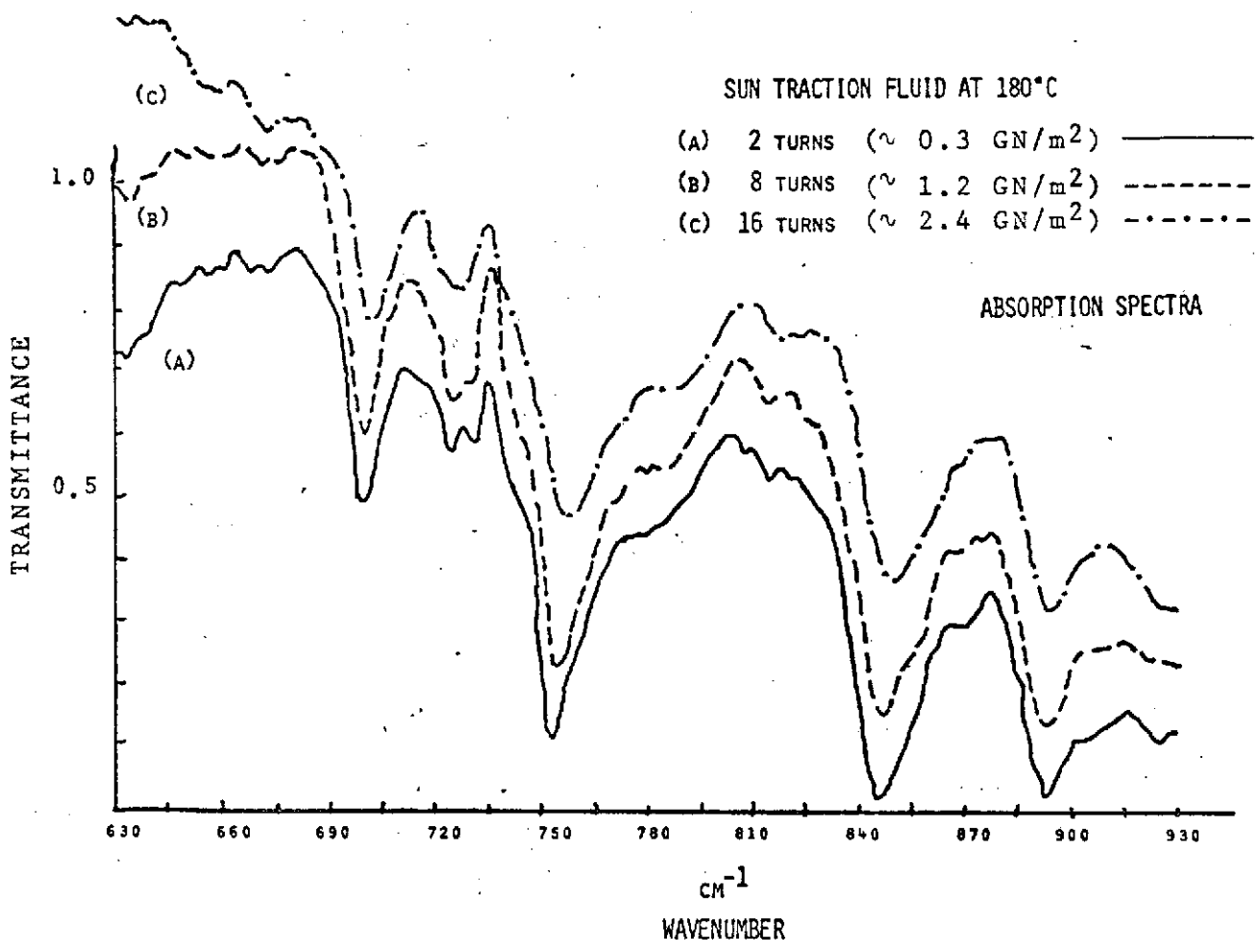

Fig. 28 - Sun Fluid, Absorption Spectra at 180°C and at Pressures of 2, 8, and 16 Turns (∿ 0.3, 1.2, and 2.4 GN/m^2) (Note that the ordinates of curves (C), (B), and (A) are uniformly displaced upward)

728 cm^{-1}. In the 80°C spectra (Fig. 27) the "liquid state twin" at 728 cm^{-1} is present at all pressures -- though weaker than at 25° and at 0.3 GN/m^2 --, but there is still a definite presence of the solid state twin at 738 cm^{-1}, especially at the two highest pressures. On the other hand, at 180°C the 738 cm^{-1} band is hardly present at any pressure and the 728 cm^{-1} band, now having a lower frequency satellite, is present at all pressures. Thus the changes of the fundamental rocking/twisting vibration (728/738 cm^{-1}) already tell us that the fluid at 25°C is definitely solidified at 1.2 GN/m^2 or more, at 80°C only partly so, and at 180°C apparently not even at our highest pressure. However, at 180°C, the appearance of a new satellite band may be indicative of a change of solution characteristics of a multicomponent system.

But there is more information in these spectra. For example, the intense band at 842 cm^{-1} in the .3 GN/m^2 spectrum at 25°C of Fig. 26, is shifted toward higher wavenumbers -- just by 2 - 3 cm^{-1}, but nevertheless significantly -- and weakened in the corresponding 1.2 and 2.4 GN/m^2 pressure, and at 180°C (Fig. 28) the shift does not occur at all. Similar trends can be observed with bands at other frequencies. On the other hand, the band at 696 cm^{-1} shifts only monotonously with pressure toward increasing wavenumbers as the pressure is increased, i.e. not by jumps and its shifts are much smaller. Indeed, it is our present opinion that the larger "shifts", e.g. those near 842 cm^{-1}, which occur in a jumping fashion as the pressure is increased, are not just "pressure shifts", i.e. increases in frequency of the band peak caused by pressure-induced bond shortenings or molar volume contractions, but changes in conformational makeup. For the high resolution of our spectra shows clearly that the jump of the band maximum is really the enhancement of a shoulder or weak satellite band already present at lower pressure. Clearly such a change in isomeric composition can be an important clue as to what makes a satisfactory fluid and deserves further attention. It should be noticed that no such deduction could be drawn from less resolved spectra.

The shifts of wavenumber position with pressure of some of the bands can be in either direction. Some organic liquids shift to a lower frequency at low pressure and to higher frequencies at high pressures. At the solidification point, an abrupt shift can occur and it too can be toward the red or toward the blue depending on the material and the solvent (if there is any). Different solvents can influence the direction of the shifts for reasons yet unknown. Work in this direction would be very desirable to obtain a better understanding of the different types of molecular interactions. We believe that many of these changes are caused by shifts in conformational equilibria as stated above. When a solid is formed, it usually is crystallized in one conformational form only, giving rise to an abrupt band frequency shift which can be in either direction. Drickamer and co-workers[13] tried to explain some of these effects in terms of reorientation of molecules under pressure, which fixes them in a configuration where the repulsive forces are at a minimum; hence, there is a red shift. For the abrupt blue shift, on the contrary, this reorientation effect probably does not exist and the

solidification corresponds then to a very large increase in the repulsive forces. The frequency shifts on solidification observed in our work are further illustrated in Fig. 29 while the previously mentioned intensity changes are summarized in Fig. 30.

New bands appearing on solidification are usually assumed to be caused by the different symmetry of the solid environment since bands forbidden by the selection rules in the liquid may become allowed in the solid if the symmetry is relatively low. Considerable work on spectral differences between liquids and solids has been reported in the literature for a number of pure materials.[14]

In any case, even though much of the theoretical background remains to be explained, there is no question about the capability of recognizing from the vibrational spectrum, phase and structural changes caused by pressure.*

3.3 EMISSION SPECTRA OF THE FLUIDS AT AMBIENT PRESSURE USING THE GRATING SPECTROMETER

The emission spectra of the two fluids at 150° and 250°C are shown, on an absolute scale (still relative with respect to a constant factor, but containing the blackbody radiation) in Figs. 31 and 32 and Figs. 33 and 34 for the ester and the Sun fluid respectively. The emissivities (using the blackbody as, in fact, a sloping background) are shown in Figs. 35, 36, 37, and 38. When these curves are compared with the corresponding absorption spectra (Figs. 1 and 2), it is clear that all the important features correspond. It should be pointed out, however, that at the low temperature of 150°, the bands of frequency above 1700 cm^{-1} are very weak relative to those in the 1200-600 cm^{-1} region. This result is, of course, a consequence of the peak of the blackbody radiation curve lying at a much longer wavelength when the temperature is low. Since the temperatures likely to occur in an EHD contact range between 100 and 300°C -- we presume -- the 1200-600 cm^{-1} spectral region is the best to be studied by emission. As we have shown, it is also very informative, capable of telling us about phase changes, chain lengths, etc., since it includes the CH_2 - rocking/twisting vibration, which is very sensitive to the environment. This fortunate coincidence of natural phenomena is important to our work.

---

*A number of authors have shown that viscosity can be calculated from the widths and contours of selected bands. For example, the width of the 698 cm^{-1} band of the Sun Fluid clearly changes with pressure. This aspect is being pursued.

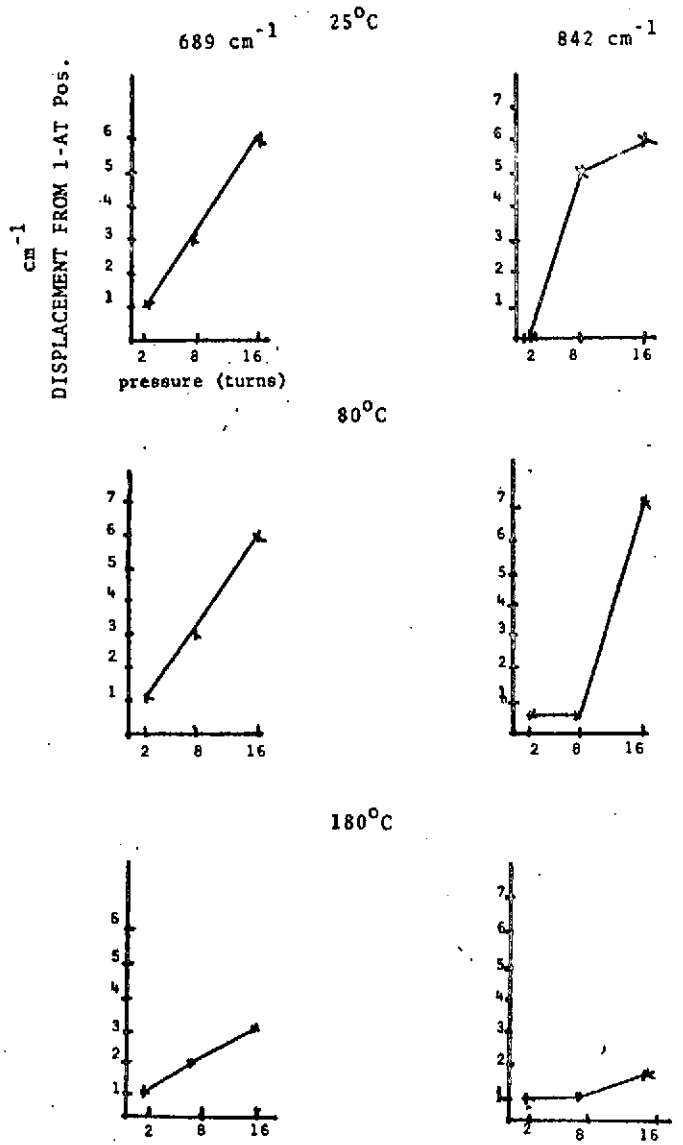

Fig. 29 - Sun Fluid, Comparison of Band Locations

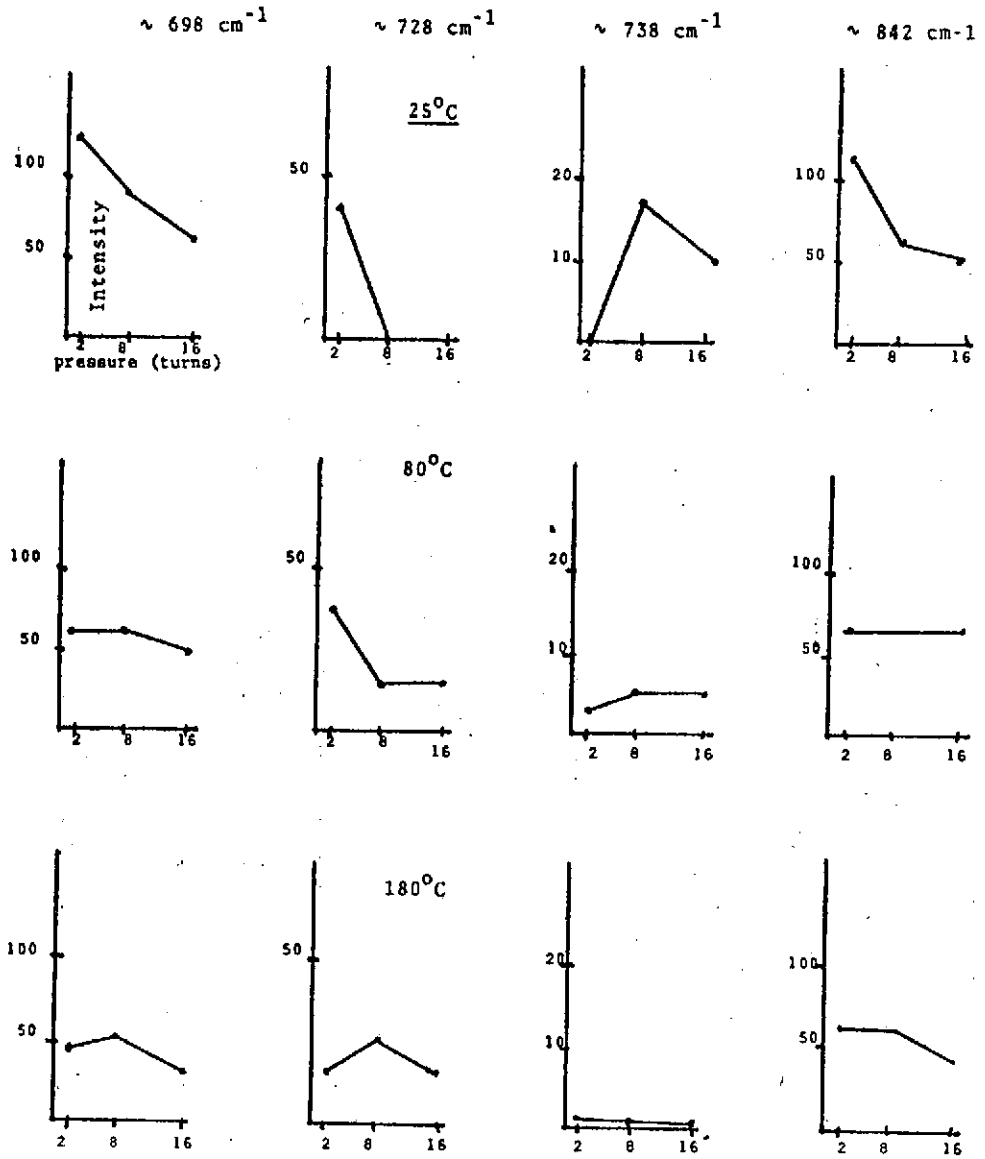

Fig. 30 - Sun Fluid, Comparison of Band Intensities

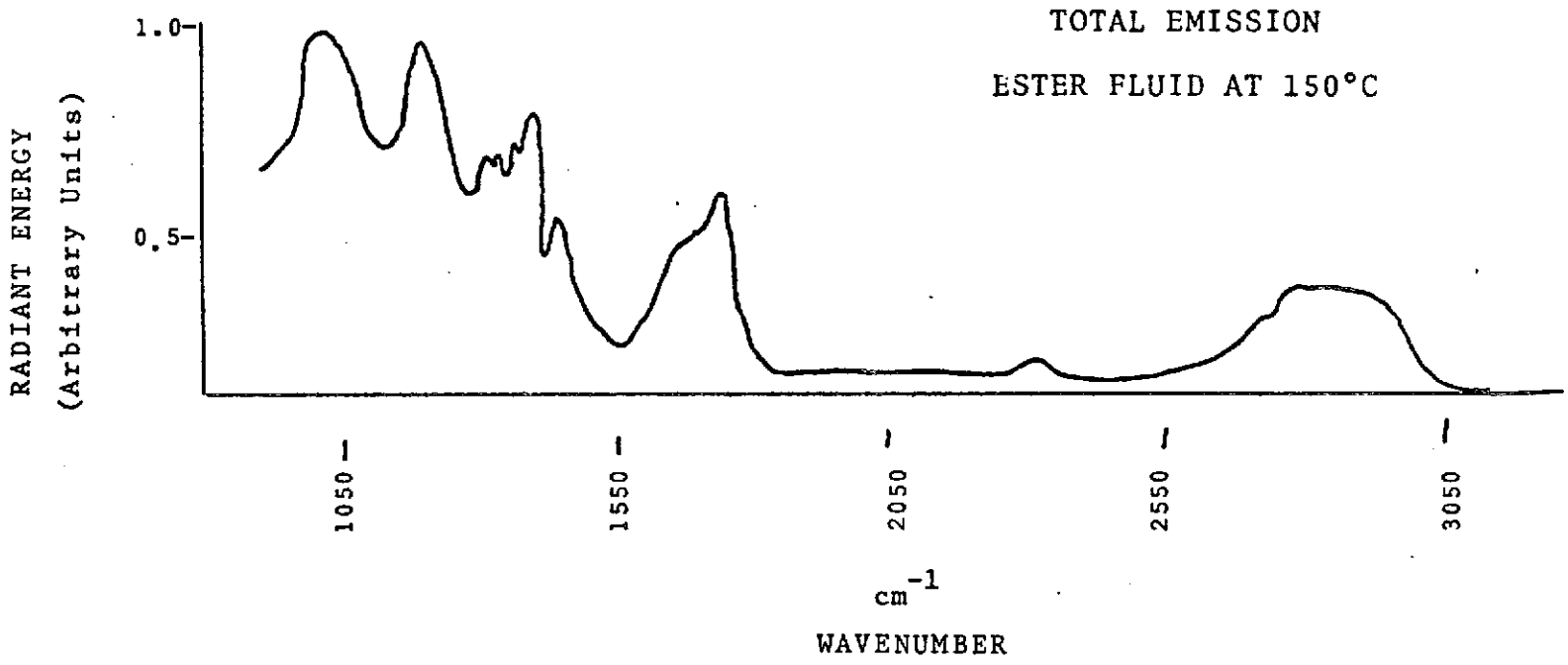

Fig. 31 - Ester Fluid at 150°C, Emission Spectrum at Ambient Pressure In Terms of Total Radiation

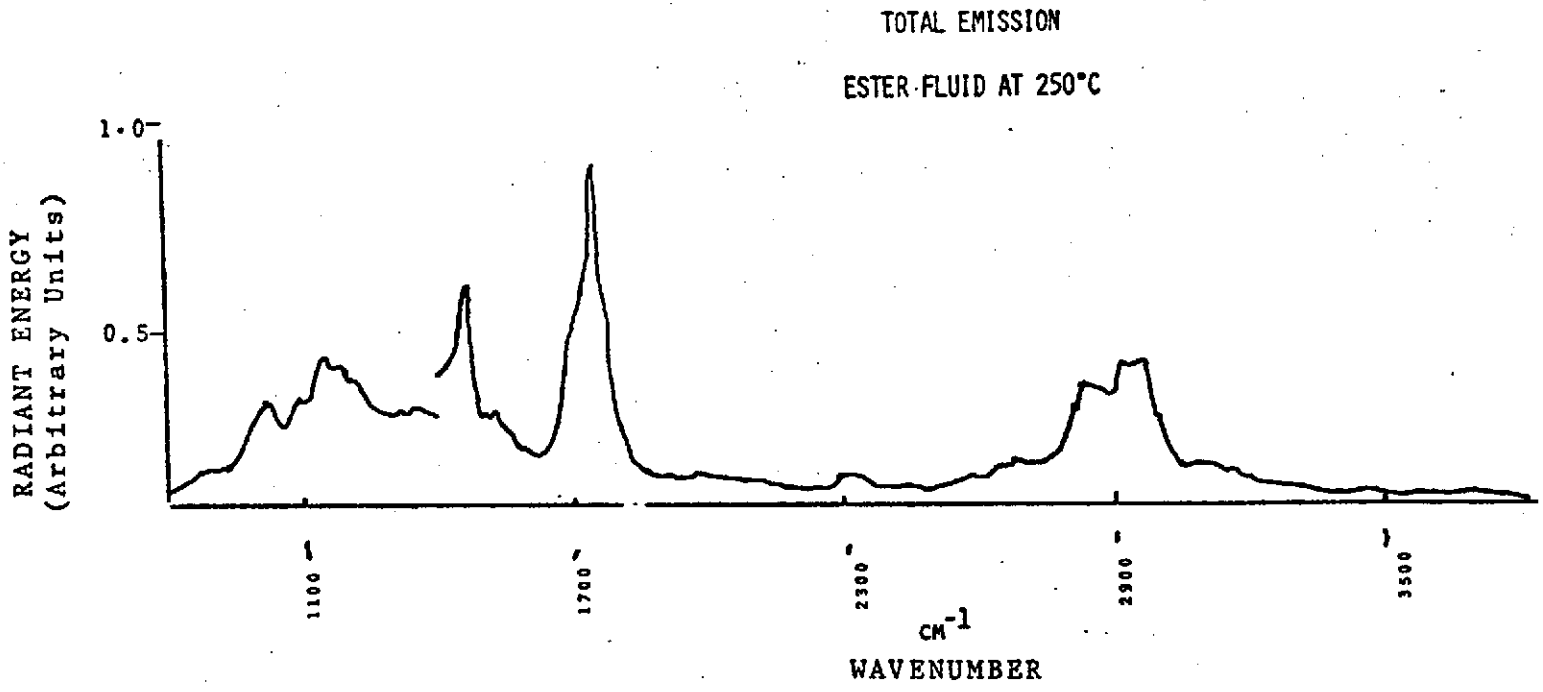

Fig. 32 - Ester Fluid at 250°C, Emission Spectrum at Ambient Pressure In Terms of Total Radiation

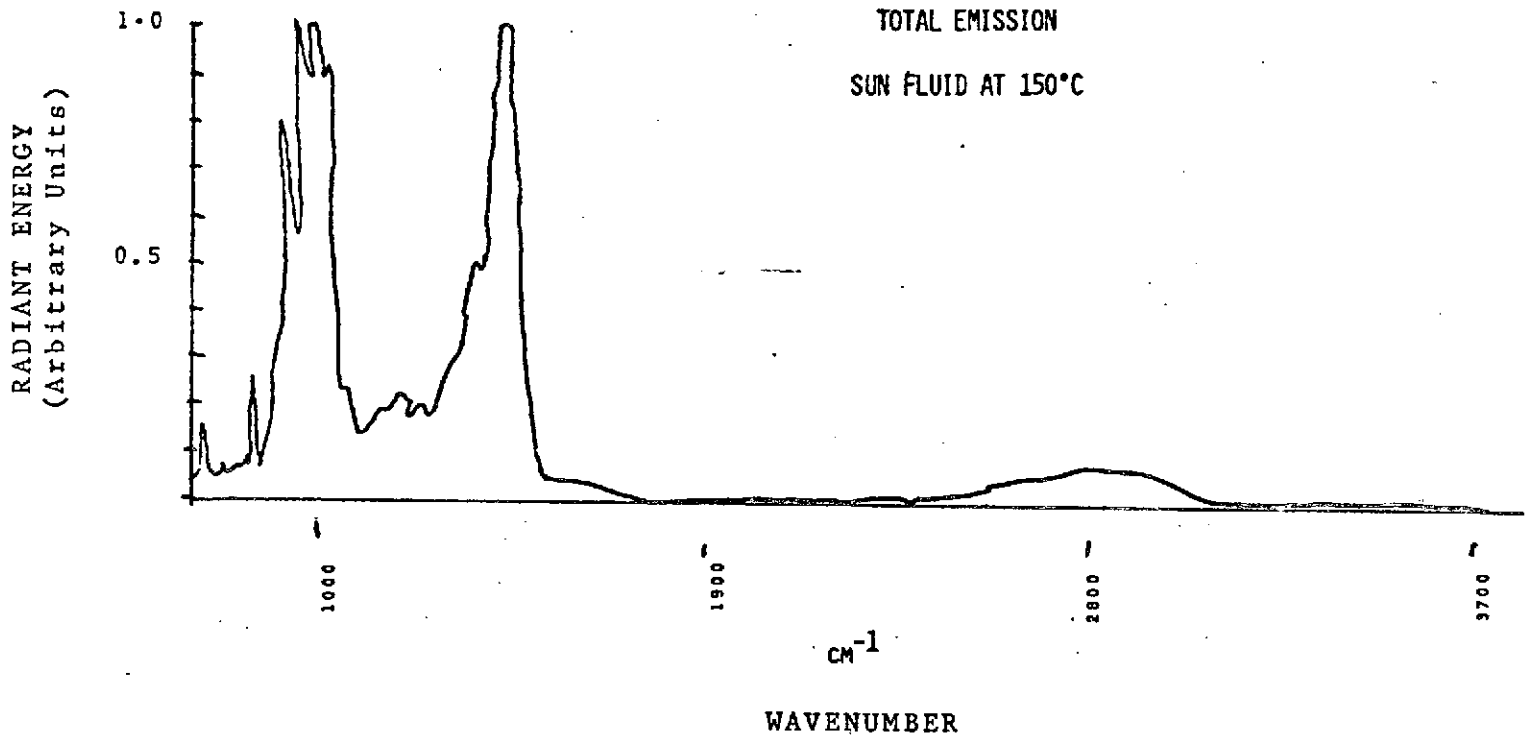

Fig. 33 - Sun Fluid at 150°C, Emission Spectrum at Ambient Pressure In Terms of Total Radiation

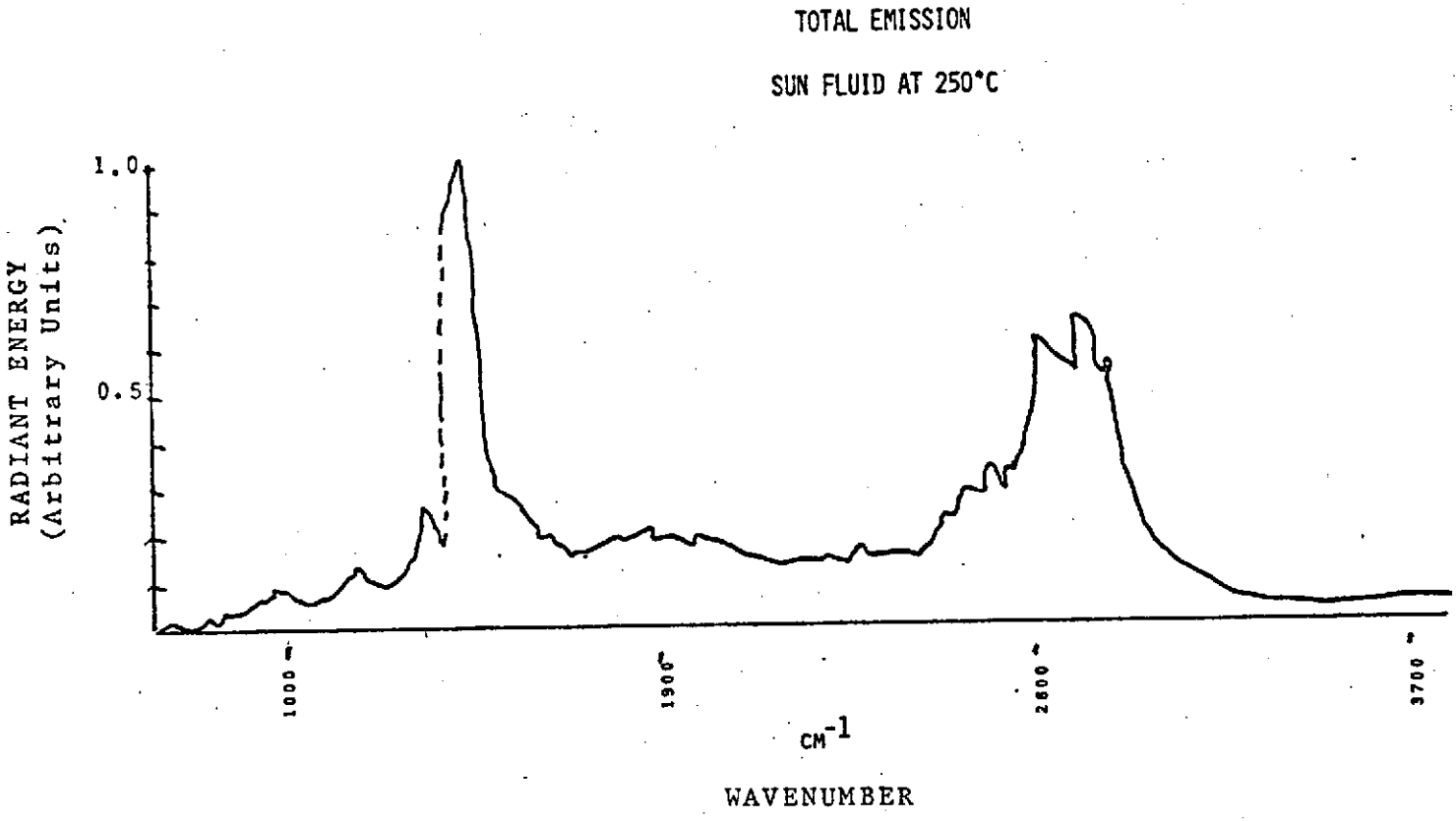

Fig. 34 - Sun Fluid at 250°C, Emission Spectrum at Ambient Pressure in Terms of Total Radiation

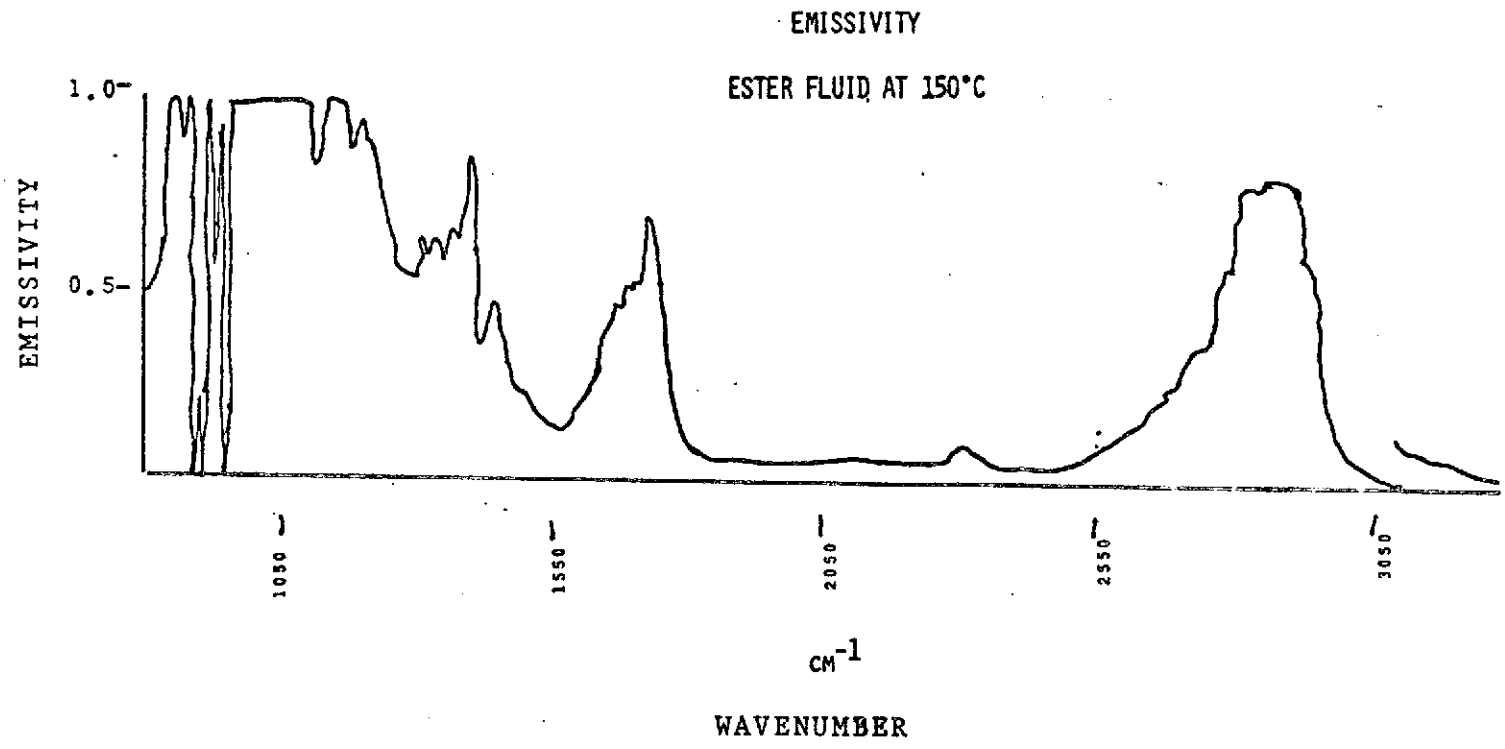

Fig. 35 - Ester Fluid at 150°C, Emissivity Spectrum

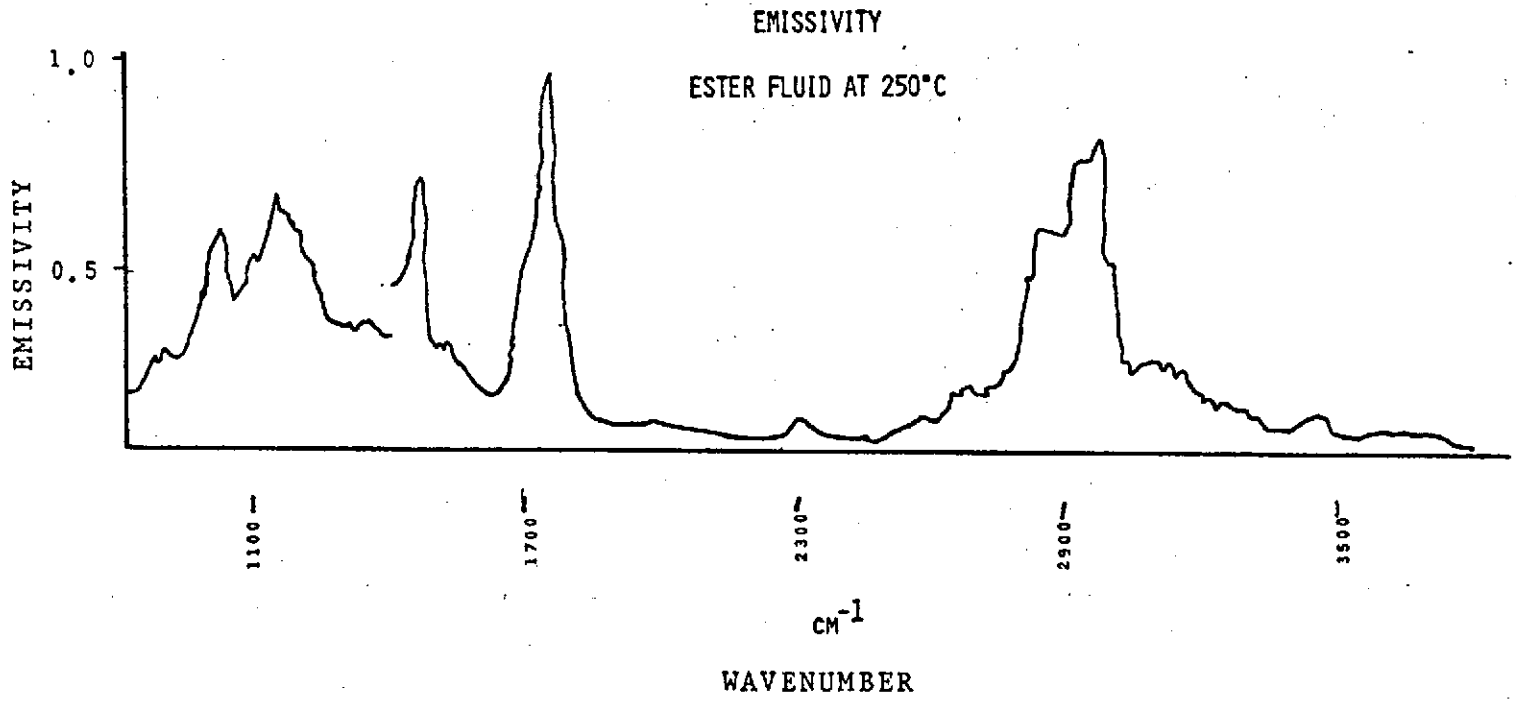

Fig. 36 - Ester Fluid at 250°C, Emissivity Spectrum

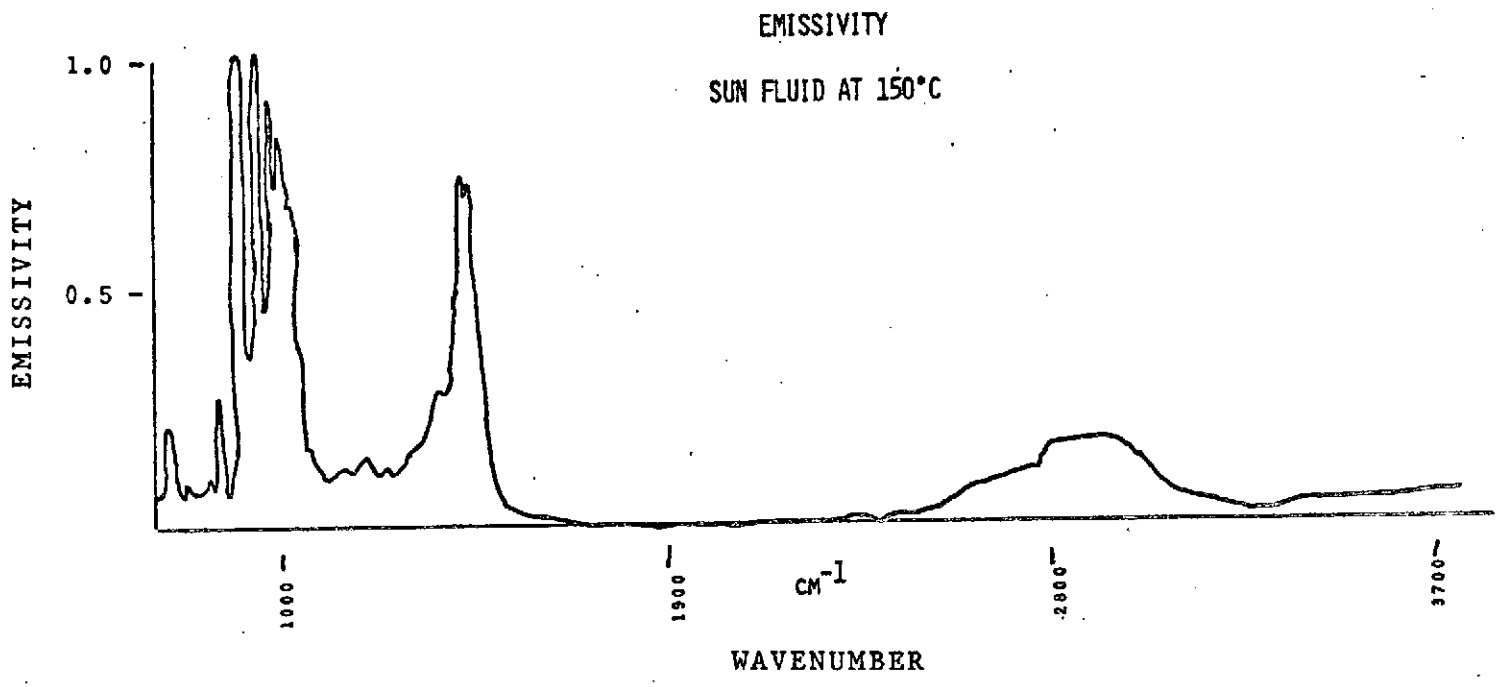

Fig. 37 - Sun Fluid at 150°C, Emissivity Spectrum

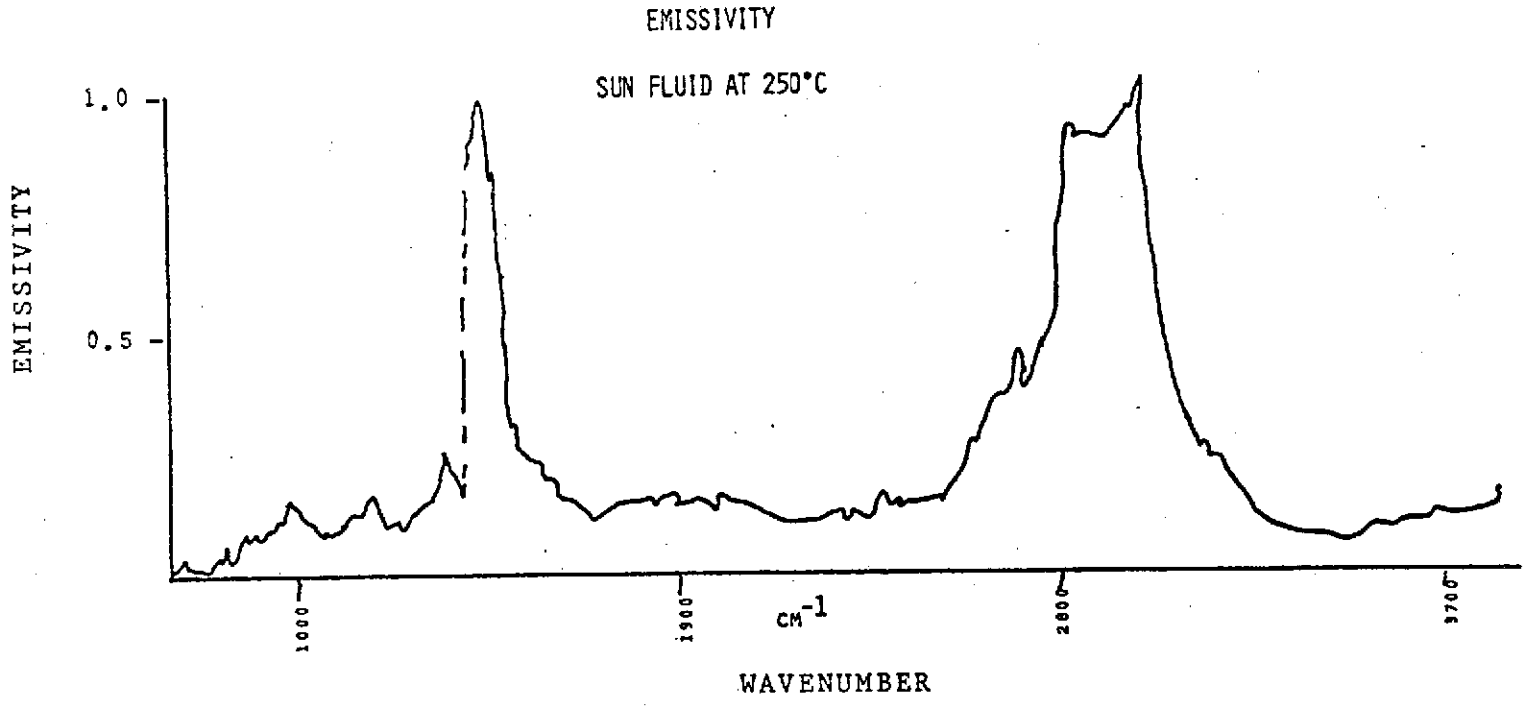

Fig. 38 - Sun Fluid at 250°C, Emissivity Spectrum

3.4 EMISSION SPECTRA OF THE FLUIDS AT HIGH PRESSURES AND ELEVATED TEMPERATURES

As described earlier in the experimental section, this was the most difficult work of this report period where the Interferometer-Microspectrometer showed its greatest value. Fig. 39 shows the first emission spectrum we obtained with the diamond cell in the 630-930 cm^{-1} region and, for comparison, the corresponding absorption spectrum is plotted on the same graph. The Sun fluid was chosen for the first experiments because it has a much richer absorption spectrum than the ester. The choice turned out to be a good one. It should be noted that the plot of Fig. 39 is exactly as it was obtained; while there is a contribution of "blackbody matter", it is not important enough to calculate it out to see the spectral features which correspond very well with those of the absorption spectrum. Fig. 40 shows the emission spectra of the same fluid at the same pressure, but at three different temperatures. It is obvious from the shapes of the bands that fluid temperature can be readily inferred from band shape changes in the emission bands. Since there is no doubt that these bands belong to the fluid, the temperatures inferred from them must be temperatures of the fluid. This observation shall prove to be very important when the technique will be applied to EHD contacts: The temperatures determined from the infrared emission spectra will be temperatures of the fluid -- not of other surfaces or of metallic debris, etc. Since direct calibrations will be involved, uncertainties regarding refractive indices, etc., which play a role in other methods of optical temperature determination, will not be present.

The changes of band shape with temperature in the case of the Sun Fluid are probably due to satellite bands. In the harmonic approximation a fundamental vibrational band should not change intensity with temperature. However, overtones and combination modes owe their existence largely to anharmonic behavior and are thus highly temperature-dependent. Rotational motion is coupled to the vibrational one; it is a major factor determining band shape and it is also viscosity-dependent. A study of the relationship between viscosity and bandshape for these and similar pure fluids is underway and will be used in later phases of this work.

Other plots of Sun Fluid emission spectra are shown in Figs. 41 to 46. Clearly pressure increases the background and the bandwidth. This may have to do with changes in band shape due to viscosity changes but it could also be caused by adsorption on metal surfaces. In one experiment where the internal surface of the back-diamond was covered with aluminum -- simulating the reflection of the ball surface in a ball-on-plate apparatus -- the background blackbody radiation was especially strong, even though great care was taken to have a good reflecting surface. Clearly much more work is needed.

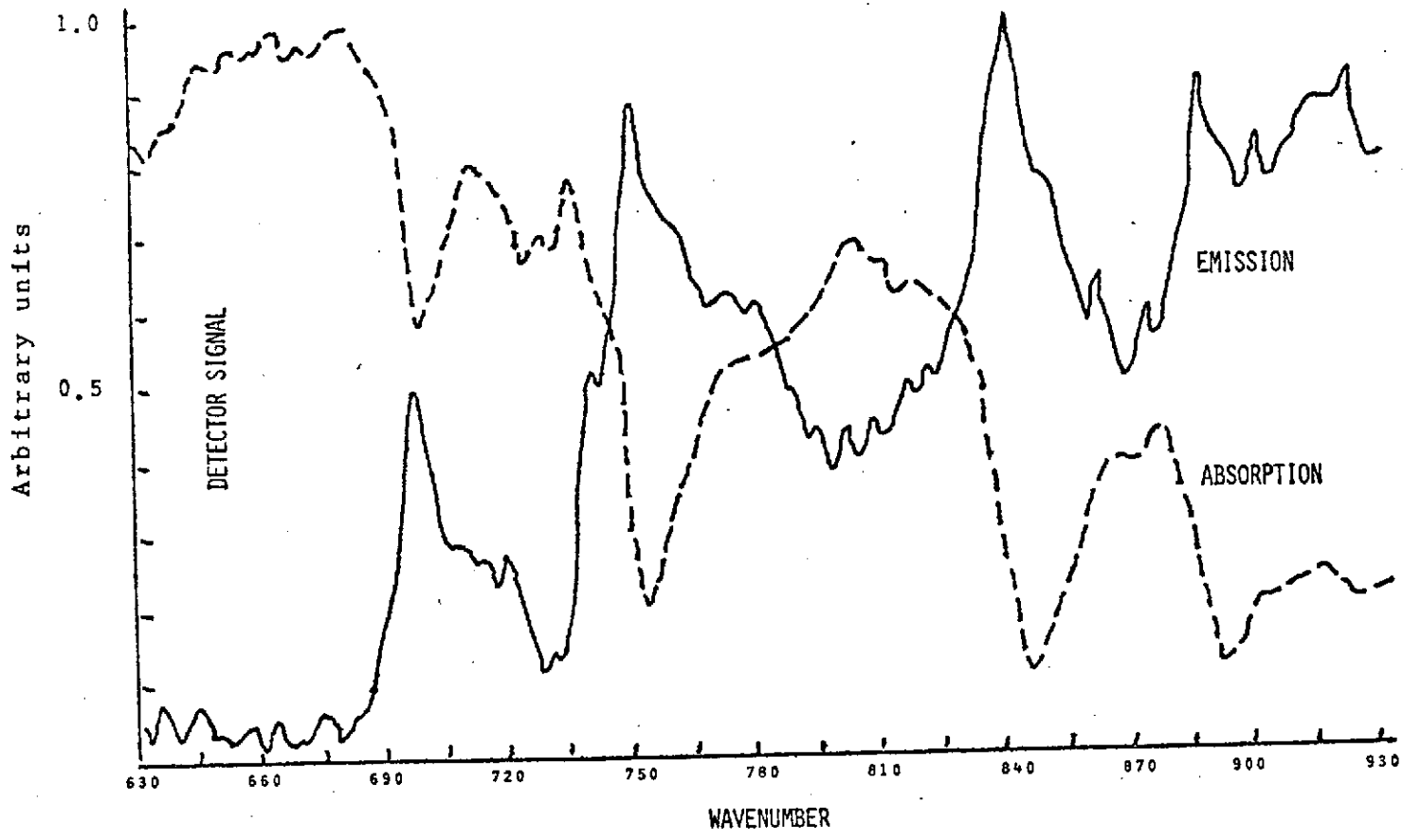

Fig. 39 - Comparison of Emission and Absorption Spectra of Sun Fluid at a pressure of 3 Turns ($\sim$ 0.4 GN/m^2) and a Temperature of 170°C. (Note that the vertical scales of both spectra were separately normalized to unity)

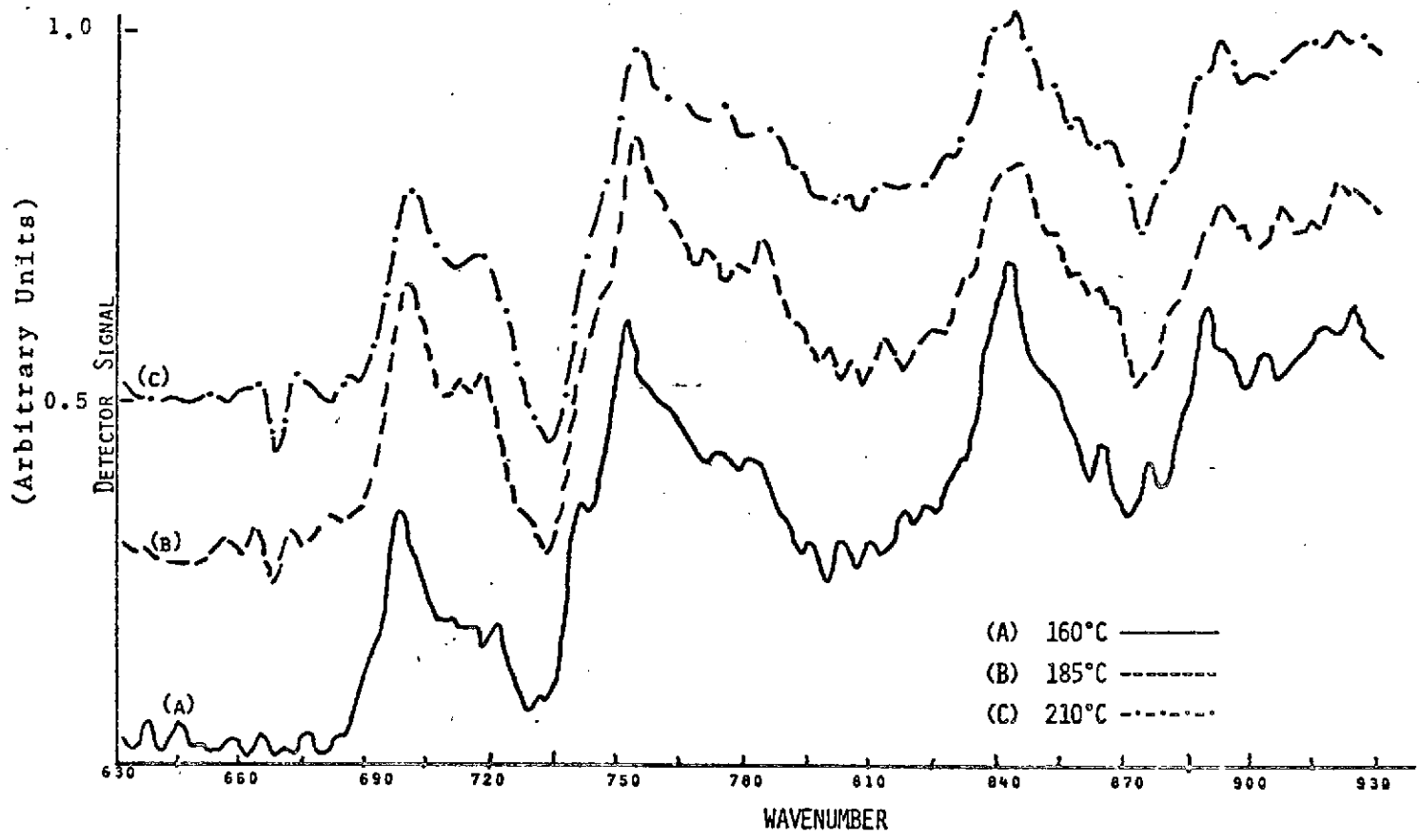

Fig. 40 - Emission Spectra of Sun Fluid at 0.4 GN/m^2 Pressure and At Temperatures of 160°, 185°, and 210°C. (Note that the ordinates of curves B and C are uniformly displaced upward)

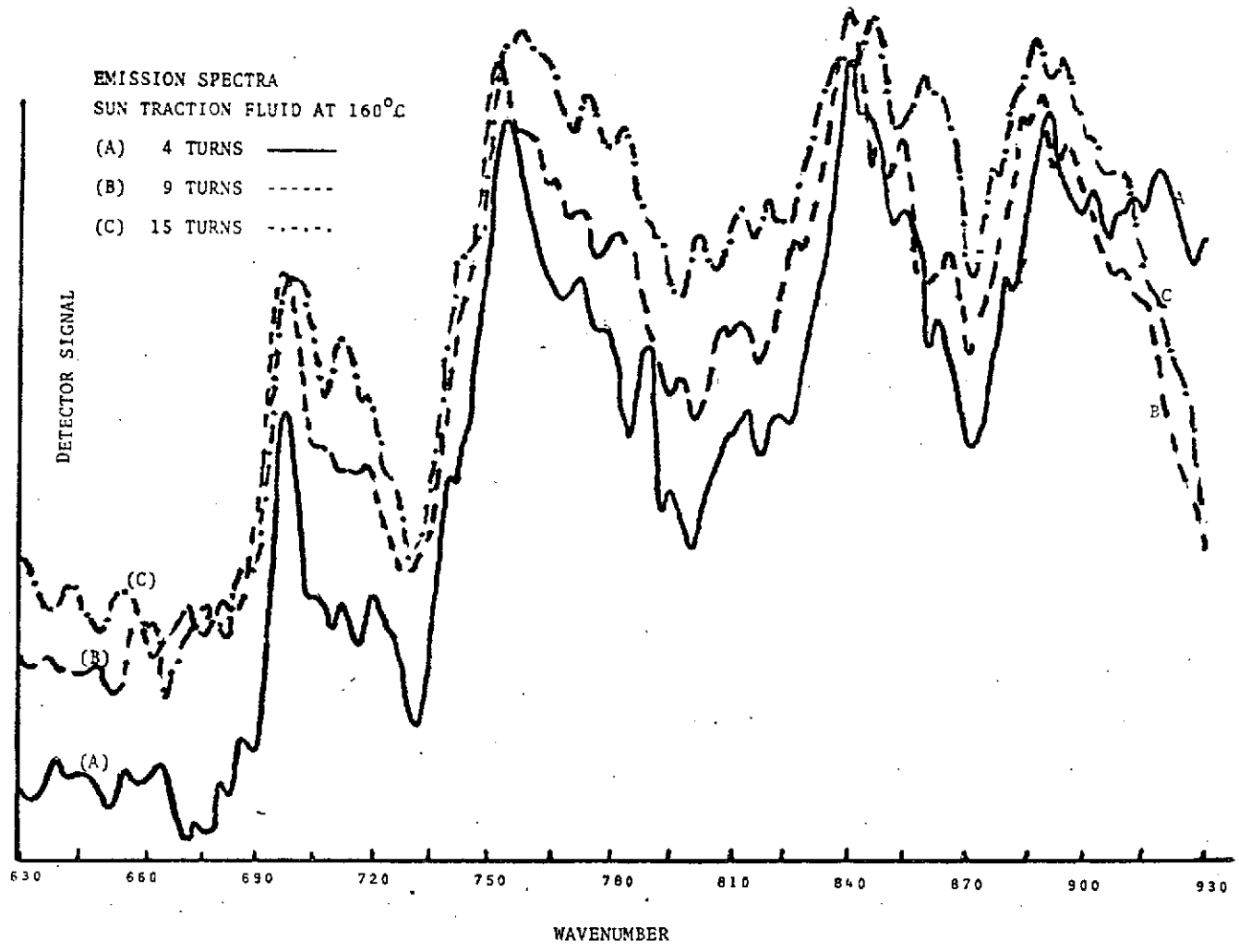

Fig. 41 - Emission Spectra of Sun Fluid at 160°C and at Pressures of 4, 9, and 15 turns (0.3, 1.2 and 2.4 GN/m^2). (Note that the ordinates of curves B and C are uniformly displaced upward).

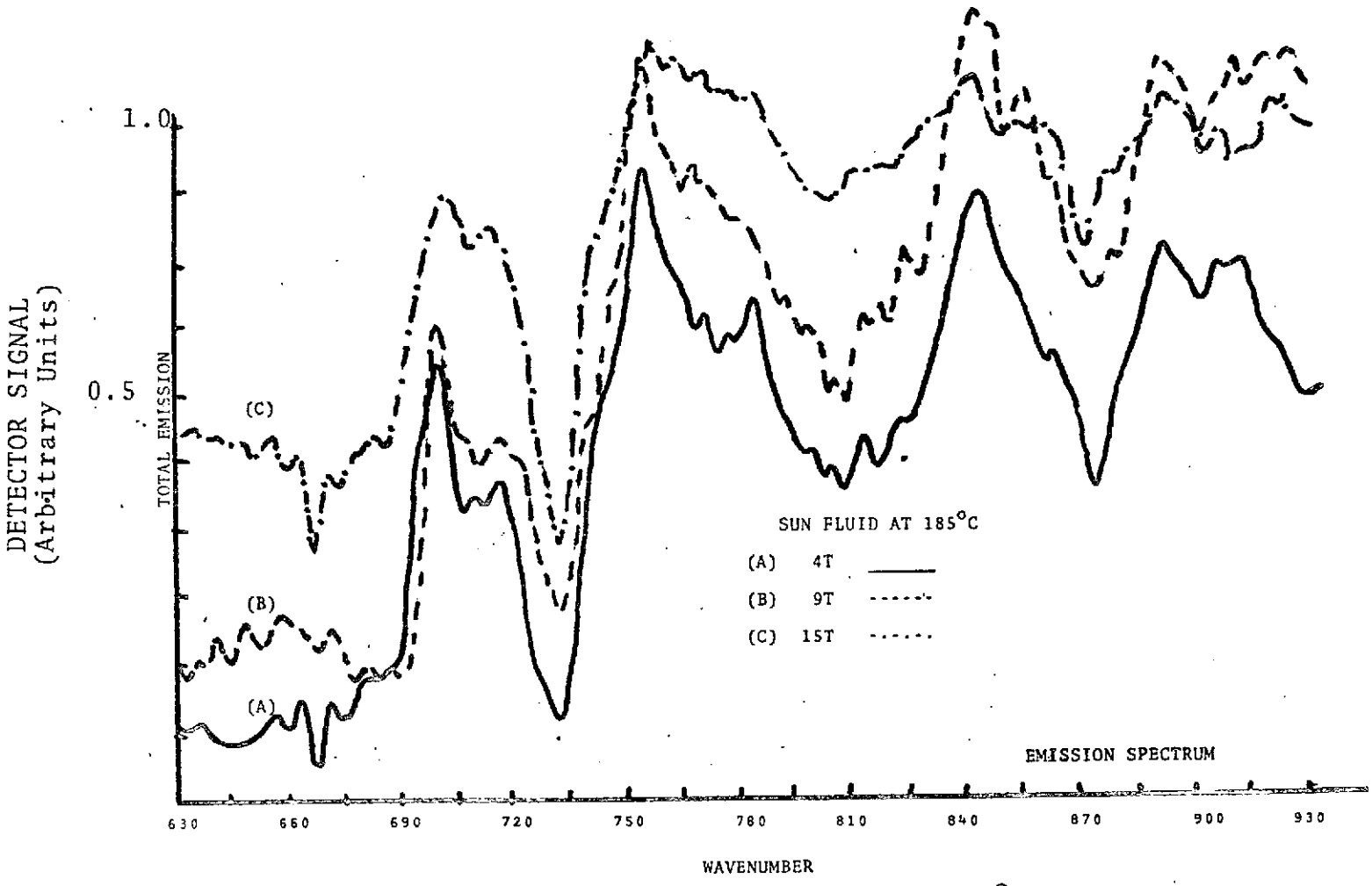

Fig. 42 - Emission Spectra of Sun Fluid at 185°C and at Pressures of 4, 9, and 15 Turns ($\sim$ 0.3, 1.2 and 2.4 GN/m^2). (Note that the ordinates of curves B and C are uniformly displaced upward).

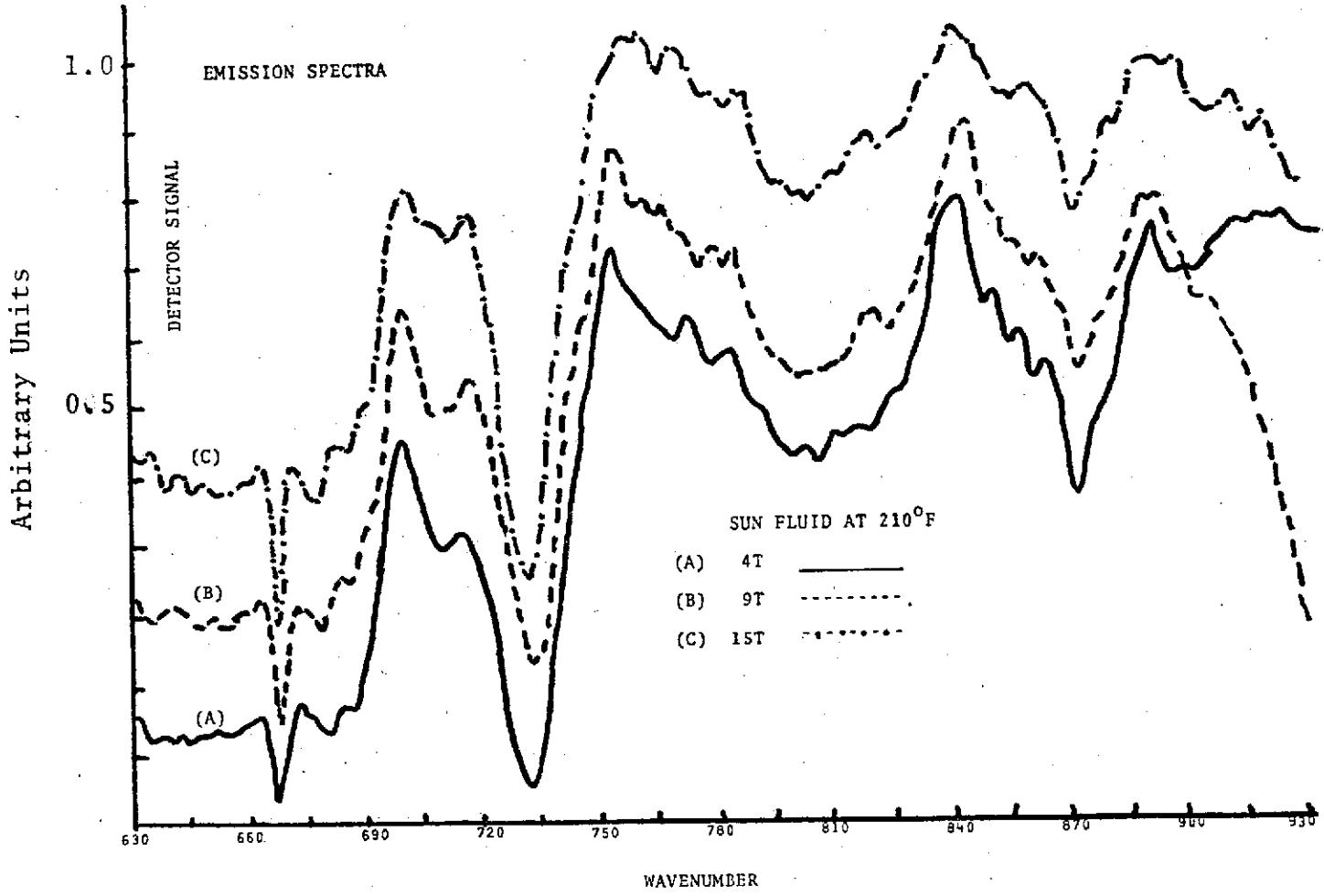

Fig. 43 - Emission Spectra of Sun Fluid at 210°C and at Pressures of 4, 9, and 15 Turns ($\sim$0.3, 1.2, and 2.4 GN/m^2). Note that the ordinates of curves B and C are uniformly displaced upward)

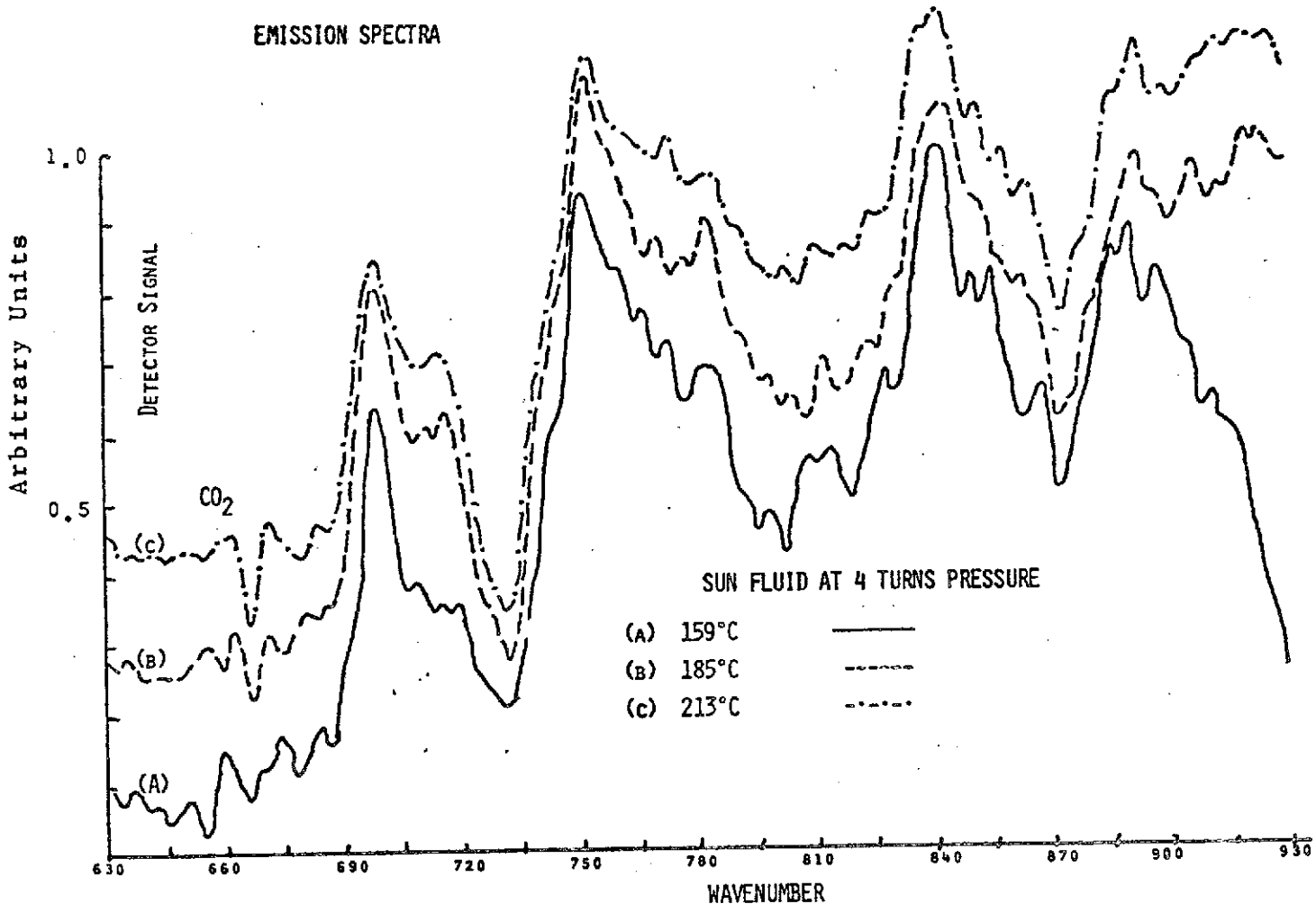

Fig. 44 - Emission Spectra of Sun Fluid at 4 turns Pressure ($\sim$ 0.3 GN/m^2) and at 159°, 185°, and 213 °C. (Note that the ordinates of curves B and C are uniformly displaced upward)

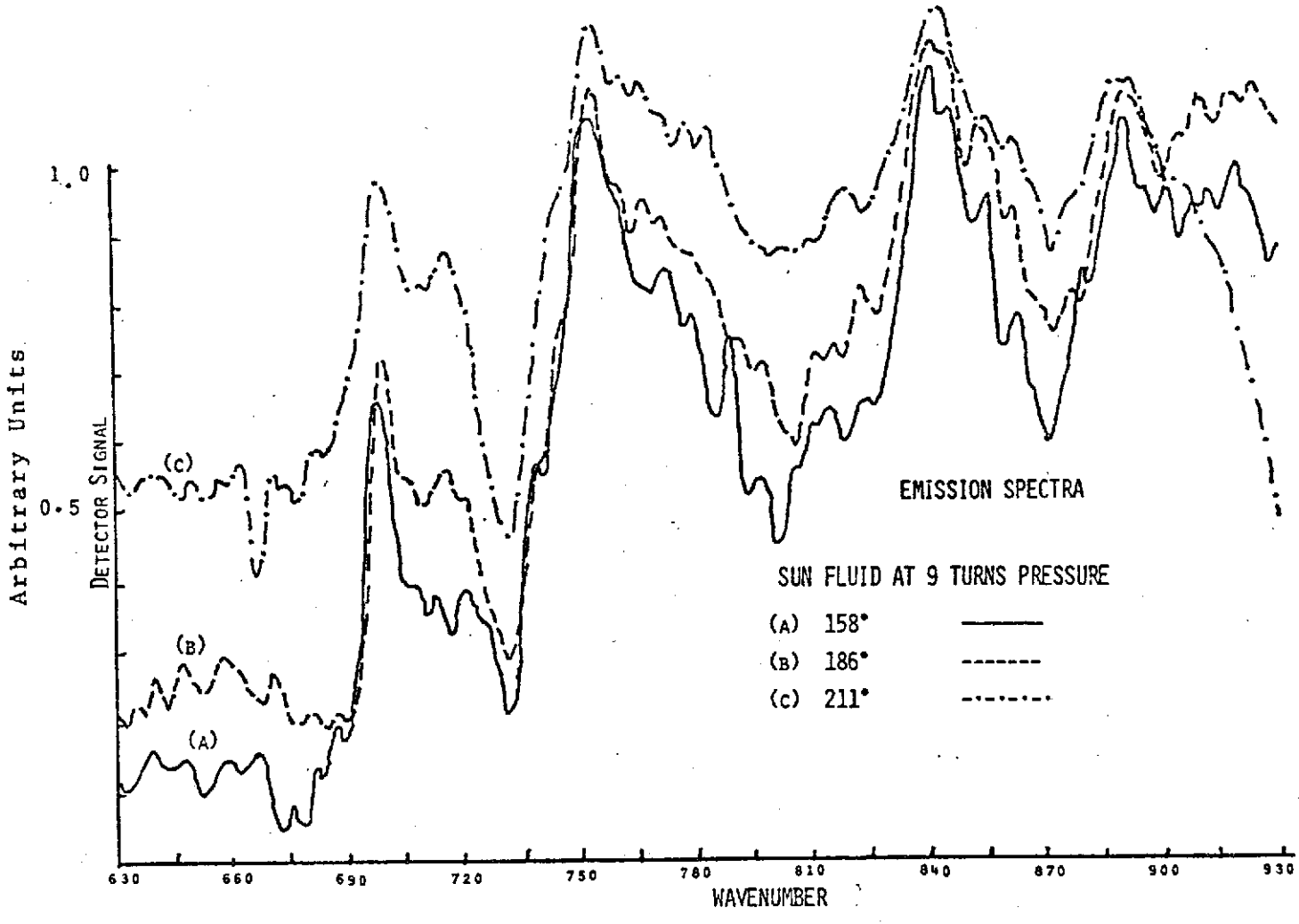

Fig. 45 - Emission Spectra of Sun Fluid at 9 Turns Pressure ($\sim$ 1.2 GN/m^2) and at 158°, 186°, and 211 °C. (Note that the ordinates of curves B and C are uniformly displaced upward.)

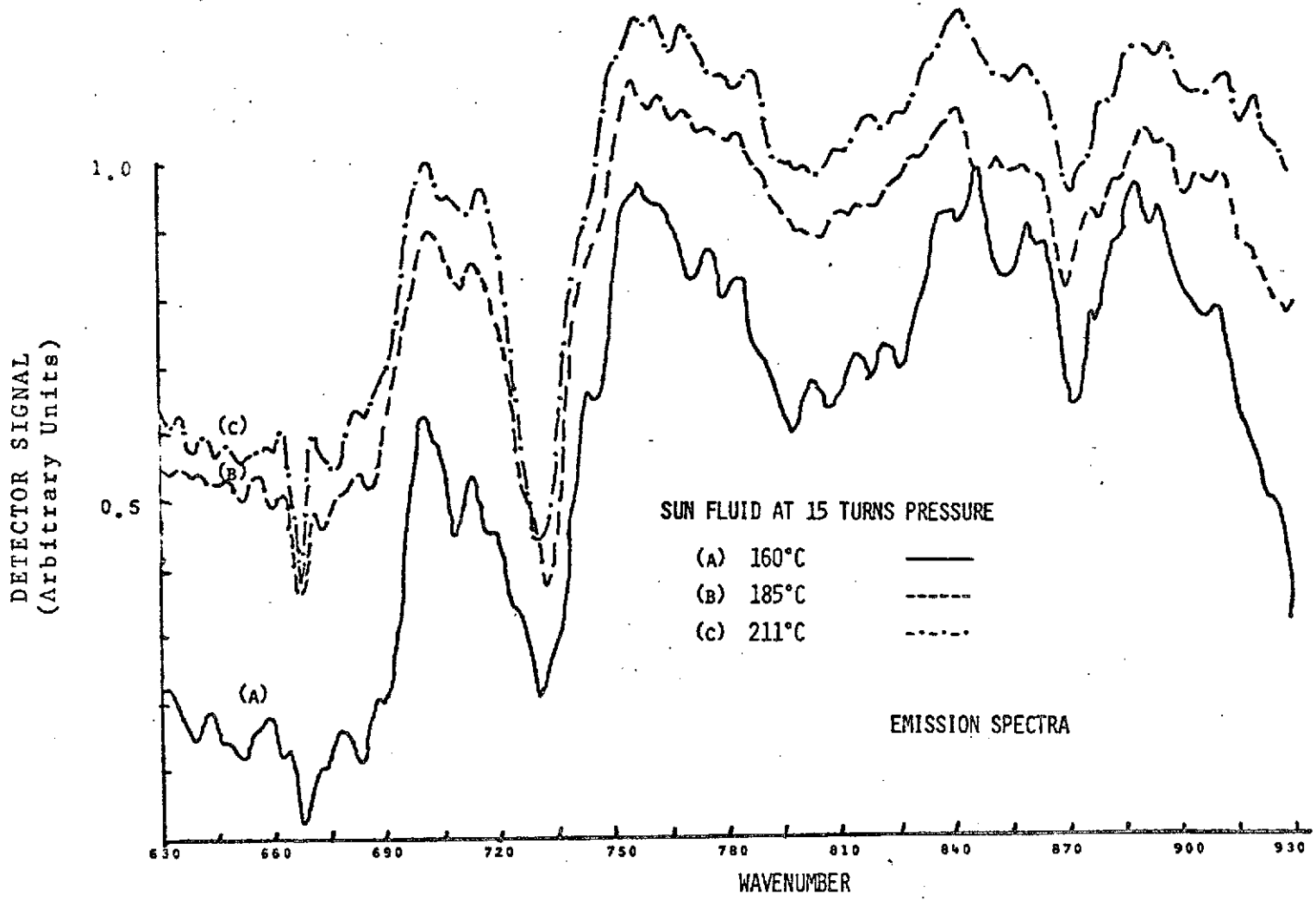

Fig. 46 - Emission Spectra of Sun Fluid at 15 Turns Pressure (~ 2.4 GN/m^2) and at 160°, 185°, and 210°C. (Note that the ordinates of curves B and C are uniformly displaced upward.)

The emission spectra from the ester exhibited much stronger blackbody background radiation than those of the Sun Fluid (Figs. 47 to 52). Here, in order to obtain characteristic emission spectra from the fluid, the procedure of Equation (7) (page), had to be applied. These are shown in Figs. 53 - 55. They show essentially only the principal CH_2 - rocking band near 728 cm^{-1}. Improved procedures of data processing (smoothing, etc.) are now being worked on.

The main aspects of these spectra are similar to those of the absorption spectra wherever the same temperature could be used. As mentioned, with modifications now in progress it will be possible to lower the temperatures for emission spectra and to enhance the signal to noise ratio.

3.5 BALL-ON-PLATE APPARATUS AND SPECTRA UNDER DYNAMIC CONDITIONS

Figure 56 shows diagramatically an optical layout of the ball-on-plate apparatus already built. Because of alignment problems -- the optical lever is too long -- the design was changed to what is essentially a four-ball tester and the optics will be identical with those now used for emission spectra from the diamond cell, i.e. the radiation will enter the source compartment of the interferometer through a window in the bottom of a cup. The radiation emitted from the EHD contact will again be imaged at the source location and brought into a horizontal plane by a 45° plane mirror. The ball-on-plate apparatus will be located above the interferometer. It will be very similar to the setup used by Professor Winer, with whom we consulted.

A preliminary experiment (already referred to) with the diamond cell, in which a piece of aluminum foil was used as a back reflector simulating the ball of the ball-on-plate apparatus, showed that a mirror surface of highly conducting metal is needed for reflection or graybody radiation will be excessive. Accordingly a silver ball may be required for the dynamic work. It will be mounted on a flexible shaft.

As already mentioned, it will be necessary to record emission spectra of fluids at temperatures below 150°C and of much thinner layers of material than those employed now. For this purpose the signal/noise ratio of the interferometer will have to be significantly improved. (The installation of some improvement is expected to come from a cold reference source, e.g. a block of dry ice, in a way similar to that used by Low.[15] The detector will alternatingly look at the cold source and at the EHD contact region.) Thus we expect to replace most of our electronic circuitry, which partly failed us and which is now obsolete in any case, with new advanced circuitry of better noise characteristics. (A new analog/digital converter has already been installed with new punch output boards, a new phase-sensitive amplifier is expected to be here soon.) These

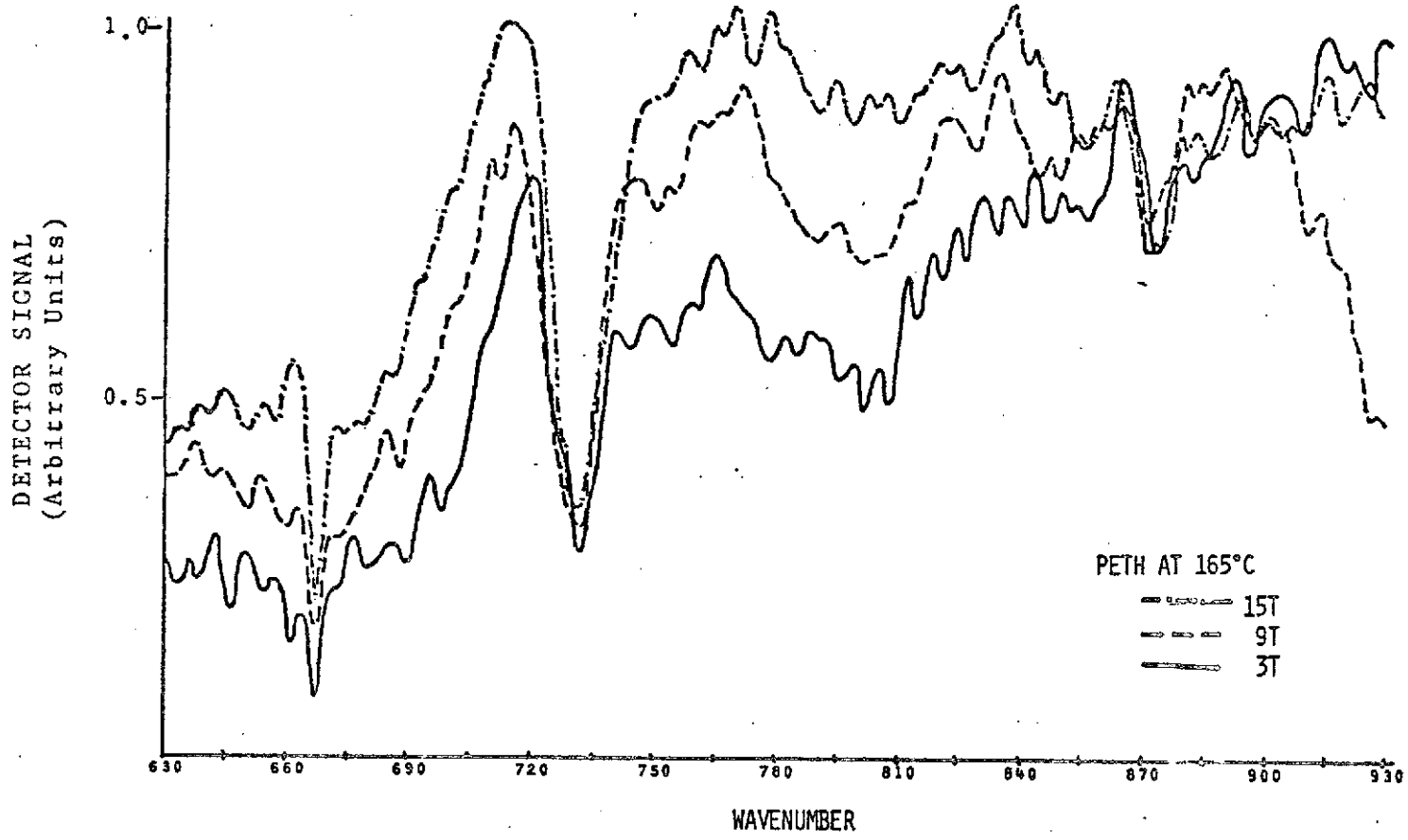

Fig. 47 - Emission Spectra of Ester Fluid at 165°C and at Pressures of 3, 9, and 15 Turns ($\sim$ 0.3, 1.2, and 2.4 GN/m^2). (Note that the ordinates of curves B and C are uniformly displaced upward.)

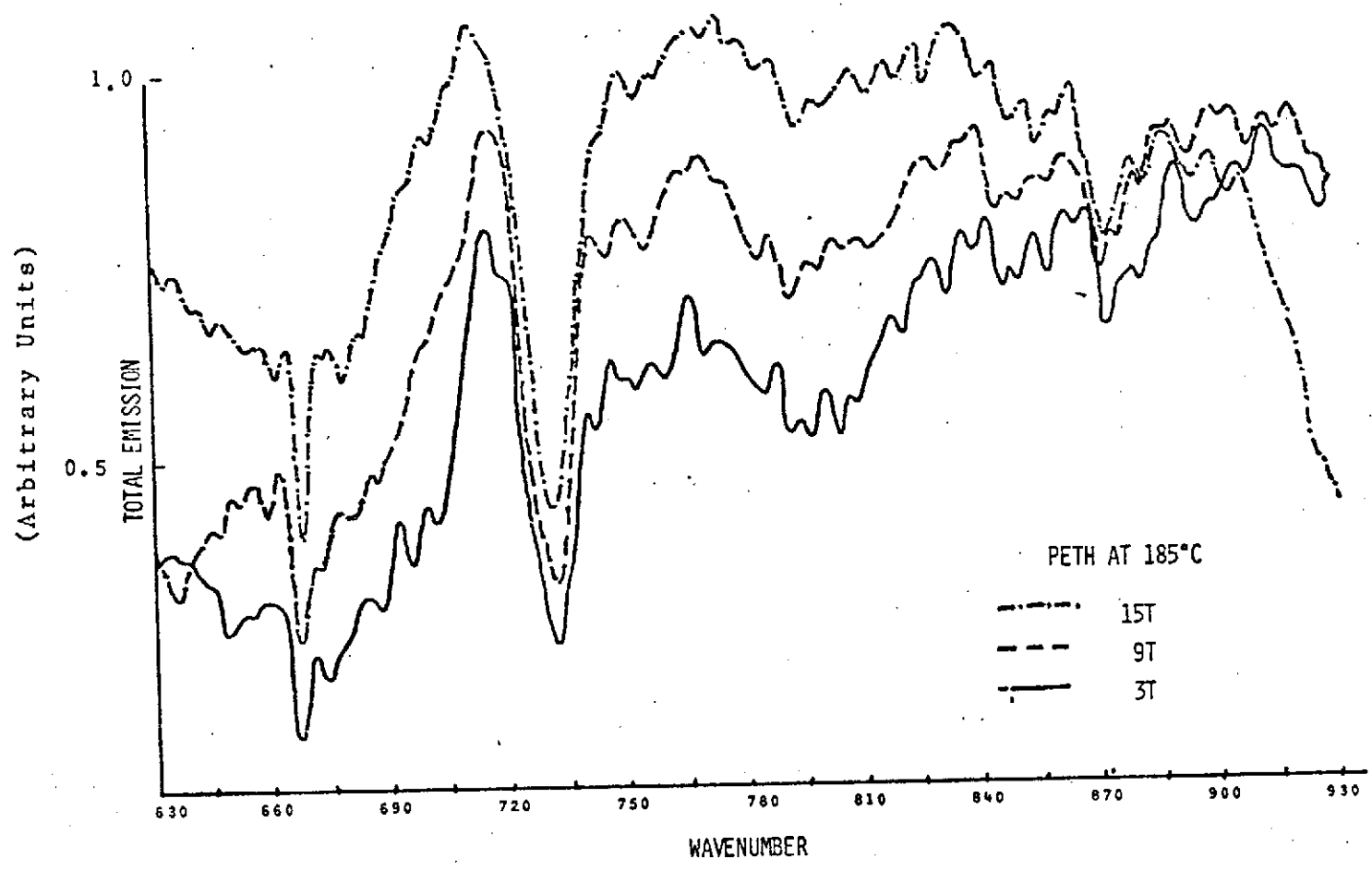

Fig. 48 - Emission Spectra of Ester Fluid at 185°C and at Pressures of 3, 9, and 15 Turns (∿ 0.3, 1.2, and 2.4 GN/m^2). (Note that the ordinates of curves B and C are uniformly displaced upward.)

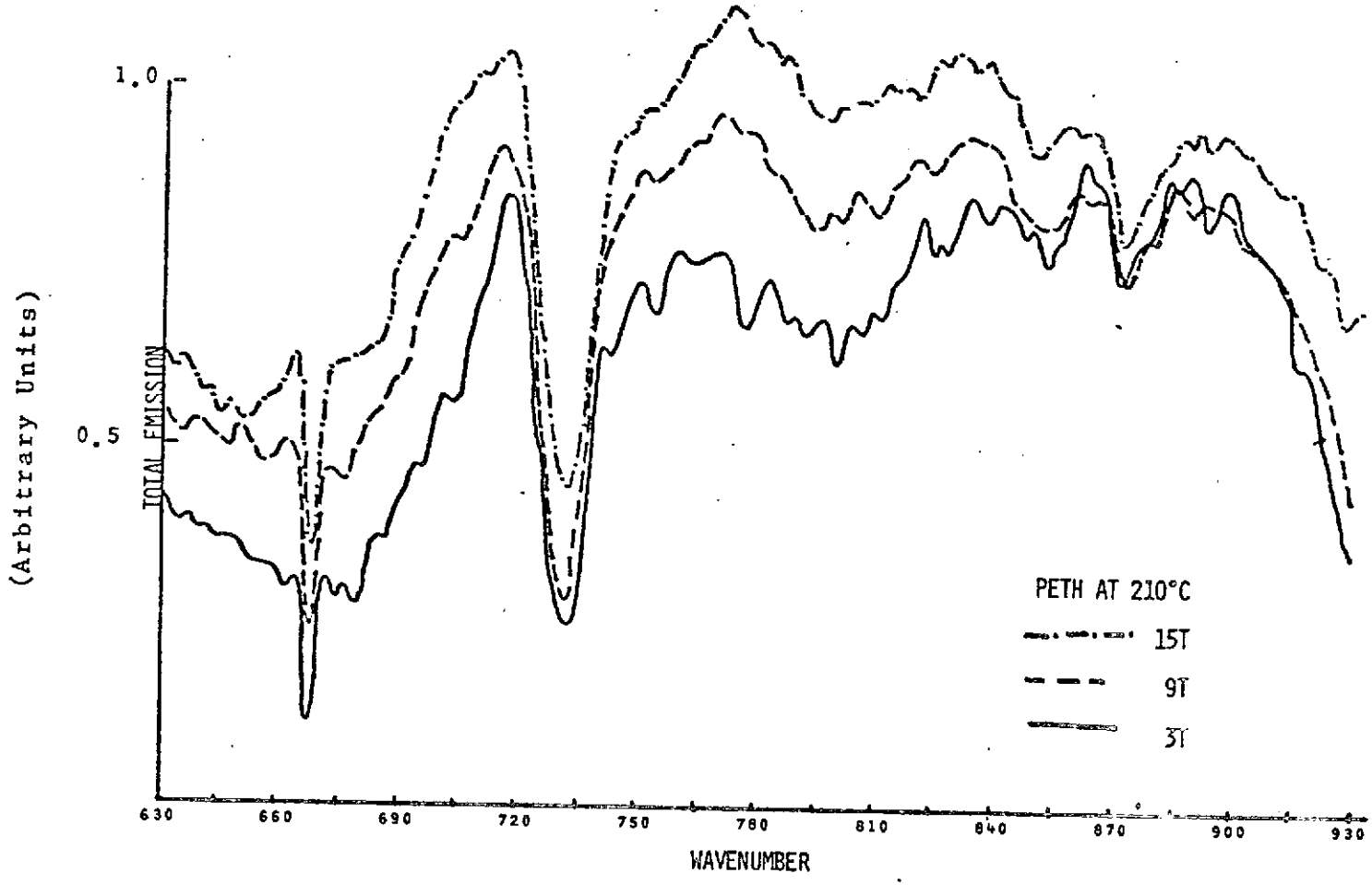

Fig. 49 - Emission Spectra of Ester Fluid at 210°C and at Pressures of 3, 9, and 15 Turns ($\sim$ 0.3, 1.2, and 2.4 GN/m^2) (Note that the ordinates of curves B and C are uniformly displaced upward.)

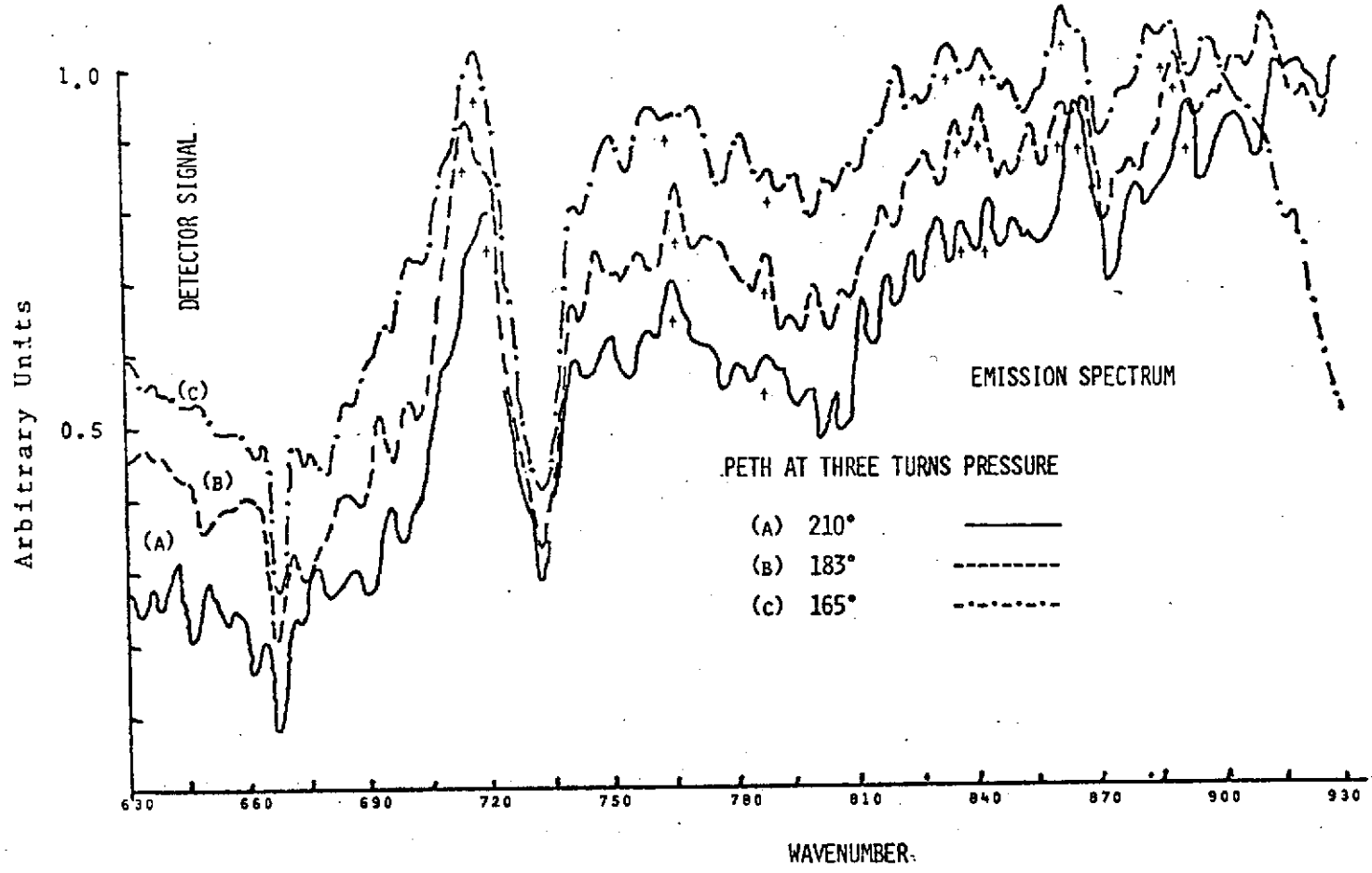

Fig. 50 - Emission Spectra of Ester Fluid at 3 Turns Pressure (~ 0.3 GN/m^2) and at 165°, 183°, and 210°C. (Note that the ordinates of curves B and C are uniformly displaced upward.)

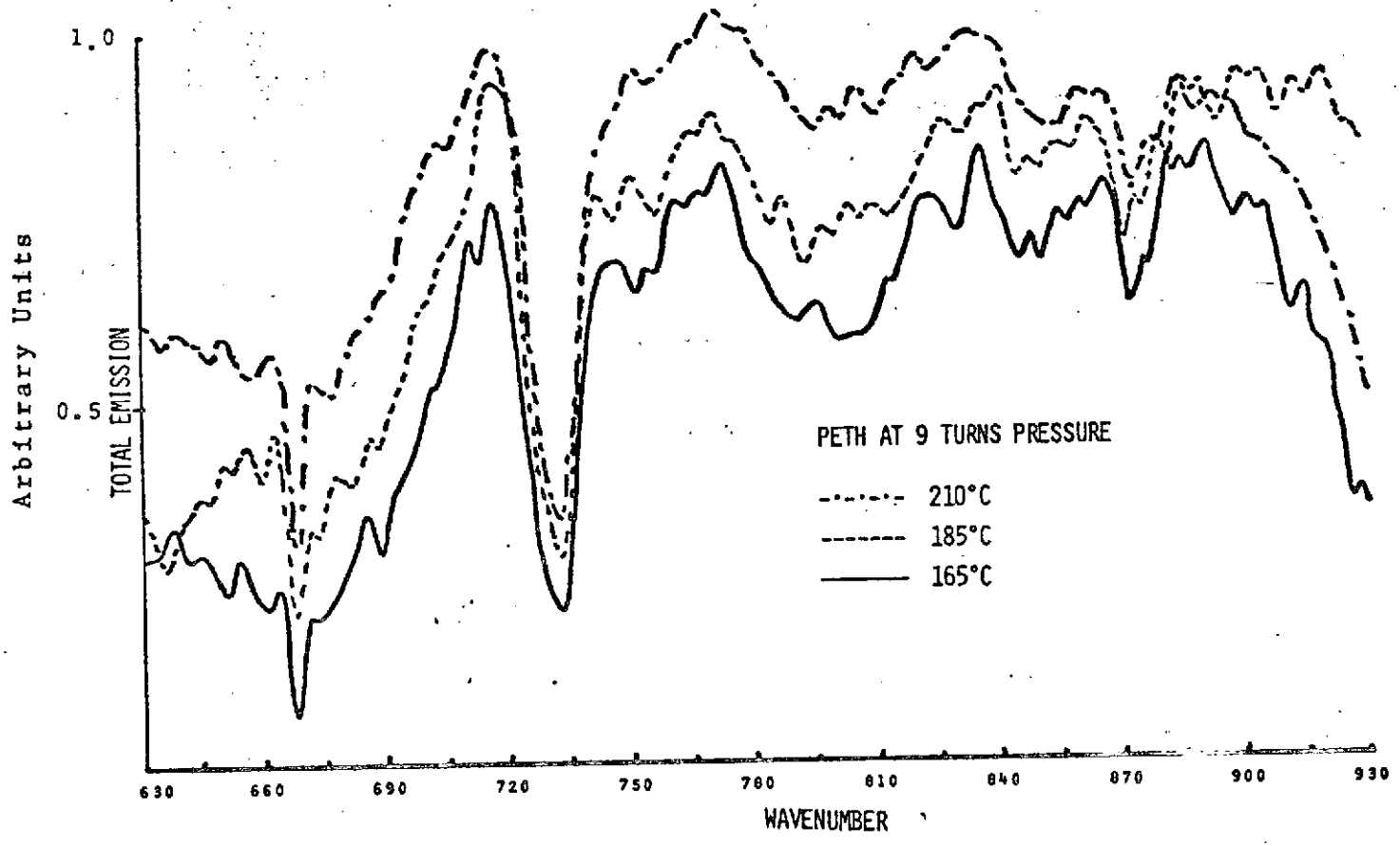

Fig. 51 - Emission Spectra of Ester Fluid at 9 Turns Pressure (~ 1.2 GN/m^2) and at 165°, 185°, and 210°C. (Note that the ordinates of curves B and C are uniformly displaced upward.)

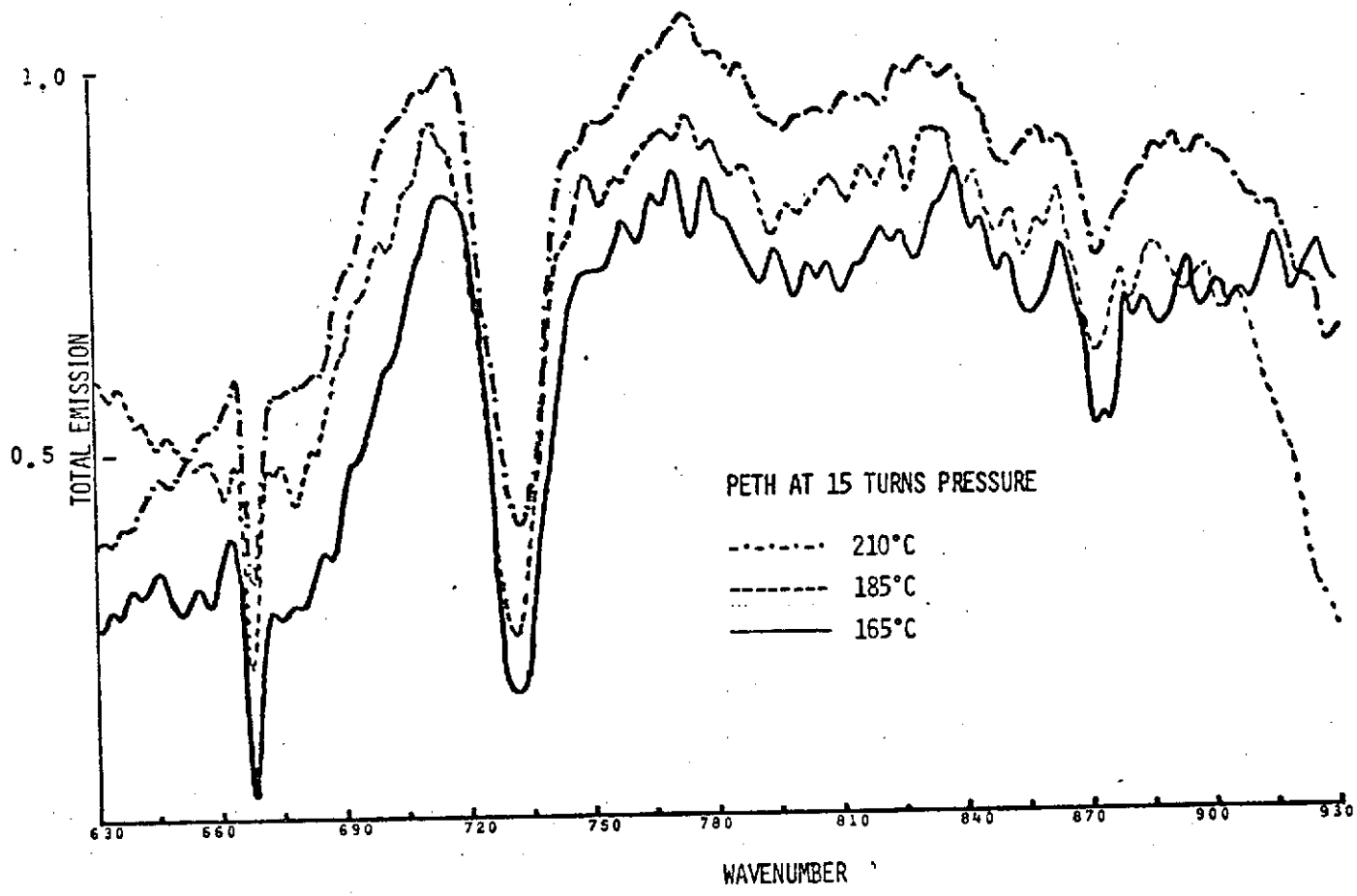

Fig. 52 - Emission Spectra of Ester Fluid at 15 Turns Pressure (~ 2.4 GN/m^2) and at 165 °, 185°, and 210°C. (Note that the ordinates of curves B and C are uniformly displaced upward.)

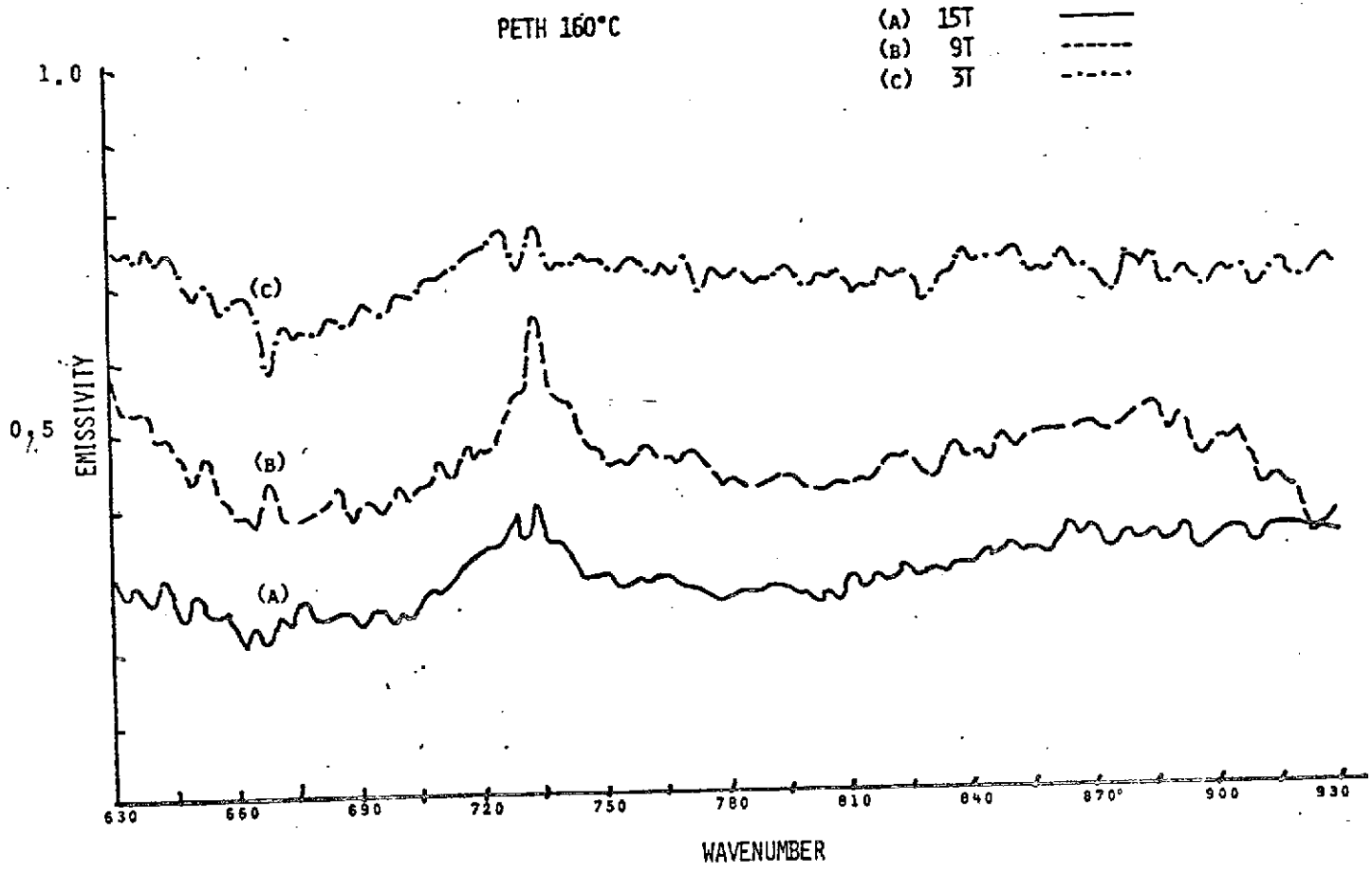

Fig. 53 - Emission Spectra of the Ester Fluid, After Background Sub-Traction, at 160°C and Pressures of 3, 9, and 15 Turns ($\sim$ 0.3, 1.2, and 2.4 GN/m^2). (Note that the ordinates of curves B and C are uniformly displaced upward.)

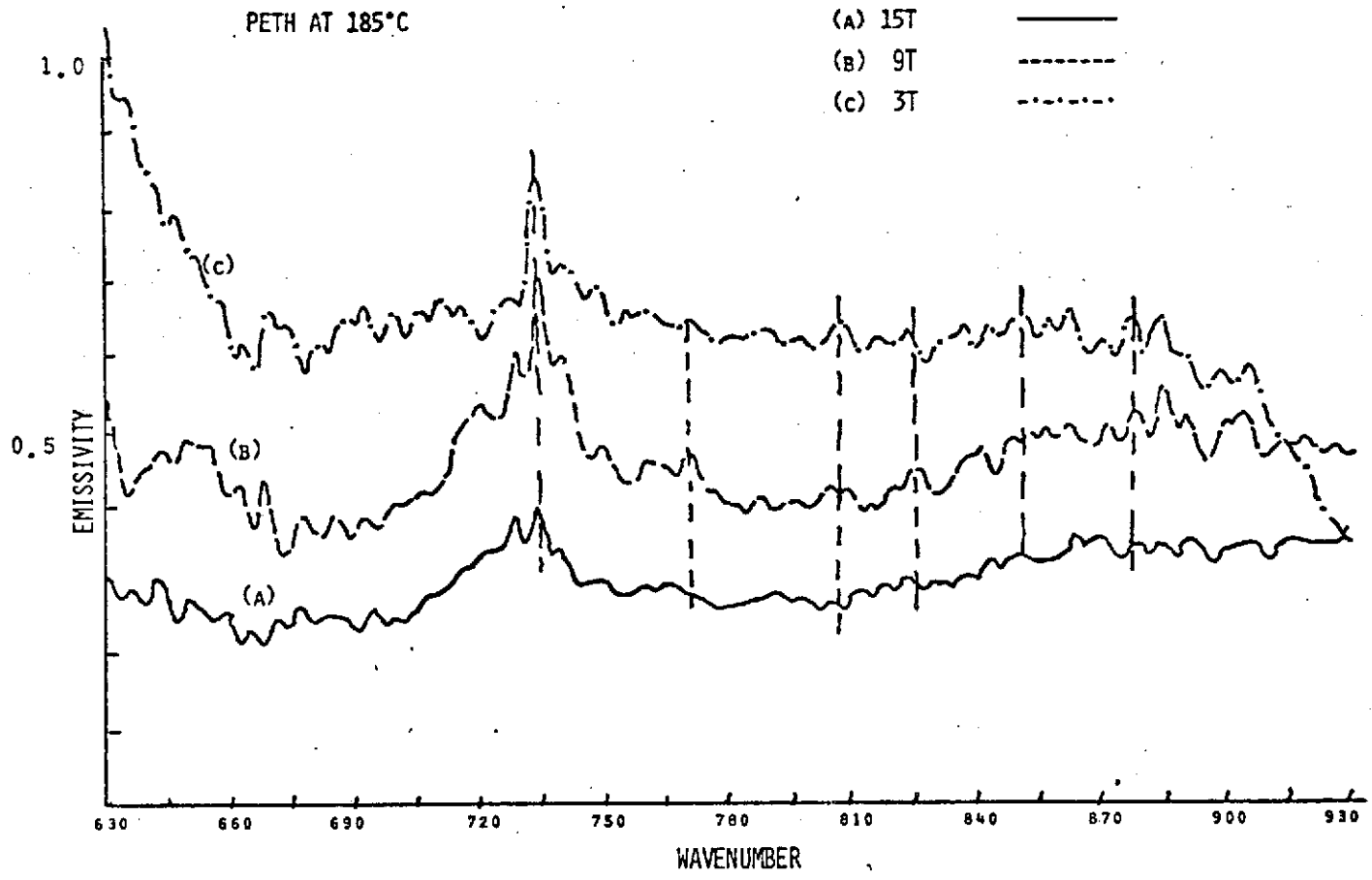

Fig. 54 - Emission Spectra of the Ester Fluid, After Background Subtraction, at 185°C and Pressures of 3, 9, and 15 Turns (~ 0.3, 1.2, and 2.4 GN/m^2). (Note that the ordinates of curves B and C are uniformly displaced upward.)

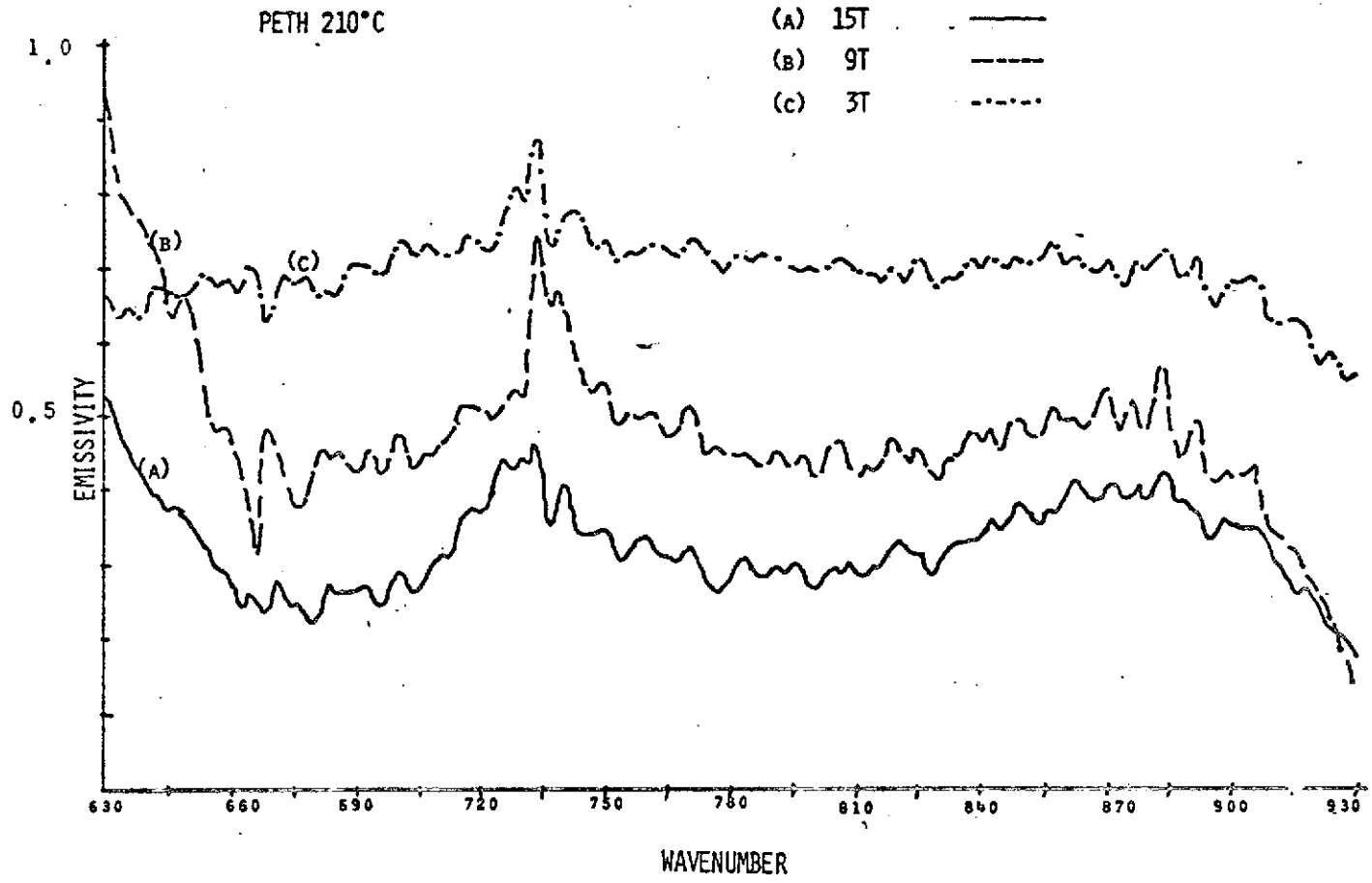

Fig. 55 - Emission Spectra of the Ester Fluid, after Background Sub-Traction, at 210°C and Pressures of 3, 9, and 15 Turns (~ 0.3, 1.2, and 2.4 GN/m^2).

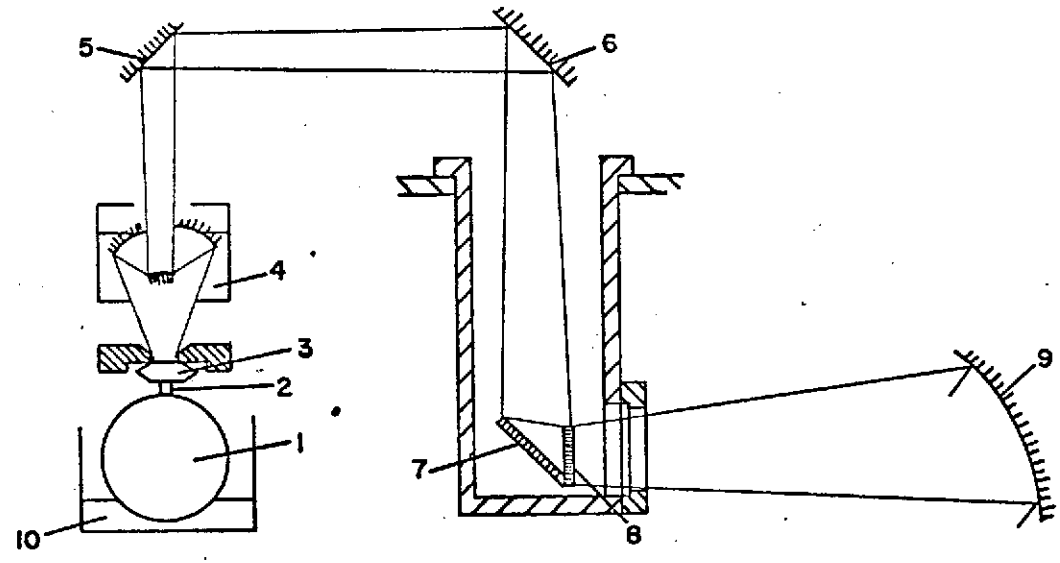

1. ROTATING BALL
2. EHD CONTACT
3. DIAMOND ANVIL
4. BECK 15X REFLECTING OBJECTIVE
5. PLANE MIRROR
6. PLANE MIRROR
7. PLANE MIRROR
8. REAL IMAGE OF EHD CONTACT
9. COLLIMATING MIRROR
10. FLUID RESERVOIR

Fig. 56 - Adapter Considered for Measuring Emission Spectra From a Ball-On-Plate Apparatus

changes will also increase our sensitivity. The improvement of our already extensive software has also been a continuing process.

A new Beck Objective 36X has been ordered to take the place of our present 15X lens. With the new lens a field only 0.5 mm in diameter will provide the same energy (because of the greater solid angle) as the present lens. With the help of masks in the image plane, an attempt will be made to scan smaller portions of the EHD contact region. If successful, we may even substitute a 72X objective, for we think we could approach the EHD region more closely than the high pressure area of our diamond cell (increased magnification implies a shorter distance from lens to object). We will then be in a position to determine fluid temperatures directly from emission band contours in different regions of the Hertzian contact and, hopefully, find new chemical species as well. Since we can deduce film thickness from spectral density, we might be able to correlate chemical fluid degradation with film thickness and temperature. By excluding unwanted graybody radiations the new Beck lenses should improve the effective strength of fluid infrared smission.

Furthermore the spectral region studied may be expanded beyond the present 630-930 cm^{-1} spread. Another region may be preferable in view of the thinner fluid films, lower temperatures and other factors encountered in the dynamic situation and, of course, with different fluids. In fact, our present interferometer scans with the diamond cell contain spectral information from 930-1100 cm^{-1}, which can be readily calculated from the available data when time permits. With some instrument modifications, it might be possible to extend our range to 2000 cm^{-1} and beyond or to below 630 cm^{-1}.

4. CONCLUDING REMARKS

Infrared absorption and emission spectra have been obtained for two fluids in the 630-930 cm^{-1} range under static conditions. Spectral changes indicative of phase changes have been found at pressures between ambient and 2 GN/m^2 and temperatures between ambient and 210°C. The present work provides a firm basis for similar work under dynamic EHD conditions.

APPENDIX A

LIST OF SYMBOLS USED

Symbol	Description
c	Apparatus constant related to radiation measurements
C_o	Velocity of light in vacuo
C_1	First radiation constant in Planck's equation
C_2	Second radiation constant in Planck's equation
d	Fluid layer thickness
E_B	Energy radiated from cell containing a gray-body and dispersed and analyzed by a grating spectrophotometer
E_C	Energy radiated from empty cell and dispersed and analyzed by grating spectrophotometer
E_N	Energy radiated from a Nernst glower and dispersed and analyzed by grating spectrophotometer
E_S	Energy radiated from cell containing a fluid sample and dispersed and analyzed by grating spectrophotometer
$E\ (T_B)$	Energy radiated by a blackbody at temperature T_B
$E\ (T_C)$	Energy radiated by chopper blade, regarded as a blackbody at temperature T_C
$E\ (T_S)$	Energy radiated by a blackbody at temperature T_S
F_B	Attenuation factor of screen used to read R_B
F_C	Attenuation factor of screen used to read R_C

Symbol	Description
F_S	Attenuation factor of screen used to read R_S
G_B	Interferometer-spectrometer gain corresponding to signal S_B
G_S	Interferometer-spectrometer gain corresponding to signal S_S
h	Plank's constant
I	Sum of radiant fluxes I_1 and I_2
I_1	Radiant flux transmitted by a hot liquid film normally through its boundary
I_2	Radiant flux reflected by a metal surface at one boundary of a hot liquid film and transmitted normally through the other boundary
k	Boltzmann's constant
$k(\omega,t)$	Absorption coefficient at wavenumber ω and temperature t
$n=n(\omega,t)$	Index of refraction of fluid at wavenumber ω and temperature t
$p(\omega,t)$	Radiant power per unit volume in the wavenumber region ω to $\omega + d\omega$ at temperature t
$R = R(\omega,t)$	Reflectivity, i.e. ratio of energy reflected to energy incident in the wavenumber region ω and $\omega + d\omega$ at temperature t
R_B	Reading on "Percent Transmission" scale of grating spectrophotometer for infrared transmission from cell containing a graybody
$R_b(\omega,t)$	Radiant flux emitted by a blackbody in the wavenumber region ω and $\omega + d\omega$ at temperature t
R_C	Reading on "Percent Transmission" scale of grating spectrophotometer for infrared transmission from cell containing air
R_S	Reading on "Percent Transmission" scale of grating spectrophotometer for infrared transmission from cell containing a fluid sample

Symbol	Description
S_B	Interferometer-spectrometer detector signal at wavelength λ or wavenumber ω resulting from the radiation of a blackbody reference at temperature T_B when the chopper blade temperature is T_C
S_F	Interferometer-spectrometer signal at wavelength λ or wavenumber ω resulting from the radiation of only the fluid at temperature T_S in a diamond cell
S_G	Interferometer-spectrometer signal at wavelength λ or wavenumber ω resulting from the radiation of the background when a fluid at temperature T_S is contained in a diamond cell
S_S	Interferometer-spectrometer detector signal at wavelength λ or wavenumber ω resulting from the radiation of diamond cell containing fluid at temperature T_S when the chopper blade temperature is T_C
$T(\omega,t)$	Transmissivity, i.e. ratio of energy transmitted to energy incident in the wavenumber region ω to $\omega + d\omega$ at temperature t
T_B	Temperature of a blackbody reference
T_C	Temperature of chopper
T_S	Temperature of fluid sample
χ	D stance from a point within a fluid film to the film boundary through which radiation is transmitted
$\epsilon(\omega,t)$	Sample emissivity in the wavenumber region ω and $\omega + d\omega$ at temperature t
ϵ_λ	Spectral emissivity at wavelength λ
λ	Wavelength
ω	Wavenumber

REFERENCES

1. Van Valkenburg, A., High Pressure Microscopy, in High Pressure Measurements, edited by Giardini and Lloyd, London, Butterworths, 1963.

2. Piermarini, G. J., Block, S., and Barnett, J. D., Hydrostatic Limits in Liquid and Solids to 100 kbar, J. Appl. Physics 44, 5377-82 (1973)

3. Bridgman, P. W., The Physics of High Pressures, London, G. Bell & Sons, Ltd., 1952

4. Barnett, J. D., Block, S. and Piermarini, G. J., An Optical Fluorescence System for Quantitative Pressure Measurement in the Diamond Anvil Cell, Rev. of Sci. Instruments, 44, 1-9 (1973)

5. Lauer, J. L., and Peterkin, M. E., Infrared Spectra of Some Dimethylcyclohexanes at Very High Pressures, in Developments in Applied Spectroscopy, Vol. 10, New York, Plenum Press, 1972

6. Low, M. J. D., McManus, J. C., and Abrams, L., Recording Infrared Spectra at Low Signal Levels, Applied Spectroscopy Reviews, 1972, p. 171-210, Marcel Dekker, Inc., New York, 1972

7. Griffith, P. R., Applied Spectroscopy 26, 73 (1972)

8. McMahon, H. O., Thermal Radiation from Partially Transparent Reflecting Bodies, J. Opt. Soc. Am. 40, 376-380 (1950)

9. Aronson, James R., and Emslie, A. G., The Influence of Physical Variables on Spectral Signatures of Natural Targets. Arthur D. Little Report ADL C-69339, Air Force Cambridge Research Laboratories Report AFCRL-70-0083 (December 31, 1969)

10. Fabbri, G., and Baraldi, P., Infrared Emission Spectra of Solids Applied Spectroscopy, 26, No. 6, 593-599 (1972

11. deRuig, W. G., Infrared Spectra of Monoacid Triglycerides, Agricultural Research Reports 759, Publication No. 167, Rijkszuivelstation-Leiden, Centre for Agricultural Publishing and Documentation, Wageningen, The Netherlands, 1971

12. Barrall, E. M. II, and Guffy, J. C., The Polymorphism of Tristearins, in Advances in Chemistry Series, No. 63, Ordered Fluids and Liquid Crystals, Washington, American Chemical Society, 1967, p. 1-12

13. Slykhouse, T. E., and Drickamer, H. G., Colloquium on "Les proprietes optiques et acoustiques des fluides comprimes et actions intermoleculaires" E.N.R.S. (1957), p. 129. Also, Kliouev, Yu., and Oksengorn, A. B., Doklady Akad. Nauk SSSR, 150, 171 (1963)

14. Davies, J. E. D., The Effect of Phase and Pressure Changes on Vibrational Spectra, J. Molec. Struct. 10, 1-30 (1971)

15. Low, M. J. D., and Coleman, I., Measurement of the Spectral Emission of Infrared Radiation of Minerals and Rocks Using Multiple-Scan Interferometry, Applied Optics, 5, No. 9, 1453-55 (1966)

16. Hewko, L. O., Rounds, F. G., and Scott, K. L., "Tractive Capacity and Efficiency of Rolling Contacts." Proceedings of the Symposium on Rolling Contact Phenomena, Joseph B. Bidwell, Ed., Elsevier, Amsterdam, 1962, p. 157-185.

DISTRIBUTION LIST

CR-134671, NASA Contract NAS3-17593

ADDRESSEE	NUMBER OF COPIES
NASA Lewis Research Center	
21000 Brookpark Road	
Cleveland, OH 44135	
Attn: Contract Section A, MS 500-206	1
Technology Utilization Office, MS 3-19	1
Director of Aeronautics, MS 3-3	1
Library, MS 60-3	2
Report Control Office, MS 5-5	1
N. T. Musial, MS 500-118	1
A. Ginsburg, MS 5-3	1
C. H. Winzig, MS 5-3	1
R. L. Johnson, MS 23-2	2
W. R. Jones, MS 23-2	10
W. R. Loomis, MS 23-2	1
L. D. Wedeven, MS 23-2	1
H. E. Sliney, MS 23-2	1
W. J. Anderson, MS 23-2	1
E. V. Zaretsky, MS 6-1	1
Lt.Col. G. J. Weden, MS 77-5	1
NASA Headquarters	
Washington, D.C. 20546	
Attn: N. F. Rekos (RLC)	1
J. Maltz (RWM)	1
NASA Scientific and Technical Information Facility	
P.O. Box 33	
College Park, MD 20740	
Attn: Acquisitions Branch	30
Air Force Aero Propulsion Laboratory	
Wright Patterson AFB, OH 45433	
Attn: Howard Jones, APFL/SFL	1
Air Force Materials Laboratory	
Wright Patterson AFB, OH 45433	
Attn: Major L. Fehrenbacher, AFML/MBT	1
C. E. Snyder, Jr., AFML/MBT	1
G. J. Morris, AFML/MBT	1
F. Brooks, AFML/MBT	1
Office of Naval Research	
Code 411	
Arlington, VA 22217	
Attn: Lt. R. Miller	1

ADDRESSEE	NUMBER OF COPIES
Battelle Memorial Institute Columbus Laboratories 505 King Ave. Columbus, OH 43201 Attn: C. M. Allen	1
Chevron Research Company 576 Standard Avenue Richmond, CA 94802 Attn: D. Godfrey	1
Exxon Research & Engineering Company P.O. Box 51 Linden, NJ 07036 Attn: A. Beerbower	1
Midwest Research Institute 425 Volker Blvd. Kansas City, MO 64110 Attn: V. Hopkins	1
Mobil Research & Development Corp. P.O. Box 1025 Princeton, NJ 08540 Attn: C. N. Rowe P. E. Fowles	1 1
Southwest Research Institute P.O. Box 28510 San Antonio, TX 78284 Attn: P. M. Ku	1
Stauffer Chemical Company Westport, CT 06880 Attn: J. Hwa	1
Trans-Sonics, Inc. P.O. Box 326 Lexington, MA 02173 Attn: V. C. Westcott	1
Carnegie-Mellon University Dept. of Chemical Engineering Schenley Park Pittsburgh, PA 15213 Attn: T. Fort, Jr.	1

ADDRESSEE	NUMBER OF COPIES
Pennsylvania State University Dept. of Chemical Engineering University Park, PA 16802 Attn: E. E. Klaus	1
Mr. E. E. Bisson 20786 Eastwood Avenue Fairview Park, OH 44126	1
Northwestern University The Technology Institute Evanston, IL 60201 Attn: H. S. Cheng	1
Texaco Research Center Research & Technical Department Fundamental Research Station Beacon, NY 12508 Attn: R. Fein	1
University of Virginia Thornton Hall Charlottesville, VA 22091 Attn: J. J. Kauzlarich W. Jamison	1 1
University of Michigan Dept. of Mechanical Engineering Ann Arbor, MI 48105 Attn: K. Ludema	1
Georgia Institute of Technology School of Mechanical Engineering Atlanta, GA 30332 Attn: W. O. Winer D. M. Sanborn	1 1
Imperial College Dept. of Mechanical Engineering Exhibition Road London SW7 2BX England Attn: A. Cameron	1
National Engineering Laboratory East Kilbride, Glasgow Great Britain Attn: D. Scott	1
The Catholic University of America Vitreous State Laboratory Washington, D.C. 20017 Attn: J. F. Dill	1